NANOPARTICLE-BRIDGE ASSAY FOR AMPLIFICATION-FREE ELECTRICAL DETECTION OF OLIGONUCLEOTIDES

by

MANOUCHEHR TEIMOURI

Presented to the Faculty of the Graduate School of

The University of Texas at Arlington in Partial Fulfillment

of the Requirements

for the Degree of

DOCTOR OF PHILOSOPHY

THE UNIVERSITY OF TEXAS AT ARLINGTON

DECEMBER 2015

Acknowledgements

I would like to express my gratitude to my supervisor, Dr. Seong Jin Koh, for his guidance and support during past five years. This work could not have been done without his help, encouragement, and perseverance.

I'm truly grateful to my colleagues, Jason and Pradeep, who gave me many lessons and shared with me their precious experiences. I would like to thank all the professors and staffs in the department of materials science and engineering and Nanofab Research Center for providing a wonderful friendly atmosphere during my program. I give many thanks to all my friends who I can't list all the names here for their help, thoughts, well-wishes, and being there whenever I needed a friend.

I have to thank the committee members, Dr. Hao, Dr. Liu, Dr. Yum, and Dr. Vasilyev, for generously spending their time and guiding throughout the proposal preparation and reviewing this dissertation.

Finally, I have to thank my family for their love, support, and encouragement. This work is dedicated to my parents for their endless love and sacrifices throughout my life.

This work was supported by US National Science Foundation (ECCS-0925997) and in part by US Office of Naval Research (N00014-12-1-0492).

November 23, 2015

Abstract

NANOPARTICLE-BRIDGE ASSAY FOR AMPLIFICATION-FREE ELECTRICAL DETECTION OF OLIGONUCLEOTIDES

Manouchehr Teimouri, PhD

The University of Texas at Arlington, 2015

Supervising Professor: Seong Jin Koh

The aim of this research is to investigate a highly sensitive, fast, inexpensive, and field-applicable oligonucleotide detection method which does not rely on any enzymatic or signal amplification processes. In this approach, target oligonucleotides are detected through the formation of nanoparticle satellite conjugates which make electrical paths between two electrodes. This method enables an extremely sensitive oligonucleotide detection because even a few oligonucleotide molecules can form a nanoparticle satellite conjugate which can provide an electrical path between electrodes and produce an electrical output signal. It is demonstrated that this oligonucleotide detection method can detect oligonucleotide molecules at concentrations as low as 50 femtomolar without any amplification process. This detection method can be implemented in many fields such as disease detection, biodefense, food safety, clinical research, and forensics.

Table of Contents

Acknowledgements iii

Abstract iv

List of Illustrations xi

List of Tables xx

Chapter 1 Introduction 1

1.1 Motivation to Oligonucleotide Detection 1

1.2 Outline 2

Chapter 2 Background of Oligonucleotide Detection Methods 4

2.1 Introduction to DNA and micro-RNA Structure 4

2.1.1 DNA 4

2.1.1.1 DNA Structure 4

2.1.1.2 DNA Hybridization 7

2.1.1.3 Probe DNA 7

2.1.2 Micro-RNA 8

2.2 Enzymatic Target Amplification-Based Detection Methods 9

2.3 Signal/Probe Amplification-Based Detection Methods Using Gold Nanoparticles 15

2.3.1 Optical detection 17

2.3.1.1 Light Absorption 17

2.3.1.2 Light Scattering 20

2.3.1.3 Surface Plasmon Resonance 23
2.3.1.4 Chemiluminescence and Electrochemiluminescence 25
2.3.2 Electrical Detection 27
2.3.3 Bio-Bar Code Assay 29
2.4 Other Detection Methods 35
2.4.1 Electrochemical Detection Methods 35
2.4.2 Quartz Crystal Microbalance (QCM)-based Detection Methods 36
2.4.3 Magnetic Particle-based Detection Methods 37
2.4.4 Quantum Dot-based Detection Methods 38
2.4.5 Nanotube- and Nanowire-based Detection Methods 40
2.5 Disadvantages of Current Detection Methods 44
Chapter 3 A New Amplification-Free Oligonucleotide Detection Method 46
3.1 Concept of the Amplification-Free Nanoparticle-Bridge Oligonucleotide Sensor 46
3.2 Procedure of the Amplification-Free Nanoparticle-Bridge Oligonucleotide Sensor Fabrication 48
Chapter 4 Experimental Procedure 51
4.1 Background of DNA-Functionalized Gold Nanoparticles 52
4.1.1 Effect of salt on DNA surface loading 52

4.1.2 Effect of spacer type on DNA surface loading 54
4.1.3 Effect of gold nanoparticle size on DNA surface loading 56
4.1.4 Dissociation and degradation of thiolated DNA on gold nanoparticles 57
4.2 Background of Self-Assembled Monolayers (SAMs) 58
4.2.1 Amino-terminated Self-Assembled Monolayers on Silicon Oxide Surface 58
4.2.2 Carboxyl-terminated Self-Assembled Monolayers on Gold Surface 62
4.3 Electrostatic Funneling 64
4.4 Experimental Materials 66
4.4.1 Reagents 66
4.4.2 Reagents Setup 70
4.5 Experimental Instruments 71
4.6 Experimental Procedure 72
4.6.1 Chip Preparation 72
4.6.2 Gold Nanoparticle Functionalization with Single-Strand DNAs (DNA-AuNP) 75
4.6.2.1 30 nm AuNP functionalization with probe-DNA (P-AuNP) 75

4.6.2.2 50-nm AuNP functionalization with capture-DNA (C-AuNP) 78
4.6.3 Quantification of oligonucleotides loaded onto gold nanoparticles 79
4.6.3.1 Quantification of loaded P-DNAs on 30-nm AuNPs..... 79
4.6.3.2 Quantification of loaded C-DNAs on 50-nm AuNPs 80
4.6.4. Engineering of Silicon Dioxide and Gold Surfaces through the Formation of Self-Assembled Monolayers (SAMs) 81
4.6.4.1. Formation of positively-charged SAM onto SiO2 surface 81
4.6.4.2. Formation of negatively-charged SAM onto Au surface..... 82
4.6.5. Formation of Nanoparticle Satellite Conjugates between two Electrodes..... 82
4.6.5.1. Accurate placement of *C*-AuNPs between two electrodes onto the center of SiO2 surface 83
4.6.5.2. Removing free APTES molecules from SiO2 surface..... 83
4.6.5.3. Hybridization of Target DNA (T-DNA) with C-DNA onto C-AuNP 83
4.6.5.4. Stringency washing..... 83
4.6.5.5. Pre-hybridization of P-DNA of P-AuNP with T-DNA onto C-AuNP 84

4.6.5.6. Hybridization of P-DNA of P-AuNP with T-DNA onto C-AuNP 84
4.6.6. I-V measurement and SEM characterization 84
Chapter 5 Results and Discussion 85
5.1 Characterization and Quantitative Analysis of Oligonucleotide-Functionalized Gold Nanoparticles 85
5.2 Formation of Self-Assembled Monolayers onto Silicon Dioxide and Gold Surfaces 90
5.3 Placement of C-AuNPs between Two Gold Electrodes 92
5.4 Formation of Nanoparticle Satellite Conjugates onto Silicon Dioxide Surface 96
5.5 Analysis of DNA Detection Using Amplification-Free Nanoparticle-Bridge DNA Sensor 99
5.5.1 SEM characterization 99
5.5.2 I-V measurements 106
Chapter 6 Conclusion and Future Work 110
6.1 Conclusion 110
6.2 Future Work 111
6.2.1 Applying Electric Field to Accelerate Oligonucleotide Hybridization and Detection 111
6.2.2 Implementing Microfluidic System 112

References.. 114

Biographical Information.. 138

List of Illustrations

Figure 2-1 the molecular structure of a segment of DNA [10] 5

Figure 2-2 Base pairing of Adenine with Thymine and of Cytosine with Guanine in DNA [10] 6

Figure 2-3 Schematic demonstration of PCR [26] 10

Figure 2-4 Schematic comparison of ELISA and IPCR An antibody–enzyme conjugate in ELISA converts a substrate into a detectable product (a), a conjugate comprising an antibody and a DNA marker is utilized in IPCR. The marker is amplified by PCR for signal generation (b) [28] 11

Figure 2-5 Schematic Typical results of the three optional qIPCR detection strategies (sequential qIPCR (gray bars), modular qIPCR (green bars) and direct qIPCR (blue bars)) for human IL-6 in human serum, compared to the analogous control ELISA (black line) [34]. 12

Figure 2-6 Schematic demonstration of RCA [42] 13

Figure 2-7 Schematic demonstration of RT-PCR to form the first DNA [51] 14

Figure 2-8 Schematic of strategies for gold nanoparticle functionalizing [55] 16

Figure 2-9 Red color DNA-AuNPs at 80 °C in unhybridized state (left), blue color at room temperature before DNA-AuNPs settlement to the bottom (center), and transparent at room temperature after settlement (right) [60]. 17

Figure 2-10 Comparison of the thermal dissociation curves for AuNP-modified DNA (black squares) and unmodified DNA (red squares) in the presence of target DNA [61]. 18
Figure 2-11 Comparison of Au nanoparticles functionalized with oligonucleotides before and after treatment with a complementary target oligonucleotides [62]. .. 18
Figure 2-12 Oligonucleotide-modified glass slide- target-nanoparticle probe sandwich assay (left), flatbed scanner images of slides before hybridization of target and nanoparticle probe (A and D), after hybridization with 10nM and 100 pM (B and E), and after exposure to silver amplification solution (C and F). 19
Figure 2-13 Schematic representation of oligonucleotide array based on scattered light (left); microscope images of model DNA arrays functionalized with oligonucleotide sequences c and d and incubated with 50 and 100-nm DNA-AuNPs in the presence of both targets a'c' and b'd' (A), just b'd' (B), just a'c' (C), and neither a'c' nor b'd' (D) [64]. 20
Figure 2-14 The Raman spectra of six dye-labeled nanoparticle probes after Ag enhancing on a chip (A) and six DNA sandwiches assays with corresponding target analysis systems (B) [8]. 21
Figure 2-15 Colorimetric detection of nucleic acid sequence: Step 1: DNA-GNP probes (A and B) are hybridized to a DNA target in solution. Step 2: illumination with white light in the plane of the slide [65]. 22

Figure 2-16 Scanometric identification (left) and the corresponding quantization (right) of the net signal intensities of various concentrations of PSA in buffer after (a) one silver deposition, (b) two silver depositions, (c) one gold deposition, (d) two gold depositions, and (e) three gold depositions [7]. 23
Figure 2-17 SPR curves of surfaces prepared in sequential steps: a MHA-coated Au film modified with a 12- mer oligonucleotide (A), after hybridization with its complementary 24-mer target (B), and followed by introduction of 12- mer oligonucleotide:Au conjugate (C) to the surface [66]..... 24
Figure 2-18 Schematic of CL quantitative assay based on Au and CuS NPs [70] 25
Figure 2-19 Schematic of sensing platform based on energy transfer between CdS:Mn nanocrystals and gold nanoparticles [73] 26
Figure 2-20 Schematic of sandwich assay in ECL-based detection [74]..... 27
Figure 2-21 Schematic demonstration of electrical detection of DNA [6]. 28
Figure 2-22 DNA duplex denaturation curve as a function of sodium ion concentration for the complementary oligonucleotide (X=A) and the 1-bp mismatch strand (X=G) [6]. 28
Figure 2-23 The DNA-BCA assay (A) NP and magnetic microparticle probe preparation (B) NP-based PCR-less DNA amplification scheme [4]. 30
Figure 2-24 The 30-nm AuNPs scanometric data quantified and normalized from five independent experiments. The dashed line indicates five standard deviations above the negative control [75]..... 31

Figure 2-25 Schematic presentation of the multiplexed biobarcode assay for detection of four DNA target [76]. 33
Figure 2-26 The bio-barcode assay method. (A) Probe design and preparation. (B) PSA detection and barcode-DNA amplification and identification [77] 34
Figure 2-27 Scanometric detection of the barcodes [79] 34
Figure 2-28 Dependence of anodic current at 0.7 V on the concentration of target DNA (the control line corresponds to the mean current in the absence of target DNA) [84] 36
Figure 2-29 Schematic illustration of the sensing process of AuNP-covered QCM surface [88] 37
Figure 2-30 Schematic of single-QD-based DNA nanosensors, a) conceptual scheme, b) fluorescence emission from reporter, and c) experimental setup [97] 39
Figure 2-31 (A) Schematic illustration of optical coding. Large spheres represent polymer microbeads; small colored spheres represent quantum dots. Molecular probes (A–E) are attached to the bead surface for biological binding. (B) Ten distinguishable emission colors of ZnS-capped CdSe QDs (C) Fluorescence micrograph of a mixture of CdSe/ZnS QD-tagged beads emitting single-color signals [98] 40
Figure 2-32 Conductance versus time for PNA-functionalized NW during flow of DNA-free solution (1), 100 fM mismatched DNA (2), DNA-free solution 3), and 100 fM complementary DNA (4) [99] 41

Figure 2-33 Detection of labeled DNA sites with nanotube tips; the arrow points to the streptavidin tag. The image height scale is 3 nm, and the white bar corresponds to 100 nm [100] 42
Figure 2-34 TEM image of magnetic bead-target-CNT sandwich [103] 43
Figure 2-35 Nanowire-based detection of single viruses. Nanowire 2 is modified with antibody which is specific to virus [105]..... 44
Figure 3-1 Schematic demonstration of amplification-free nanoparticle-bridge Oligonucleotide sensor. C-AuNPs placement between two electrodes (a). Formation of nanoparticle satellite conjugates (b)..... 48
Figure 3-2 Schematic demonstration of nanoparticle-bridge Oligonucleotide sensor fabrication. Functionalization of SiO2 and Au surfaces with positively and negatively charged (SAMs), respectively (a). Placement of C-AuNPs onto the center locations of the electrode gap (b). Removal of APTES SAMs from SiO2 surface (c). Formation of nanoparticle-satellite conjugates (d). Producing an electrical sensor output by applying a voltage bias across the electrodes (e)..... 50
Figure 4-1 Surface density of the thiolated ssDNA on 13 nm gold nanoparticles as a function of NaCl concentration [108]. 53
Figure 4-2 DNA loading vs NaCl concentration on 15-nm gold nanoparticles. .. 53
Figure 4-3 DNA loading values as a function of spacer for 15, 30, and 50-nm gold nanoparticles [107]..... 55

Figure 4-4 Curves showing fluorescence intensity at 520nm for Au-DNA conjugate samples heated at varying temperatures for 24h [113]..... 57
Figure 4-5 Chemical structure of APTES..... 58
Figure 4-6 Schematic APTES hydrolysis followed by condensation [128]. 59
Figure 4-7 An APTES-derived layer with structural irregularities: individual silane molecules can be incorporated into the layer via (a) hydrogen bonding, (b) electrostatic attraction, (c) covalent bonding with the substrate, and (d) horizontal and (e) vertical polymerization with neighboring silanes; (f) oligomeric/polymeric silanes can also react/interact with functionalities present at the interface [126]. 60
Figure 4-8 APTES film thickness as a function of temperature, (75C left, 25C right), time and APTES concentration [128]. 61
Figure 4-9 Zeta potentials of ionic SAMs [133]..... 62
Figure 4-10 Schematic of carboxylic acid terminated SAMs [142]. 63
Figure 4-11 Plots of the surface coverages of carboxylic acid and carboxylate as a function of pH. Circles represent acid and triangles represent carboxylate anion 63
Figure 4-12 Wafer-scale nanoparticle placement with electrostatic funneling (a) A schematic of the electrostatic interaction energy in an aqueous solution for a negatively charged nanoparticle near a substrate surface functionalized with positively and negatively charged molecules. (b) The nanoparticles (red dots) are guided to the centers of positively charged lines (of width W) where the interaction energy is minimum [144]..... 65

Figure 4-13 Properties of as-received (a) 30 and (b)50nm AuNPs 66

Figure 4-14 Schematic demonstration of e-beam lithography..... 74

Figure 4-15 SEM images of the comb-structure patterns onto chip 74

Figure 4-16 Schematic demonstration of NAP-5 instruction 77

Figure 4-17 Schematic demonstration of gold nanoparticle functionalizing with DNAs 78

Figure 4-18 Schematic demonstration of fluorescent marker-labeled ss-DNA displacement from gold nanoparticles using MCH 81

Figure 5-1 UV-vis spectra of non- and Oligonucleotide -functionalized 30-nm gold nanoparticles 86

Figure 5-2 UV-vis spectra of non- and Oligonucleotide-functionalized 50-nm gold nanoparticles 86

Figure 5-3 Standard linear calibration curves for fluorescence-labeled P-DNA (a) and C-DNA (b) 87

Figure 5-4 Number of DNA per gold nanoparticle (a) and immobilized DNA spacing (b) for P-AuNP and C-AuNP..... 89

Figure 5-5 Oligonucleotide-functionalized 30nm AuNPs attachment on SiO_2 (dark) and Au (bright) surfaces (scale bar: 500nm)..... 91

Figure 5-6 Singe particle placement of oligonucleotide-functionalized 30nm AuNPs (bright and dark areas are Au and SiO_2 surfaces; scale bar: 500nm)..... 91

Figure 5-7 SEM images of three C-AuNPs placed onto gap between two electrodes (scale bar: 500nm) 92
Figure 5-8 Deviation of C-AuNPs location from center of the gap between two electrodes for 100 C-AuNPs 93
Figure 5-9 Effect of ion concentration on attachment of DNA-AuNPs at 1 mM PB pH 7.25 (a&b) and 10 mM PB pH 7.25 (c&d) (scale bars: 200nm)..... 95
Figure 5-10 Effect of pH on attachment of DNA-AuNPs at 1 mM PB pH 6.0 (a) and 1 mM PB pH 7.0 (b) (scale bars: 200nm) 95
Figure 5-11 Formation of nanoparticle satellite conjugates onto silicon dioxide surface for 5 nM complementary (a) and 1-base pair mismatched (b) T-DNA (scale bars: 200nm) 97
Figure 5-12 Formation of nanoparticle satellite conjugates onto silicon dioxide surface for 50 fM complementary (a) 50 fM 1-base pair mismatched (b), and 100 aM complementary (c) T-DNA (scale bars: 200nm) 98
Figure 5-13 SEM images and statistical analysis of nanoparticle satellite conjugates at 5 nM T-DNA (scale bars: 100nm) 101
Figure 5-14 SEM images and statistical analysis of nanoparticle satellite conjugates at 50 pM T-DNA (scale bars: 100nm) 102
Figure 5-15 SEM images and statistical analysis of nanoparticle satellite conjugates at 500 fM T-DNA (scale bars: 100nm)..... 103

Figure 5-16 SEM images and statistical analysis of nanoparticle satellite conjugates at 50 fM T-DNA (scale bars: 100nm)..... 104
Figure 5-17 SEM images and statistical analysis of nanoparticle satellite conjugates at 5 nM 1-base pair mismatched T-DNA (scale bars: 100nm)..... 105
Figure 5-18 I-V measurement for 5 nM T-DNA (device is same as the one which was analyzed statistically in figure 5-13)..... 107
Figure 5-19 I-V measurement for 50 pM T-DNA (device is same as the one which was analyzed statistically in figure 5-14)..... 107
Figure 5-20 I-V measurement for 500 fM T-DNA (device is same as the one which was analyzed statistically in figure 5-15)..... 108
Figure 5-21 I-V measurement for 50 fM T-DNA (device is same as the one which was analyzed statistically in figure 5-16)..... 108
Figure 5-22 I-V measurement for 5 nM 1-bp mismatched T-DNA (device is same as the one which was analyzed statistically in figure 5-17)..... 109

List of Tables

Table 4-1 Comparison of surface coverage for A20 and T20 spacers..... 54

Table 4-2 Average values including standard deviations for particle sizes, absolute number of oligonucleotides per particle, surface Coverage, and effective footprint..... 55

Table 4-3 Comparison of surface coverage of DNA on 15 to 250 nm gold nanoparticles for different spacers from. 56

Table 4-4 Target, Capture, and Probe DNAs product information (all sequences are from 5' to 3')..... 68

Chapter 1

Introduction

1.1 Motivation to Oligonucleotide Detection

Detection of DNA or RNA molecules has become an important part of research in many areas such as disease diagnostics, food safety, forensics, and biodefence. MicroRNA (miRNA) profiling plays a crucial role in diagnosis of cancer. Discovering pathogenic agents in foods is essential to prevent foodborne illnesses. DNA analysis of samples left at crime scene can provide evidence for police investigations. Therefore, it would be highly beneficial to have a DNA or RNA detection method which is sensitive, fast, inexpensive, and field-applicable.

Currently, the main techniques of DNA or RNA molecule detection rely on amplification processes, such as enzymatic target amplification, or signal/probe amplification process. For example, million to billion copies of a particular DNA sequence can be generated from a few DNA molecules using polymerase chain reaction (PCR) [1-3]. Bio barcode assay is used for detection of amplified target DNA in the form of barcode DNA [4, 5]. Silver reduction is used to enlarge the size of gold nanoparticle probes [6, 7]. Raman scattering signal is enhanced by modification of Raman dye-labeled nanoparticles [8, 9]. However, these amplification-based techniques necessarily involve many process steps, which cause a number of considerable drawbacks. They are time-consuming,

costly, sensitive to contamination, and require laboratories and complex instruments. This work aims to develop a highly sensitive, fast, inexpensive, and portable oligonucleotide detection method which does not rely on any amplification process and can be easily used in point-of-care settings.

The concept of our detection method is to directly detect target oligonucleotides with no need of amplification through the formation of gold nanoparticle satellite conjugates between two electrodes. In the presence of even a few target oligonucleotides, probe oligonucleotide-functionalized gold nanoparticles are attached to central capture oligonucleotide-functionalized gold nanoparticles, to form nanoparticle satellite conjugates. Nanoparticle satellite conjugates make electrical path between two electrodes and generate electrical output signal.

1.2 Outline

The aim of this research is to develop an ultra-sensitive amplification-free nanoparticle-bridge DNA oligonucleotide sensor. Here, first the fundamental of DNA structure and hybridization will be presented. Then, current methods of oligonucleotides detection will be reviewed. In chapter 3, concept of our oligonucleotides detection method and procedure for the sensor fabrication will be introduced. In chapter 4, first the theory and a review to three experimental techniques which are applied in our detection method will be presented. These

techniques contain synthesize of DNA-functionalized gold nanoparticles, formation of self-assembled monolayers, and electrostatic funneling. After reviewing the background, experimental procedure for fabrication and testing of our detection method will be explained. In chapter 5, results of our DNA oligonucleotides detection method including SEM and I-V measurements will be discussed. In chapter 6, conclusion and suggestions for future work will be given.

Chapter 2

Background of Oligonucleotide Detection Methods

The aim of this research is to develop a new method for amplification-free detection of oligonucleotides, in particular a DNA oligonucleotide. In this chapter, a brief description to DNA structure and micro-RNA will be presented. After that, current oligonucleotide detection methods including target-enzymatic amplification- and signal/probe-amplification-based methods will be reviewed. Disadvantages of current detection methods will be mentioned at the end of this chapter.

2.1 Introduction to DNA and micro-RNA Structure

2.1.1 DNA

2.1.1.1 DNA Structure

DNA (Deoxyribonucleic acid) molecules consist of two polynucleotides. Each nucleotide is composed of three components: nucleobase in the form of Adenine (A), Thymine (T), Cytosine (C), or Guanine (G), saccharide sugar or deoxyribose, and phosphate group. The molecular structure of a nucleotide is shown in figure 2-1. Nucleotides are bound together via covalent bonds and nucleobases of two polynucleotides are paired together through hydrogen bond in a specific way such that A always pairs up with T and C always pairs up with G

(figure 2-2). Note that G-C base pairs form three hydrogen bonds while A-T base pairs form two hydrogen bonds. This makes G-C base pairs more stable than A-T base pairs. Nucleotide pairing between strands allows the sequence in one strand to determine the sequence in the complementary strand. The two ends of a strand are not identical. Note that one end of each strand a 3 prime hydroxyl group of the deoxyribose sugar is not involved in the backbone while the other end of the same strand the 5 prime hydroxyl group of the deoxyribose sugar at that end is free or may contain a phosphate that is free and not bonded to another deoxyribose sugar. This dissimilarity of the two ends of a strand creates the ability to uniquely distinguish each end of the strand.

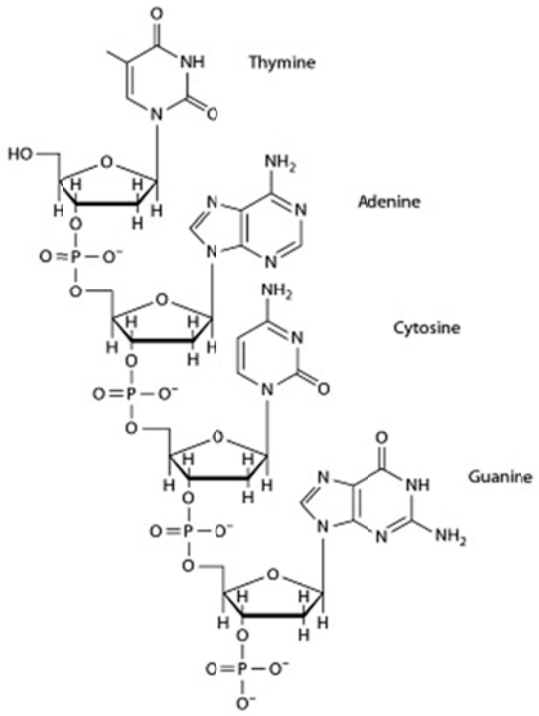

Figure 2-1 the molecular structure of a segment of DNA [10]

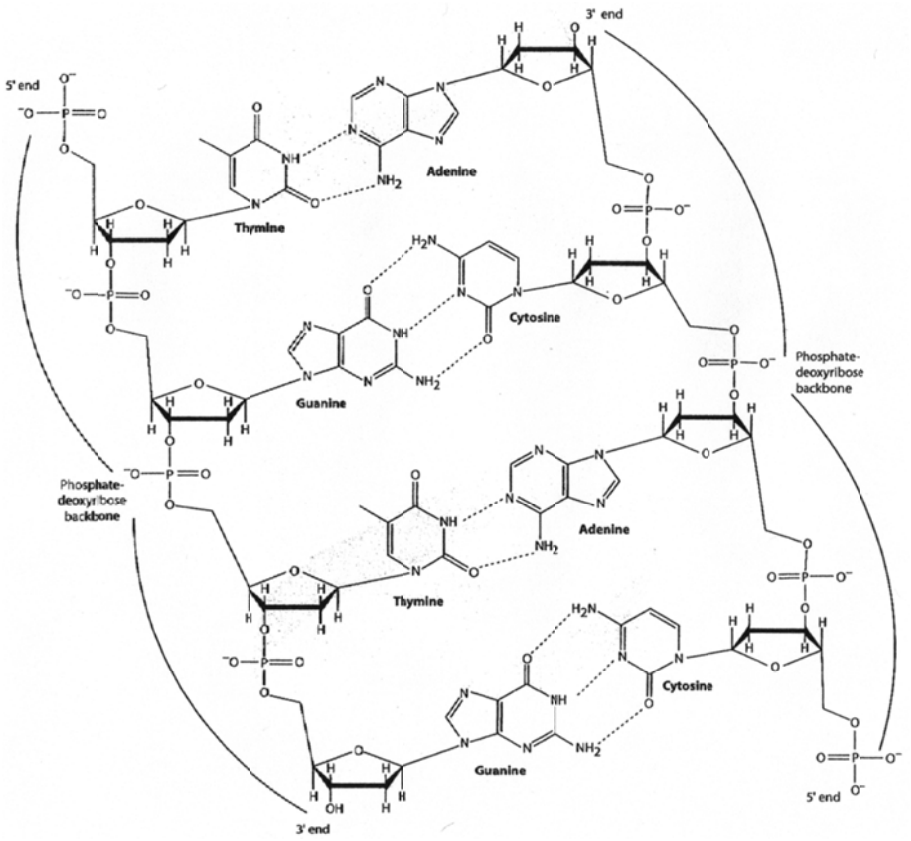

Figure 2-2 Base pairing of Adenine with Thymine and of Cytosine with Guanine in DNA [10]

DNA molecules are two polymer strands which are bound together in a helical configuration by hydrogen bonds. This double-stranded structure (dsDNA) can be melted to form two single-stranded DNA molecules (ssDNA). Melting occurs at high temperature and low salt. A common way to determine the stability of a DNA molecule is measuring the "melting temperature" at which 50% of the double-stranded molecules are separated into two single-stranded molecules.

2.1.1.2 DNA Hybridization

DNA hybridization refers to the process in which two complementary pieces of DNA (or a piece of DNA and a piece of RNA) anneal to form a double-stranded molecule through base pairing. DNA hybridization is a second-order reaction in which formation of a few base pairs from each strand, called nucleus, is the rate-limiting step. Hybridization of remaining base pairs would be quick [11]. Mechanism of the hybridization between DNA oligonucleotide immobilized on the gold nanoparticle and DNA oligonucleotide in the solution was reported to be first adsorption of free DNA oligonucleotide onto the gold nanoparticle surface and then two-dimensional diffusion to hybridizes with an immobilized DNA oligonucleotide [12, 13].

2.1.1.3 Probe DNA

Probe DNA is usually a single-stranded DNA that is labeled with a molecular marker of either radioactive or fluorescent molecule and is used to identify a complimentary DNA sequence of interest. The probe DNA hybridizes to single-stranded nucleic acid (DNA or RNA) whose base sequence allows probe-target base pairing due to complementarity between the probe and target.

Identification of DNA sequences with high or low homology depends on hybridization stringency. High stringency, such as high hybridization temperature and low salt in hybridization buffers, allows only hybridization between nucleic

acid sequences that are highly homologous, whereas low stringency, such as lower temperature and high salt, allows hybridization between sequences which are less homologous.

2.1.2 Micro-RNA

MicroRNAs (miRNAs) are a class of naturally occurring, small non-coding RNA molecules, about 19–25 nucleotides in length. miRNAs are short single stranded RNA molecules, which serve as master regulators of gene expression. Their abnormal levels in tumours have important pathogenetic consequences: miRNAs that are overexpressed in tumours contribute to oncogenesis by downregulating tumour suppressors, whereas miRNAs lost by tumours generally participate in oncogene overexpression [14]. The alterations of miRNA expression are involved in the initiation, progression and metastasis of various types of human cancers, such as breast cancer [15], lung cancer [16], prostate cancer [17], and colon cancer [18].

It is known that miRNA expression patterns can characterize the developmental origins of tumors more effectively than mRNA expression signatures and can be used as an efficient tool for the diagnosis and prognosis of human cancer. To block the function of miRNAs and consequently to inhibit their oncogenic effects, several approaches have been developed. These accomplishments have revealed a potential for miRNA to be used as a clinical

tool in cancer diagnosis and as a target for therapy [19]. To determine the expression pattern of all known miRNAs, developing an accurate and inexpensive profiling method is essential. Detection of miRNA using RT-PCR method has been studied although this is challenging due to the short size of miRNAs which makes PCR amplification complicated [20].

2.2 Enzymatic Target Amplification-Based Detection Methods

Currently, the main assays of DNA detection are based on polymerase chain reaction (PCR) coupled with molecular fluorophores [1, 2, 21-25]. PCR is a method for making many copies of specific segments of DNA starting with a very small amount. This technology can be used to identify specific micro-organisms from small amount of DNA.

The DNA to be amplified is mixed with deoxyribonucleotides, a thermal-stable DNA polymerase called Tag polymerase, and DNA primers. The DNA primers hybridize to the ends of the genes to be amplified and provide starting point for the Tag polymerase. The mixture is heated to break the hydrogen bonds on the DNA forming single strands of molecules. The mixture is then cooled sufficiently to allow DNA primers to anneal to each end of the segment to be copied. Tag polymerase then synthesized the complementary strands of DNA using the primers as the starting point. The temperature is raised again to separate the DNA strands and then lowered sufficiently to allow the primers to attach Tag

polymerase new synthesized another set of new complementary strands. This process is repeated until enough DNA has been produced to be identified (figure 2-3). After 21 cycles, one molecule of DNA can be amplified to over a million copies.

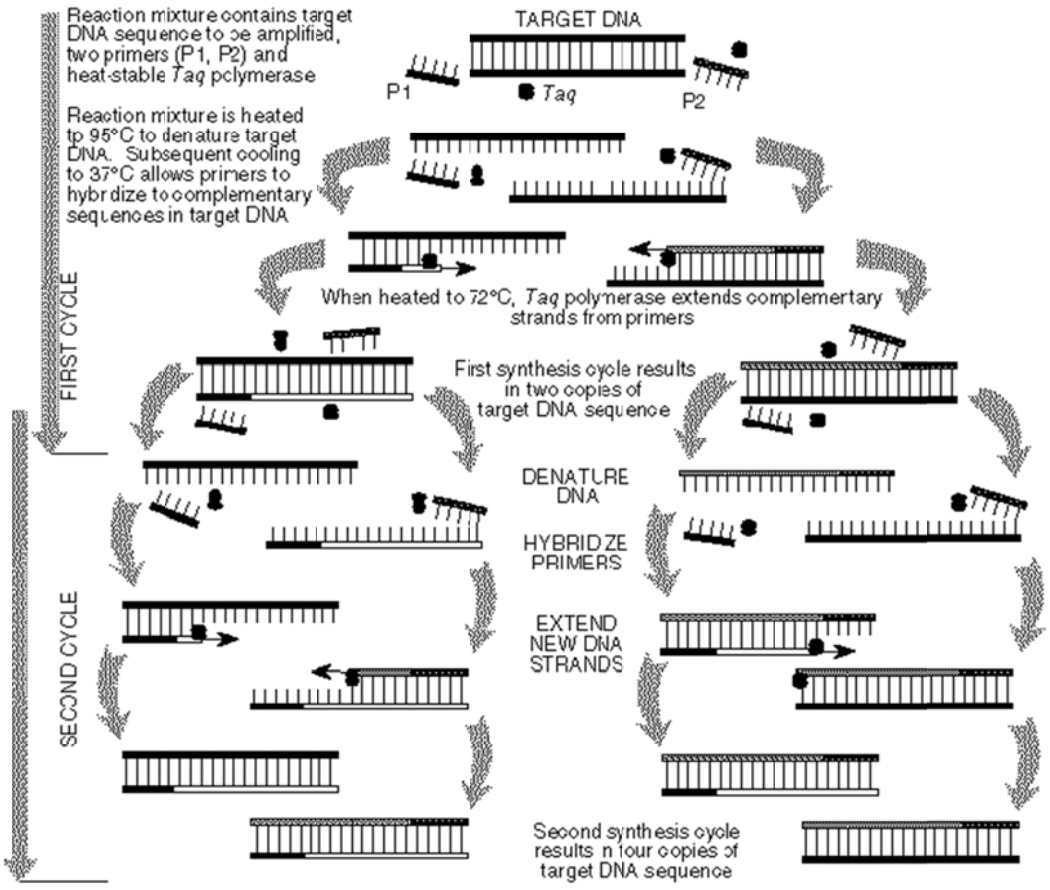

Figure 2-3 Schematic demonstration of PCR [26]

Immuno-polymerase chain reaction (Immuno-PCR) is an antigen detection system which was first developed by Sano et al [27]. In this method, a specific DNA molecule is used as the marker to attach to antigen. Then, a segment of the attached DNA was amplified by PCR. Analysis of the PCR products allowed detection of a few antigen molecules. A comparison in setup between I-PCR and ELISA (the most typical protein detection method) is shown in figure 2-4. As a consequence of signal amplification using PCR, the limit of detection (LOD) of a given ELISA is enhanced 100–10,000 fold [28].

Real-time (qPCR) is a sensitive method for detection and quantification of nucleic acids levels [29]. It is based on detection and quantification of fluorescence emitted from a reporter molecule at real time.

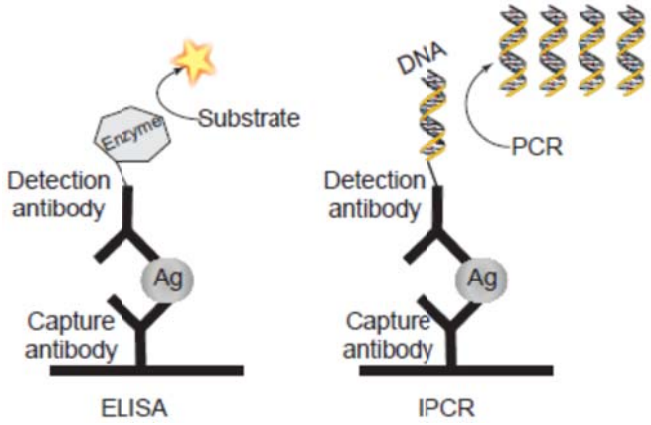

Figure 2-4 Schematic comparison of ELISA and IPCR An antibody–enzyme conjugate in ELISA converts a substrate into a detectable product (a), a conjugate comprising an antibody and a DNA marker is utilized in IPCR. The marker is amplified by PCR for signal generation (b) [28]

Real-time PCR has been employed to quantify miRNA expression profiles. It is used to study the potential function of miRNAs in cancer pathogenesis. Real-time PCR was employed to measure miRNA precursors in cell lines and human cancer cell lines [30, 31].

Real-time Immuno-PCR (qIPCR) has been efficiently used for detection of protein and antigens. The quantitative immuno-PCR (qIPCR) technology takes the advantages of immunoassays and signal amplification of PCR [32, 33]. Niemeyer et al. used qIPCR assay to detect human interleukin 6 (IL-6) protein [34]. They found 10-fold (sequential qIPCR) to 1,000-fold (direct qIPCR) improvement in the detection of IL-6 compared to ELISA (figure 2-5).

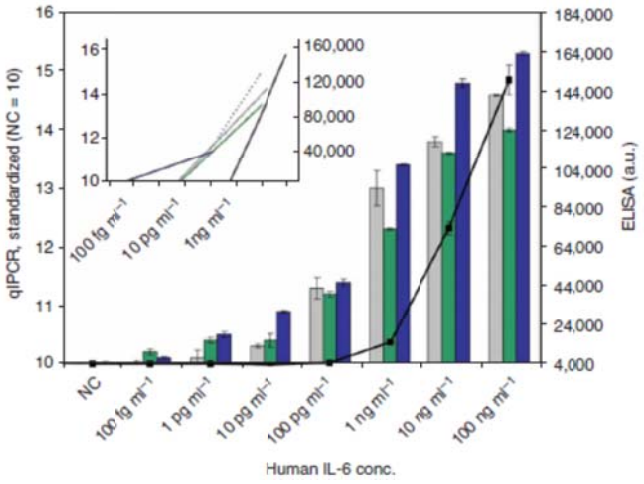

Figure 2-5 Schematic Typical results of the three optional qIPCR detection strategies (sequential qIPCR (gray bars), modular qIPCR (green bars) and direct qIPCR (blue bars)) for human IL-6 in human serum, compared to the analogous control ELISA (black line) [34].

Rolling circle amplifications (RCA) using DNA and RNA polymerases is another amplification process which has been used for detection of DNA and RNA molecules [35-39]. In rolling circle amplification, one strand is nicked and the free 3'OH is extended by DNA polymerase. The 3' end on the circle is lengthened while the growing point rolls around the circular template. The 5' end is displaced and forms a tail of single-stranded DNA that extends from the circle. The single-stranded tail is converted into double-stranded DNA by synthesis involving RNA primers, as in the synthesis of the lagging strand of normal DNA replication (Figure 2-6).

Immuno-rolling circle amplification (RCA) is another method of protein detection. In immune-RCA, an oligonucleotide primer, covalently attached to the detection antibody, is enzymatically elongated by adding a circular single-stranded DNA as template [40, 41].

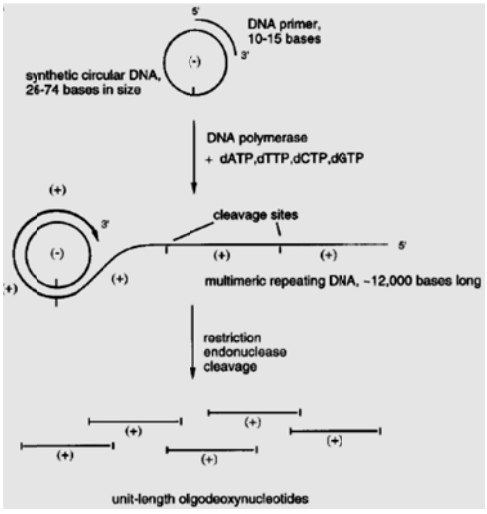

Figure 2-6 Schematic demonstration of RCA [42]

Reverse transcription polymerase chain reaction (RT-PCR) is a common amplification technique which is used in RNA detection [43-46]. In RT-PCR, the RNA molecule is first converted into a complementary DNA (cDNA) using a reverse transcriptase. The cDNA is then exponentially amplified using PCR (figure 2-7).

Asaga et al developed a reverse-transcription quantitative real-time PCR (RT-qPCR) assay for direct detection of circulating miRs in serum. They hypothesized that serum concentrations of miR-21, a biomarker increased in breast tumors, would correlate with the presence and extent of breast cancer [3].

Another efficient amplification used for DNA and RNA detection is exponential amplification reactions (EXPAR) using isothermal polymerase reaction and nicking [47-50].

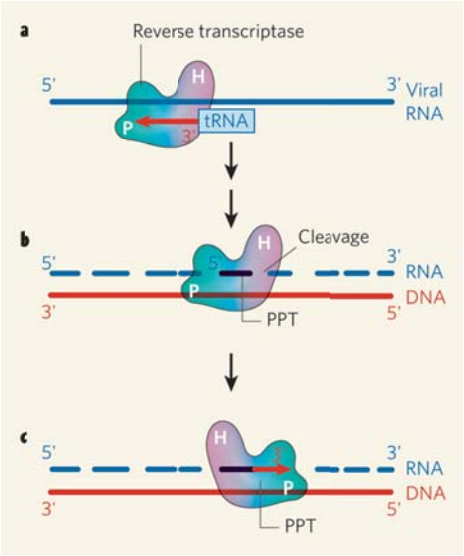

Figure 2-7 Schematic demonstration of RT-PCR to form the first DNA [51]

2.3 Signal/Probe Amplification-Based Detection Methods Using Gold Nanoparticles

Over the past twenty years, unique properties of gold nanoparticles have attracted researcher's attention to develop gold nanoparticle-based DNA detection assays. Chemical and physical properties of the gold nanoparticles determine the applications of gold nanoparticles to oligonucleotides detection. The application of gold nanoparticles in biosensors is strongly related to their properties that depend on synthetic procedures and the subsequent chemical and biological modifications of the gold nanoparticles [52].

Gold nanoparticles appear red in color with surface plasmon band at around 520 nm but they exhibited blue-purple color with shifted characteristic plasmon resonance when they get agglomerated. Physical properties of gold nanoparticles can be easily tailored using surface modification. Unique properties of gold nanoparticles which are strongly depend on their size and shape has made them an interesting nanomaterial to be used in bio-sensing applications [53, 54].

The purpose of functionalizing gold nanoparticles with biomolecules is to have both characteristic properties of biomolecules and gold nanoparticles without change respect to their individuals. There are different processes for functionalizing gold nanoparticles with biomolecules [55]. Ligand-like binding to the surface in which biomolecules are adsorbed directly onto the gold nanoparticle surface is one process. Another one is electrostatic adsorption of

positively charged molecules onto negatively charged gold nanoparticle. Covalent binding between the biomolecule and the stabilizing shell around the gold nanoparticle [56, 57], and affinity-based binding are the other processes. Schematic of biomolecule loading strategies onto gold nanoparticles are seen in figure 2-8. Gold nanoparticles are usually functionalized with oligonucleotides via covalent bond or electrostatic interaction. Thiol-modified oligonucleotides have been widely used to be immobilized onto gold nanoparticles through covalent bonding [58, 59].

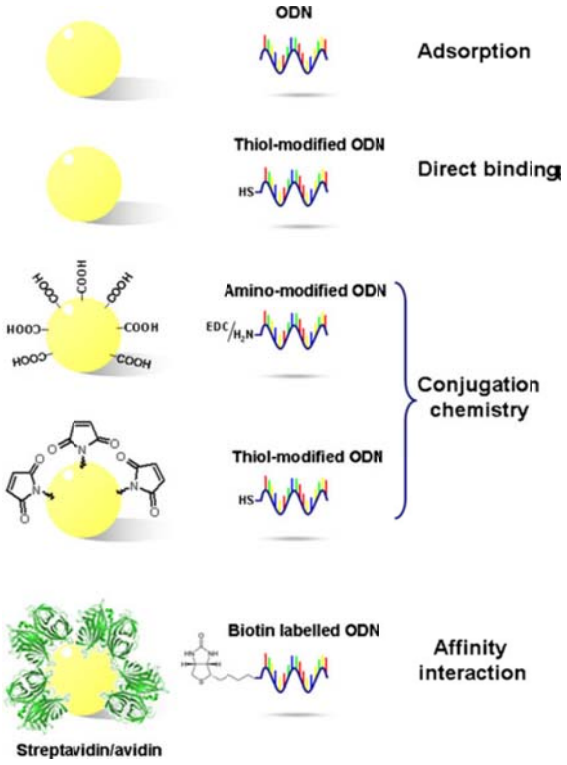

Figure 2-8 Schematic of strategies for gold nanoparticle functionalizing [55]

2.3.1 Optical detection

2.3.1.1 Light Absorption

Application of nanomaterials as biodetection agents was first indicated in 1996. Mirkin et al. reported that the intense colors of gold colloids can be used as an indicator for new DNA colorimetric sensing. In accordance with the fact that color of gold nanoparticles depend on particle size and interparticle distance, they observed color change of gold nanoparticles solution as a consequence of agglomeration of DNA-AuNPs in the presence of complementary target DNA (Figure 2-9) [60]. Limitation of their DNA detection approach was in the 1-10 nM range. Further studies revealed that melting profiles of the nanoparticle-modified DNAs are sharp occurring over a temperature range much more narrow than the transition for unlabeled DNA [61] (Figure 2-10).

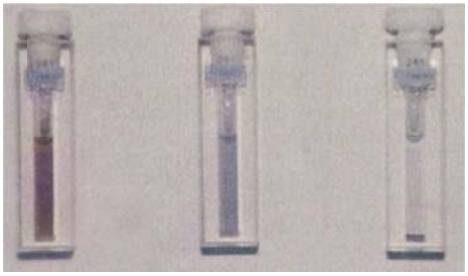

Figure 2-9 Red color DNA-AuNPs at 80 °C in unhybridized state (left), blue color at room temperature before DNA-AuNPs settlement to the bottom (center), and transparent at room temperature after settlement (right) [60].

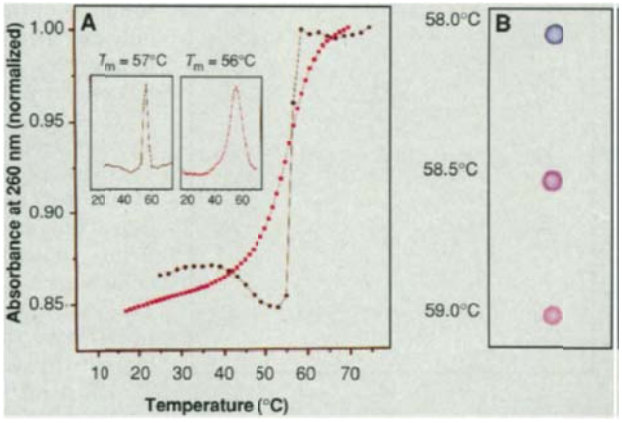

Figure 2-10 Comparison of the thermal dissociation curves for AuNP-modified DNA (black squares) and unmodified DNA (red squares) in the presence of target DNA [61].

Storhoff et al. [62] found that formation of large DNA-linked three-dimensional aggregates of Au nanoparticles in the presence of target DNA leads to a red shift in the surface plasmon resonance (figure 2-11)

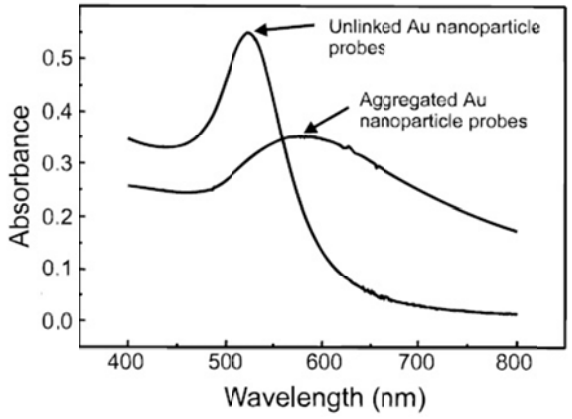

Figure 2-11 Comparison of Au nanoparticles functionalized with oligonucleotides before and after treatment with a complementary target oligonucleotides [62].

Exquisite selectivity that results from the sharp melting transitions of nanoparticle-functionalized DNA is an important advantage that has been realized in a chip-based system. This assay relies on a sandwich structure involving an oligonucleotide-modified chip, a nanoparticle probe, and target oligonucleotide. In this assay a capture DNA strand is immobilized on a chip that recognizes one section of target DNA. The other section of target DNA is then labeled with an oligonucleotide-functionalized nanoparticle probe (Figure 2-12). A thermal stringency wash removes nonspecifically bound target strands, allowing for over 10:1 selectivity for single base-pair mismatch DNA. Eventually, reduction of silver onto the gold nanoparticle surfaces is carried on to amplify the target signal. The capture-DNA/ target DNA/probe-DNA-functionalized gold nanoparticle sandwich can be then visualized with a flatbed scanner [63].

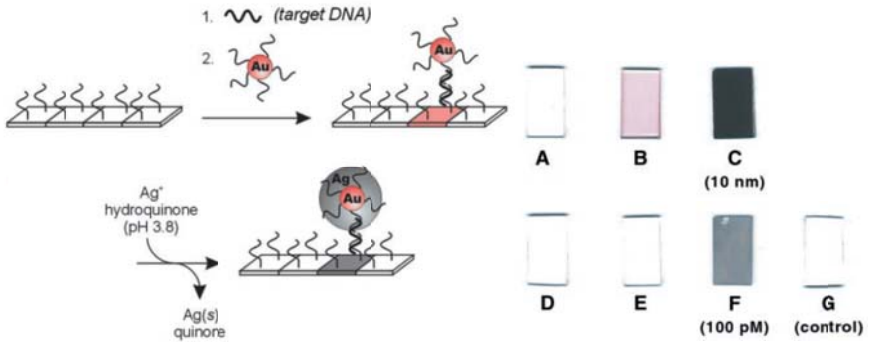

Figure 2-12 Oligonucleotide-modified glass slide- target-nanoparticle probe sandwich assay (left), flatbed scanner images of slides before hybridization of target and nanoparticle probe (A and D), after hybridization with 10nM and 100 pM (B and E), and after exposure to silver amplification solution (C and F) [63].

2.3.1.2 Light Scattering

Metal nanoparticles that differ in size and composition can be designed to scatter light of different wavelengths according to their distinct surface plasmon resonances. Taton et al designed a DNA array imaging technique which is based on scattered light from oligonucleotide-functionalized 50 and 100-nm gold nanoparticles [64]. In their array, light was scattered out of the guide plane and imaged as bright, colored spots wherever gold nanoparticle probes were attached to the surface (Figure 2-13).

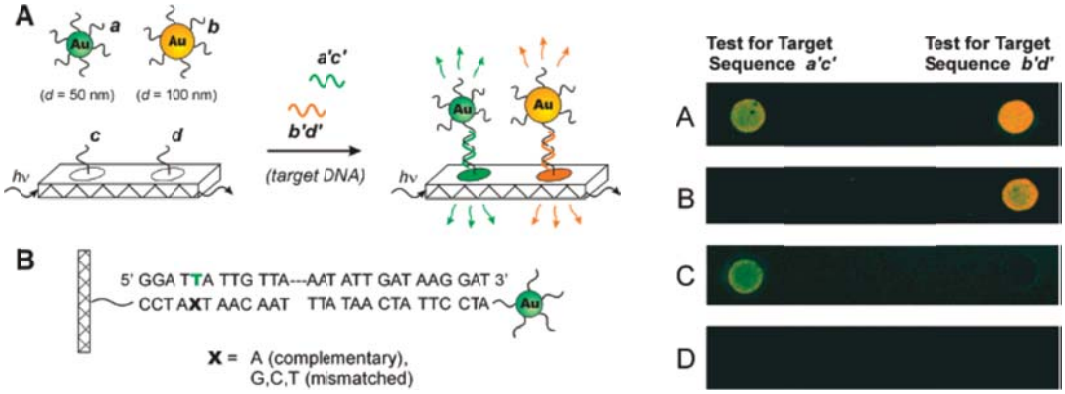

Figure 2-13 Schematic representation of oligonucleotide array based on scattered light (left); microscope images of model DNA arrays functionalized with oligonucleotide sequences c and d and incubated with 50 and 100-nm DNA-AuNPs in the presence of both targets a'c' and b'd' (A), just b'd' (B), just a'c' (C), and neither a'c' nor b'd' (D) [64].

Formation of a silver coating that acts as a surface-enhanced Raman scattering (SERS) promoter for the dye-labeled particles is facilitated by gold nanoparticles. Cao et al. distinguished six dissimilar target DNAs with raman-labeled DNA-functionalized gold nanoparticles [8]. Figure 2-14 shows the Raman spectra of six dye-labeled nanoparticle probes after silver enhancement on a chip.

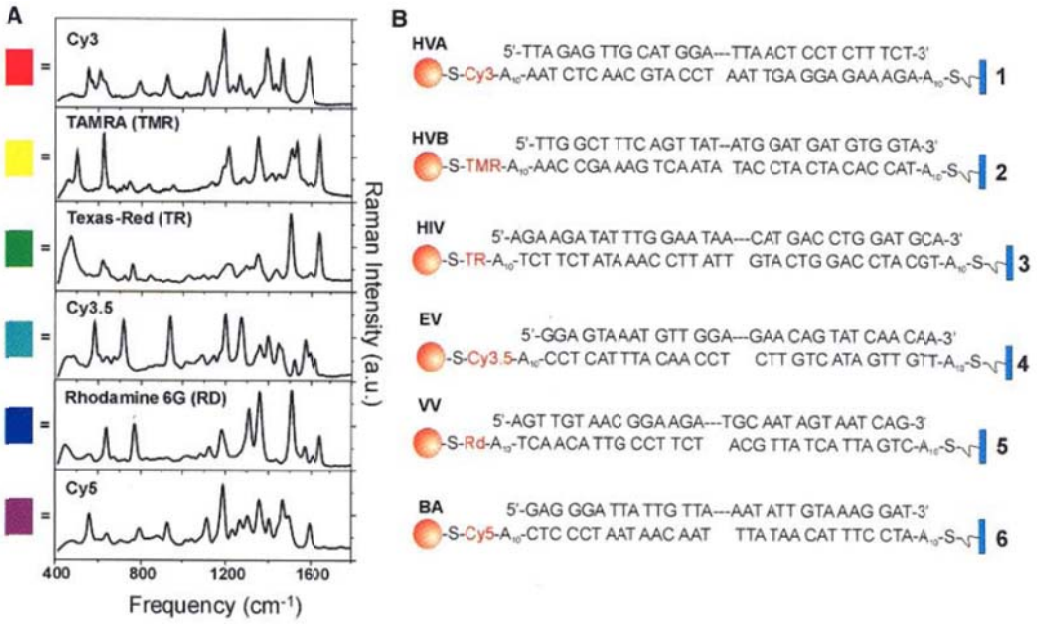

Figure 2-14 The Raman spectra of six dye-labeled nanoparticle probes after Ag enhancing on a chip (A) and six DNA sandwiches assays with corresponding target analysis systems (B) [8].

A colorimetric light scattering of gold nanoparticles was used by Storhoff et al. (figure 2-15). In their assay, pairs of 50-nm diameter gold probes, functionalized with oligonucleotides that are complementary to target DNA, are involved. The gold nanoparticle probes scatter orange light as a result of a plasmon band red shift in the presence of target and scatter green light in the absent of target [65].

Kim et al used multiple gold depositions as a signal enhancing mechanism in their scanometric assay for detection of Prostate specific antigen and three different cancer markers [7]. They found that multiple gold depositions provide greater signal than the typical single silver deposition which is because of the formation of larger probe. Their assay was capable of detecting 300 aM of Prostate specific antigen (figure 2-16).

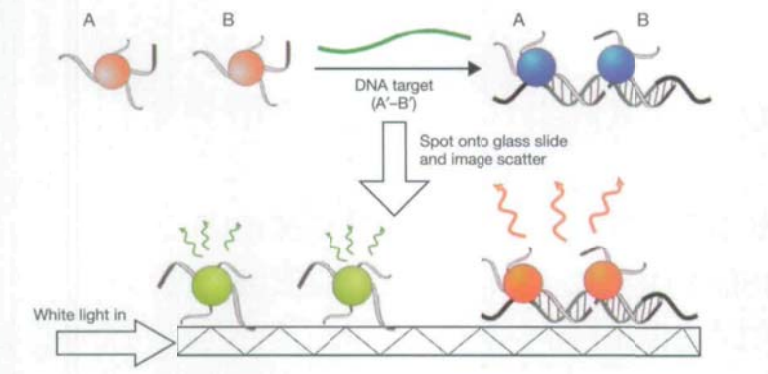

Figure 2-15 Colorimetric detection of nucleic acid sequence: Step 1: DNA-GNP probes (A and B) are hybridized to a DNA target in solution. Step 2: illumination with white light in the plane of the slide [65].

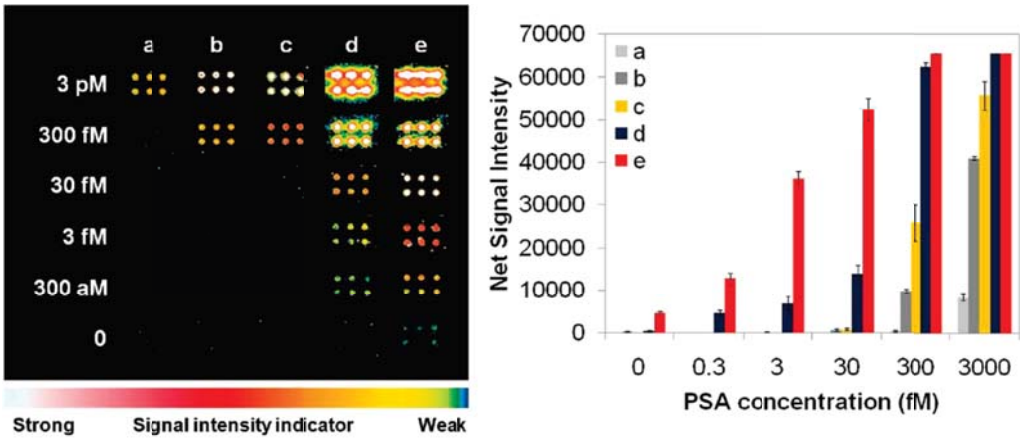

Figure 2-16 Scanometric identification (left) and the corresponding quantization (right) of the net signal intensities of various concentrations of PSA in buffer after (a) one silver deposition, (b) two silver depositions, (c) one gold deposition, (d) two gold depositions, and (e) three gold depositions [7].

2.3.1.3 Surface Plasmon Resonance

Surface plasmon resonance (SPR) is a surface-sensitive analytical technique based on the ability to detect dielectric constant changes induced by molecular adsorption at a noble metal film. A "sandwich" geometry has been developed to use SPR measurement in DNA detection. In this assay, a surface-bound oligonucleotide hybridize with target DNA leading to a very small change in SPR response. A second specifically interacting oligonucleotide loaded onto a high molecular weight or high refractive index tag, such as gold nanoparticle, is

introduced to increase the magnitude of the response. Consequently, a much larger change in SPR reflectivity can be observed.

He et al. [66] showed that use of the Au nanoparticle tags leads to a greater than 10-fold increase in angle shift (Figure 2-16), corresponding to a more than 1000-fold improvement in sensitivity for the target oligonucleotide as compared to the unamplified binding event [67]. A quantitation limit of 10 pM (≤8×108 oligonucleotides/ cm2) was also obtained for 24-mer oligonucleotides.

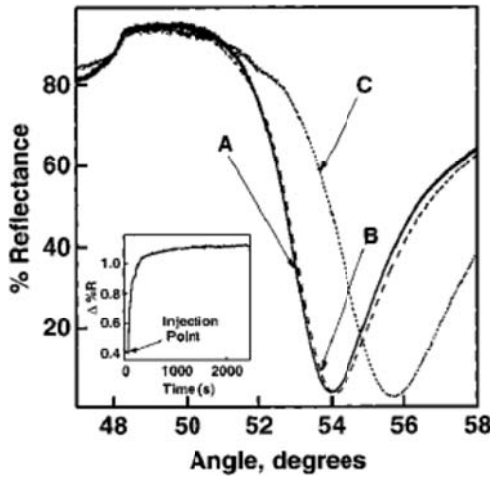

Figure 2-17 SPR curves of surfaces prepared in sequential steps: a MHA-coated Au film modified with a 12- mer oligonucleotide (A), after hybridization with its complementary 24-mer target (B), and followed by introduction of 12- mer oligonucleotide:Au conjugate (C) to the surface [66].

2.3.1.4 Chemiluminescence and Electrochemiluminescence

Detection of chemiluminescence (CL) and electrogenerated-chemiluminescence (ECL) have received considerable attention in bio-detection are due to their versatility, and simplicity [68, 69]. Excited states of an ECL luminophore can generate ECL signals in an electrochemical reaction. After discovery of ECL properties of semiconductor nanocrystals, attention to applying ECL NCs has been increased. Ding et al. quantitatively detected concentration of the one-base mutant DNA by chemiluminescence (CL) detection of the cupric ions dissolved from the CuS nanoparticles. They used gold nanoparticles to immobilize 77 CuS nanoparticles through amidization reaction to enhanced the sensitivity [70]. Schematic of their assay is shown in figure 2-18.

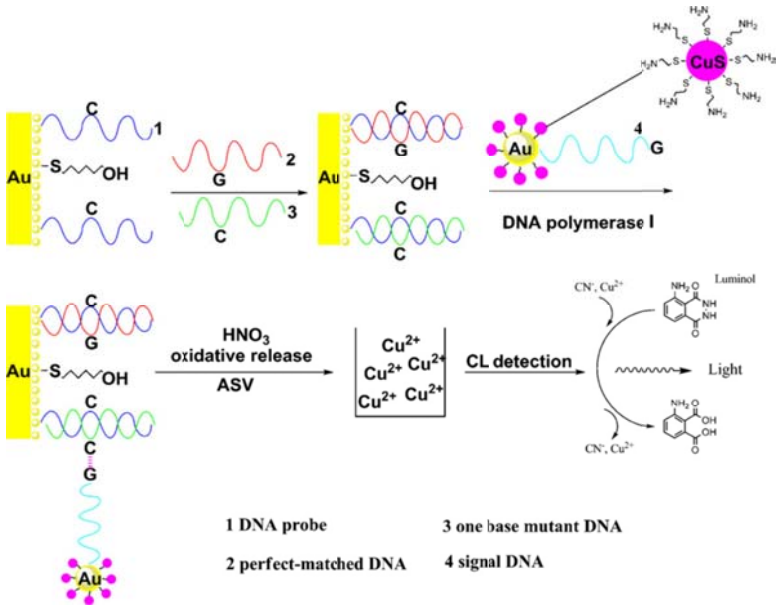

Figure 2-18 Schematic of CL quantitative assay based on Au and CuS NPs [70]

ECL signal detection has also been used for DNA detection [71, 72]. A co-reactant is usually used in ECL applications to make intermediate species that in reaction with a luminophore can generate excited states. Shan et al. used CdS:Mn nanocrystals (NCs), S2O8 2− ions, and AuNPs as ECL luminophores, coreactant, and enhancers (figure 2-19) to detect 50aM DNA [73].

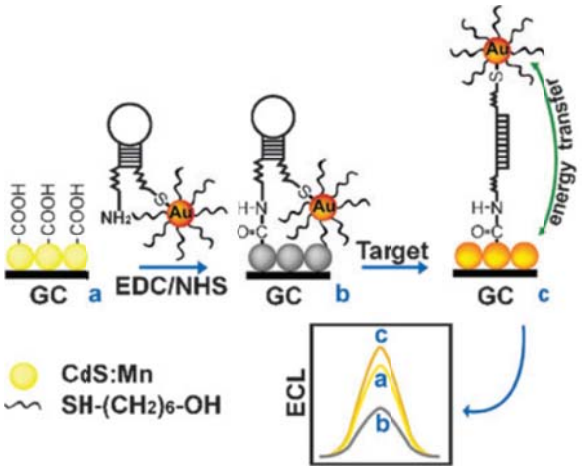

Figure 2-19 Schematic of sensing platform based on energy transfer between CdS:Mn nanocrystals and gold nanoparticles [73]

A sandwich structure made of biotinylated capture DNA immobilized onto gold nanoparticle, target DNA, and luminol-labeled DNA probe immobilized onto gold nanoparticle (figure 2-20) was reported to generate ECL signal at 0.19 aM DNA concentration [74].

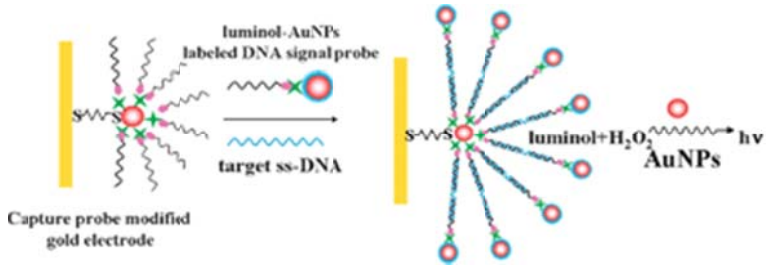

Figure 2-20 Schematic of sandwich assay in ECL-based detection [74]

2.3.2 Electrical Detection

Electrical -based DNA detection methods are the ones that could be used as field-applicable sensors. Nanoparticle sandwich assay, similar to what used in scanometric approach, combined with silver enhancement was used for electrical detection of DNA strands [6].

In this assay, capture oligonucleotides are immobilized in a gap between two electrodes. In the presence of target DNA, a nanoparticle sandwich is formed between two electrodes flowing current between two electrodes, while in the absence of target DNA there is no current flow (Figure 2-21). An impressive selectivity factor of 10000:1 is obtained when this assay is combined with salt-based stringency washing (Figure 2-22).

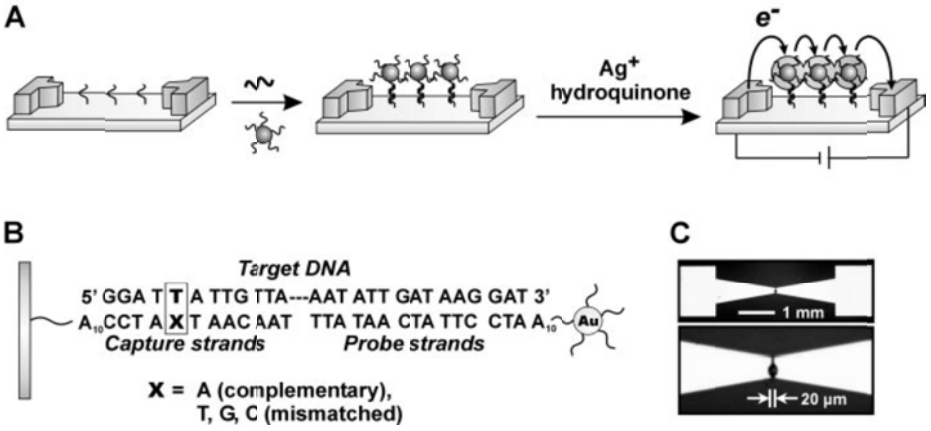

Figure 2-21 Schematic demonstration of electrical detection of DNA [6].

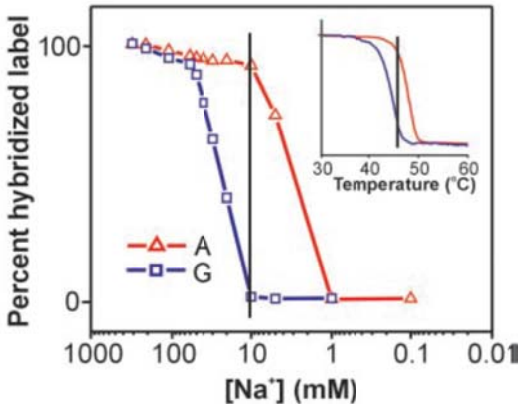

Figure 2-22 DNA duplex denaturation curve as a function of sodium ion concentration for the complementary oligonucleotide (X=A) and the 1-bp mismatch strand (X=G) [6].

2.3.3 Bio-Bar Code Assay

The bio-bar-code assay is a promising new amplification and detection system that utilizes short oligonucleotides as target identification strands and surrogate amplification units in both protein and nucleic acid detection.

The typical assay involves two types of particles. One particle is magnetic and has recognition elements for the target of interest attached to its surface. The second is a particle (e.g., a gold nanoparticle) that has a recognition agent, which can sandwich the target with the magnetic particle. The second particle also carries oligonucleotides covalently attached to its surface that support complementary oligonucleotides. The hybridized oligonucleotides are the bar-code strands. When the sandwich structures are formed, a magnetic field is used to localize and collect them. Excess sample is removed and then water or buffer at an elevated temperature is used to release and collect the bar-code strands. The strands can be identified using any number of common DNA detection modalities (e.g., scanometric detection or fluorescence detection).

Using bio-barcode assay to detect DNA targets was first reported by Nam et al. [4]. That system relies on two-component oligonucleotide-modified gold nanoparticles and single-component oligonucleotide-modified magnetic microparticles, and subsequent detection of amplified target DNA in the form of barcode DNA using a chip-based detection method (figure 2-23).

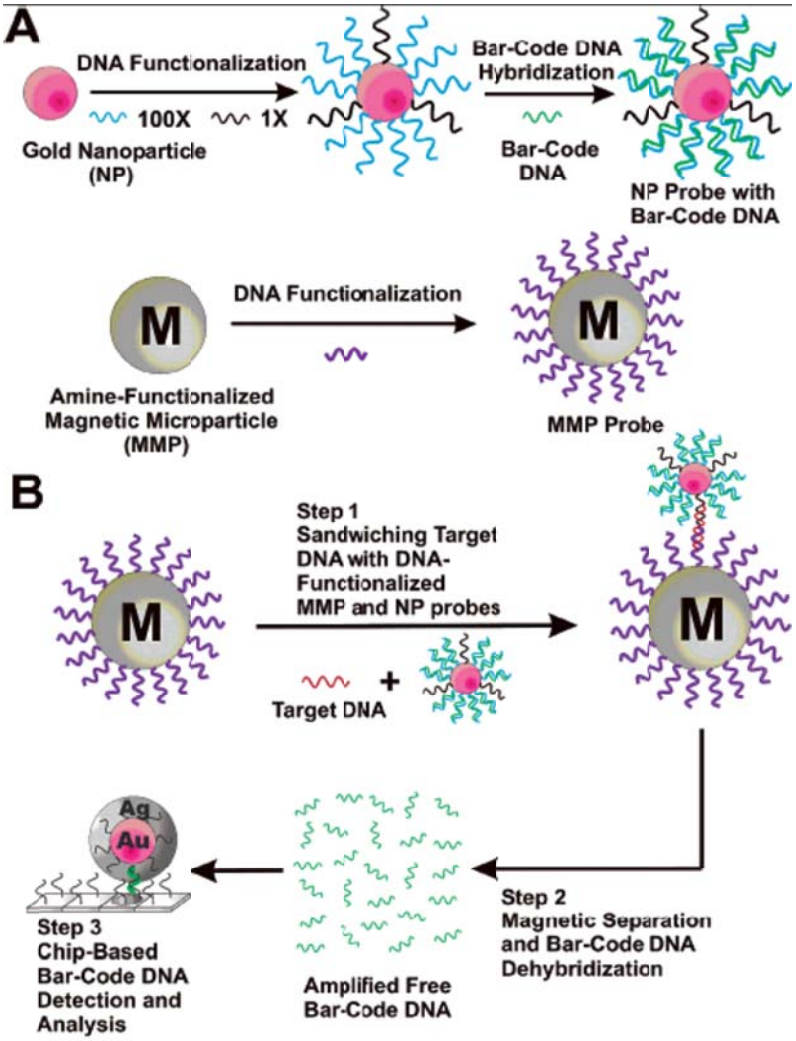

Figure 2-23 The DNA-BCA assay (A) NP and magnetic microparticle probe preparation (B) NP-based PCR-less DNA amplification scheme [4].

The bio bar-code assay relies on three oligonucleotides on the gold nanoparticle. A developed bio bar-code assay was reported by Thaxton et al. [75] and Hill and Mirkin [5] in which gold nanoparticles are functionalized with just

one oligonucleotide. This new developed bio bar-code assay relies on the ability to liberate the adsorbed thiolated oligonucleotides from the gold nanoparticles surface with dithiothreitol (DTT). Figures 2-24 shows that with either 13- or 30-nm gold nanoparticle, the DTT-based bio-barcode assay is capable of detecting target concentrations down to 7aM when coupled with the scannometric readout method [75].

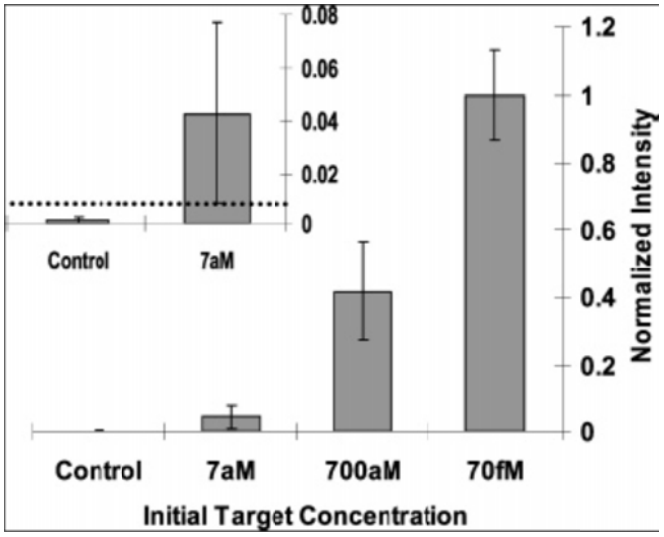

Figure 2-24 The 30-nm AuNPs scanometric data quantified and normalized from five independent experiments. The dashed line indicates five standard deviations above the negative control [75]

Simultaneous detection of multiple oligonucleotide targets by using oligonucleotide sequences associated with a) hepatitis B virus surface-antigen gene (HBV), b) variola virus (small pox, VV), c) Ebola virus (EV), and d) human immunodeficiency virus (HIV) as model systems was reported by Stoeva et. al. (figure 2-25). They demonstrated that these four DNA targets can be detected with high selectivity at mid-femtomolar concentrations [76] .

The utility of the bio-barcode assay for detecting protein markers and specifically Prostate specific antigen (PSA) has been extensively studied.

Nam et al. reported PSA detection at 30 attomolar concentration [77]. Their system relies on magnetic microparticle probes with antibodies that specifically bind PSA and nanoparticle probes that are encoded with DNA that is unique to the PSA and antibodies that can sandwich the target captured by the microparticle probes. Identifying the oligonucleotide sequence released from the nanoparticle probe allowed the determination of the presence of the BSA (figure 2-26).

Thaxton et al. developed the bio-barcode assay for the detection of PSA at 330 fg/mL [78]. They also detected PSA in the serum of men after radical prostatectomy which was 300 times more sensitive than commercial immunoassays.

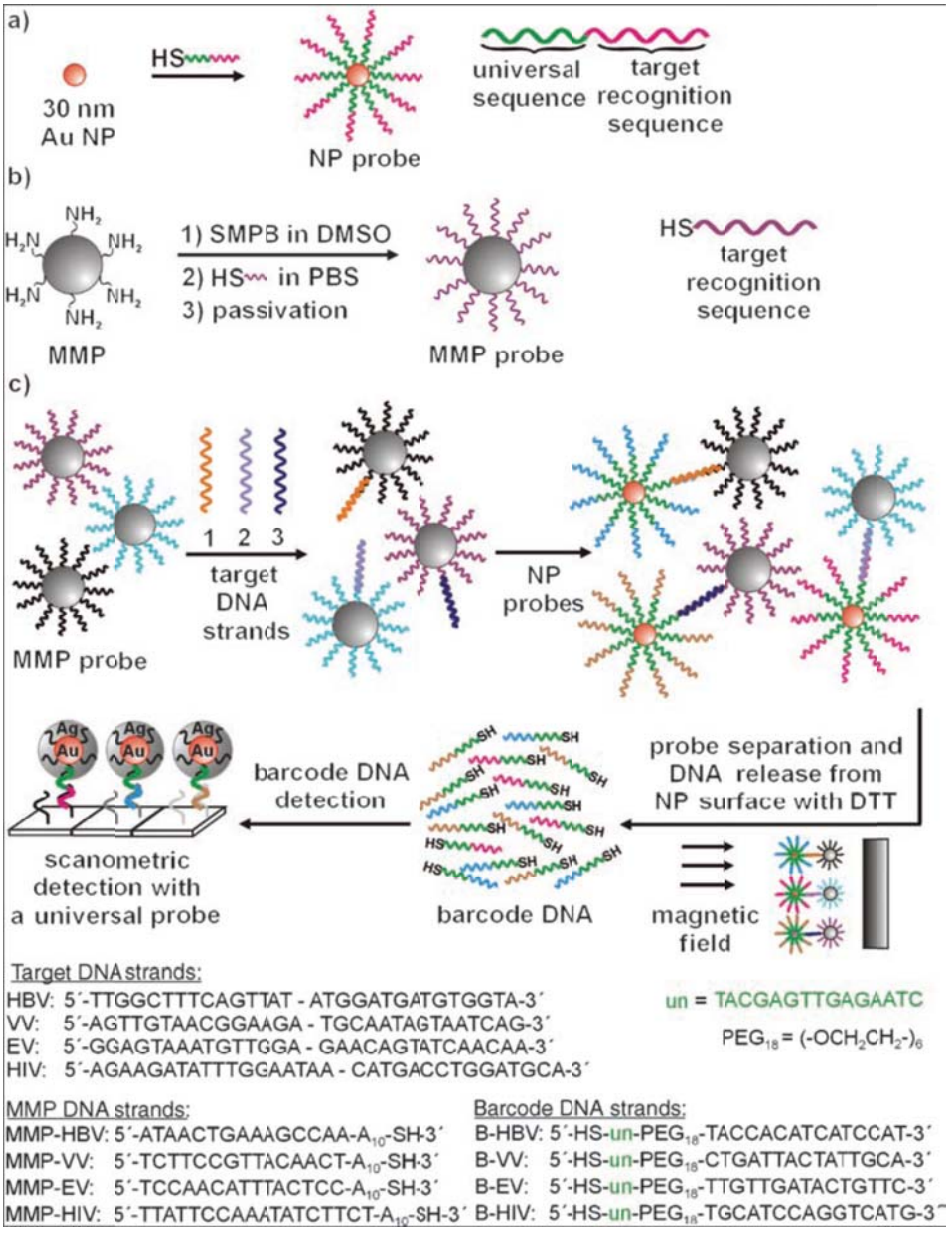

Figure 2-25 Schematic presentation of the multiplexed biobarcode assay for detection of four DNA target [76].

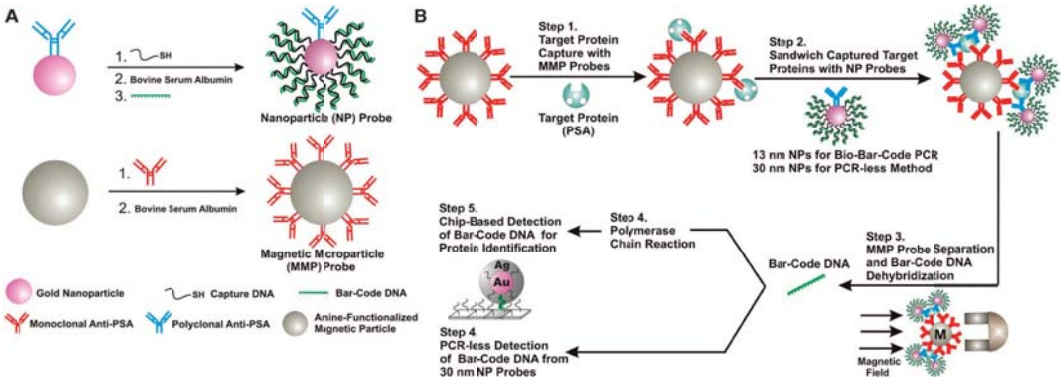

Figure 2-26 The bio-barcode assay method. (A) Probe design and preparation. (B) PSA detection and barcode-DNA amplification and identification [77]

Highly selective multiplexed detection of three protein cancer markers in buffer and serum media was demonstrated by Stoeva et al [79]. They detected three different protein cancer markers each at 170 fM concentration with high selectivity (figure 2-27).

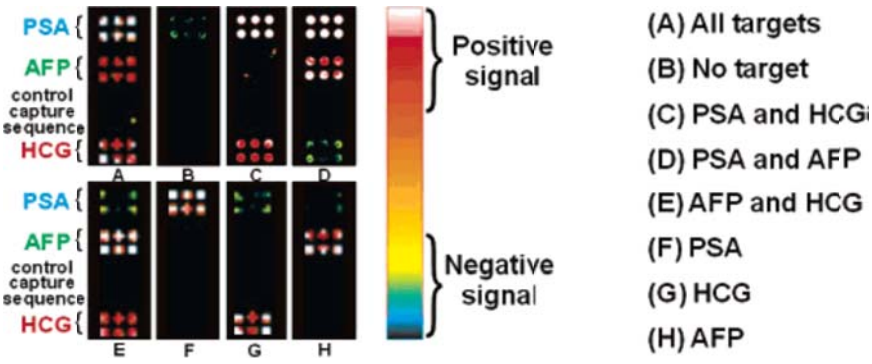

Figure 2-27 Scanometric detection of the barcodes [79]

2.4 Other Detection Methods

2.4.1 Electrochemical Detection Methods

In electrochemical oligonucleotide sensors, the hybridization event is converted into a direct electrical signal. In electrochemical sensors, by using an highly or moderately electrocatalytic electrode, such as Au,Pt, ITO (indium tin oxide), or applying a significant change in the electrocatalytic activity of an electrode, electrocatalysis can be utilized [80-83].

Das and Yang found that that DNA-conjugated AuNPs are not good enough to be used as electrocatalytic labels because of slow electron-transfer kinetics on DNA-conjugated AuNPs. So, they enhanced the electrocatalytic activity of DNA-conjugated AuNPs by NaBH4 treatment which led to significant increase in the electrocatalytic current of hydrazine on the ITO electrodes [84]. By using ITO electrode which has low background noise and modification of electrode with gold nanoparticles, they were able to detect 1fM target DNA (figure 2-28).

Selvaraju et al utilized the combination of AuNP labeling and magnetic beads (Mbs). Using capture-probe conjugated Mbs and ferrocene (Fc)-modified ITO electrodes, p-aminophenol was generated and electrooxidized. They also reported sensitivity of 1 fM [85].

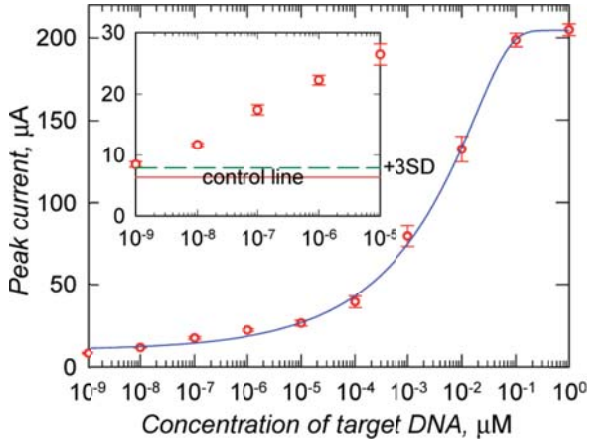

Figure 2-28 Dependence of anodic current at 0.7 V on the concentration of target DNA (the control line corresponds to the mean current in the absence of target DNA) [84]

2.4.2 Quartz Crystal Microbalance (QCM)-based Detection Methods

Gold nanoparticles can be used to enhance piezoelectric transducer frequency shifts. Weismann et al [86] reached 1 fM sensitivity using a quartz piezoelectric crystal, avidin-labeled DNA, and gold deposition onto gold nanoparticles to produce amplified frequency shifts.

Further increase in sensitivity can be obtained using nanoparticle modification of the QCM surface with DNA-functionalized AuNP signal amplification (figure 2-29). Liu et al reached 10^{-16} M sensitivity by sandwiching target DNA between gold nanoparticle immobilized on the QCM surface and oligonucleotide-functionalized gold nanoparticle [87, 88].

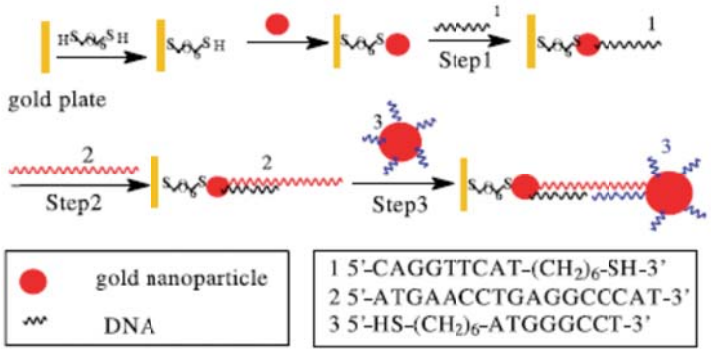

Figure 2-29 Schematic illustration of the sensing process of AuNP-covered QCM surface [88]

2.4.3 Magnetic Particle-based Detection Methods

Magnetic beads are usually used for concentration of target biomolecules and with labels such as gold nanoparticles for detection. A sandwich assay consisting gold nanoparticles, DNA and magnetic microbeads have been widely used for DNA detection. Xu et al reported significant improvement in selectivity of DNA sensors [89].

Bead-based sandwich hybridization (BBSH) is another approach for rapid analysis of specific nucleic acids. Simultaneous hybridization of target molecule with capture on the magnetic bead and probe followed by enzymatic labeling reaction and potentiometric measurement was reported [90]. The common phenomenon in these assays is that target DNA is first captured and then released for further process and detection which increase detection time. Some researchers have been modifications to overcome this problem [91-93]. Martins et al.

developed a platform involving immobilization of specic probes for target and labeling targets with paramagnetic markers. Real time monitoring of probe-target interaction was measured via variation in sensor resistance with label's magnetic stray fields [94].

2.4.4 Quantum Dot-based Detection Methods

Quantum dots are a type of nanoparticles which are used for fluorescence tagging of biomolecules. They are brighter and much photostable than organic fluorophores. It is possible to monitor different components in a system because most of the quantum dots can be excited using a single, short-wavelength excitation source [95].

Fluorescence resonance energy transfer (FRET)-based probes was studied for unamplified DNA [96]. Using this structure, Zhang et al. used probes DNA-quantum dots to capture DNA targets. The schematic of quantum dot-based assay is shown in figure 2-30. Binding to a dye-labelled reporter strand, a FRET donor–acceptor ensemble was formed. This assembly ends up in fluorescence emission from the acceptor fluorophores by means of illumination of the quantum dot donor [97].

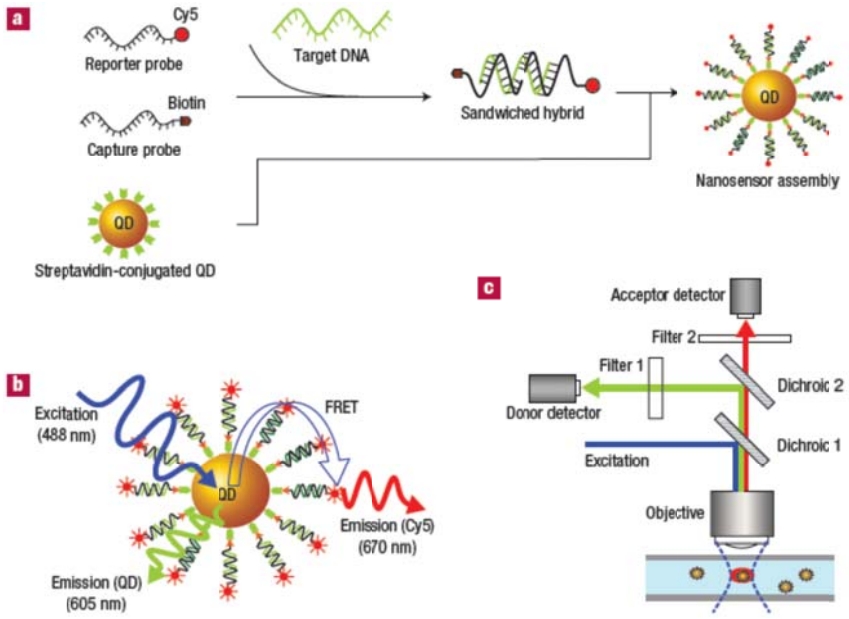

Figure 2-30 Schematic of single-QD-based DNA nanosensors, a) conceptual scheme, b) fluorescence emission from reporter, and c) experimental setup [97]

Quantum dots (QDs) are suitable fluorophores for wavelength and intensity multiplexing due to their size-dependent emission and simultaneous excitation. Multicolor optical coding assay was developed by Han et al. by embedding different sized QDs into polymeric microbeads (figure 2-31). They were able to observe different target signals simultaneously in DNA hybridization at the single-bead level [98].

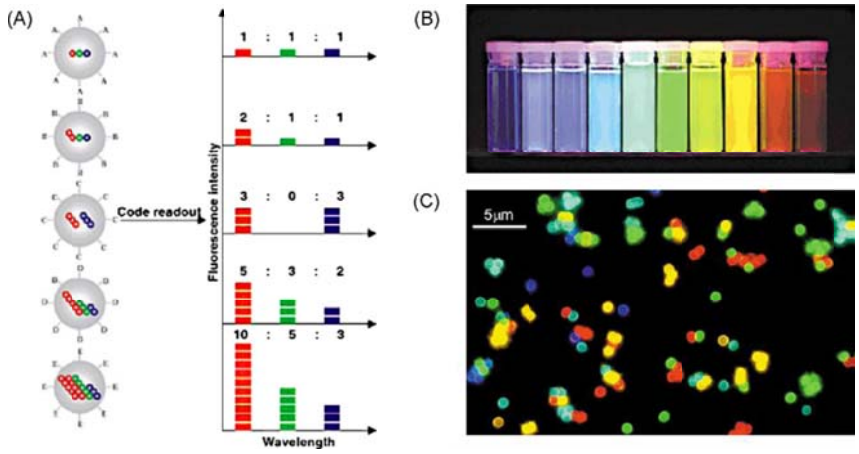

Figure 2-31 (A) Schematic illustration of optical coding. Large spheres represent polymer microbeads; small colored spheres represent quantum dots. Molecular probes (A–E) are attached to the bead surface for biological binding. (B) Ten distinguishable emission colors of ZnS-capped CdSe QDs (C) Fluorescence micrograph of a mixture of CdSe/ZnS QD-tagged beads emitting single-color signals [98]

2.4.5 Nanotube- and Nanowire-based Detection Methods

Nanowires (NWs) and Nanotubes (NTs) have been recently used for label-free electrical detection of DNA and proteins. Hahm and Lieber demonstrated that Silicon NWs (SiNWs) which is functionalized with peptide nucleic acid (PNA) receptors can operate as a real-time DNA sensors to femtomolar range [99]. In their assay, PNA-functionalized SiNW bridges two electrodes. In the present of target DNA, there would be a rapid change in the conductance of SiNW. They

saw that by adding 100 fM complementary DNA solution, the conductance increases over a longer time scale and remains unchanged while conductance of SiNW jumped and dropped immediately after adding mismatched DNA and DNA-free solution, respectively (figure 2-32).

Woolley et al. used single-walled carbon nanotube (SWNT) atomic force microscopy (AFM) probes to detect polymorphic sites and determine haplotypes in 10-kilobase-size DNA fragments [100]. They marked specific sequence of DNA with streptavidin-labeled DNA probes. Labeled DNA then imaged by AFM using SWNT probes. The presence and locations of the sequence specific tags can be readily observed in the AFM image (figure 2-33).

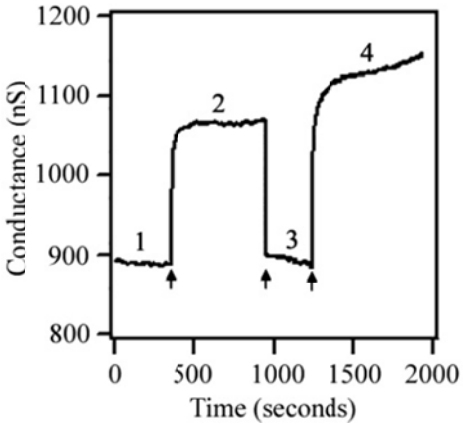

Figure 2-32 Conductance versus time for PNA-functionalized NW during flow of DNA-free solution (1), 100 fM mismatched DNA (2), DNA-free solution 3), and 100 fM complementary DNA (4) [99]

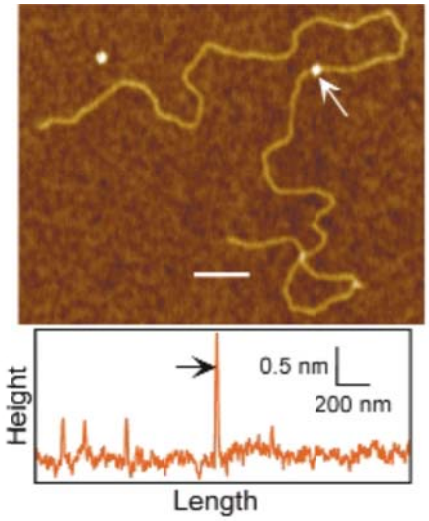

Figure 2-33 Detection of labeled DNA sites with nanotube tips; the arrow points to the streptavidin tag. The image height scale is 3 nm, and the white bar corresponds to 100 nm [100]

Wang et al. used carbon-nanotube to modify glassy-carbon electrodes (CNT/GC) in order to improve detection of nucleic acids and DNA hybridization, and guanine bases. They got to detect DNA at nanomolar range using carbon nanotube-modified electrodes by amplified electrochemical signals [101]. In a similar way, array of carbon nanotube was used for DNA detection. After hybridization of target with capture oligonucleotide loaded onto nanotubes, $Ru(bpy)_{32}^{+}$ was introduced for mediation of guanine base oxidation. Hybridization of target and capture was observed by measuring Ru(III)/Fe(III) electrocatalysis [102].

Another assay to detect amplified DNA was utilized using enzyme-coated carbon nanotube coupled with oligonucleotide-modified magnetic microparticle. In the presence of target, a magnetic microparticle-target-carbon nanotube sandwich is formed (figure 2-34). After separation of this sandwich and then formation of a naphtol product, chronopotentiometric stripping is used to detect target DNA [103].

Conducting nanotubes and nanowires were also used for detection of proteins. Boron-doped silicon nanowire was used to detect streptavidin at picomolar range. It was shown that conductivity of silicon nanowire changes in the presence of streptavidin [104]. Antibody-functionalized nanowire which is specific to influenza A virus particles was also successfully utilized to demonstrate the influence of a virus-nanowire on conductivity of nanowire (figure 2-35) [105].

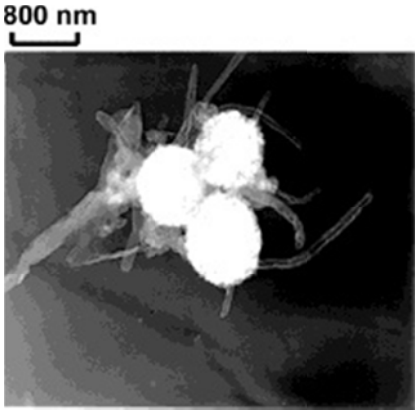

Figure 2-34 TEM image of magnetic bead-target-CNT sandwich [103]

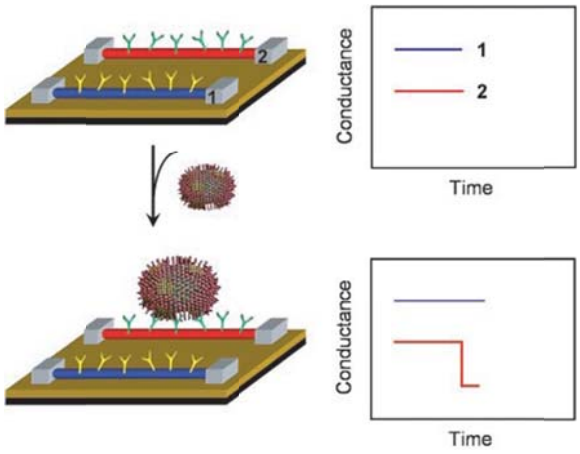

Figure 2-35 Nanowire-based detection of single viruses. Nanowire 2 is modified with antibody which is specific to virus [105]

Similar research on detecting target proteins was carried out using carbon nanotubes. Polyethylene oxide which is coated onto carbon nanotubes specifically functionalized with antibodies to probe target proteins. Decrease in nanotube conductance as a consequence of target presence was observed [106].

2.5 Disadvantages of Current Detection Methods

The limitations of the current detection methods are mostly associated with the complicated, time consuming, and requiring experimental expertise in amplification-based methods. Also, the elongated assay time and enhanced reagent consumption make these amplification-based detection methods less attractive for routine applications when there is no particular need for

ultrasensitive analysis. Considering these drawbacks, we aimed to develop a highly sensitive oligonucleotide detection method which does not rely on any amplification method. The concept of our amplification-free nanoparticle-bridge oligonucleotide sensor is explained in chapter 3.

Chapter 3

A New Amplification-Free Oligonucleotide Detection Method

In this chapter, Concept and fabrication procedure of our new amplification-free nanoparticle-bridge Oligonucleotide sensor is presented.

3.1 Concept of the Amplification-Free Nanoparticle-Bridge Oligonucleotide Sensor

The main concept of this method which is schematically demonstrated in figure 3-1 is to create an electrical path between two electrodes through the formation of nanoparticle satellite conjugates. The formation of nanoparticle satellite conjugates which indicates the presence of target oligonucleotide is examined by conducting I-V measurements. Presence of target oligonucleotide and consequently formation of nanoparticle satellite conjugate leads to the generation of a linear I-V curve. In this method, two kinds of gold nanoparticle and three kinds of single-stranded Oligonucleotide molecules are used to provide electrical path between two electrodes. Single-stranded Capture DNA (C-ssDNA), Target DNA (T-ssDNA), and Probe DNA (P-ssDNA) strands are all synthetic. C-ssDNA is immobilized onto larger gold nanoparticle (~50 nm) to form C-AuNP conjugate and P-ssDNA is immobilized onto smaller gold nanoparticle (~30 nm) to form P-AuNP conjugate. One section of T-ssDNA is complementary to C-

ssDNA and the other section is complementary to P-ssDNA. C-AuNPs are place at the center positions of the gap between two electrodes. After introducing T-ssDNA and then P-AuNPs, nanoparticle satellite conjugates are formed which bridges two electrodes. Formation of nanoparticle satellite conjugates provide electrical paths between two electrodes and produce an electrical current when a voltage bias is applied. In this method, the sensing signal is an electrical current.

The main advantage of this method is that only a few number of T-ssDNA is needed to form a nanoparticle satellite conjugate and consequently produce an electrical signal without any amplification. A 30-mer single-stranded anthrax DNA (3'-TAG GAA TAG TTA TAA ATT GTT ATT AGG GAG-5') was used as T-ssDNA.

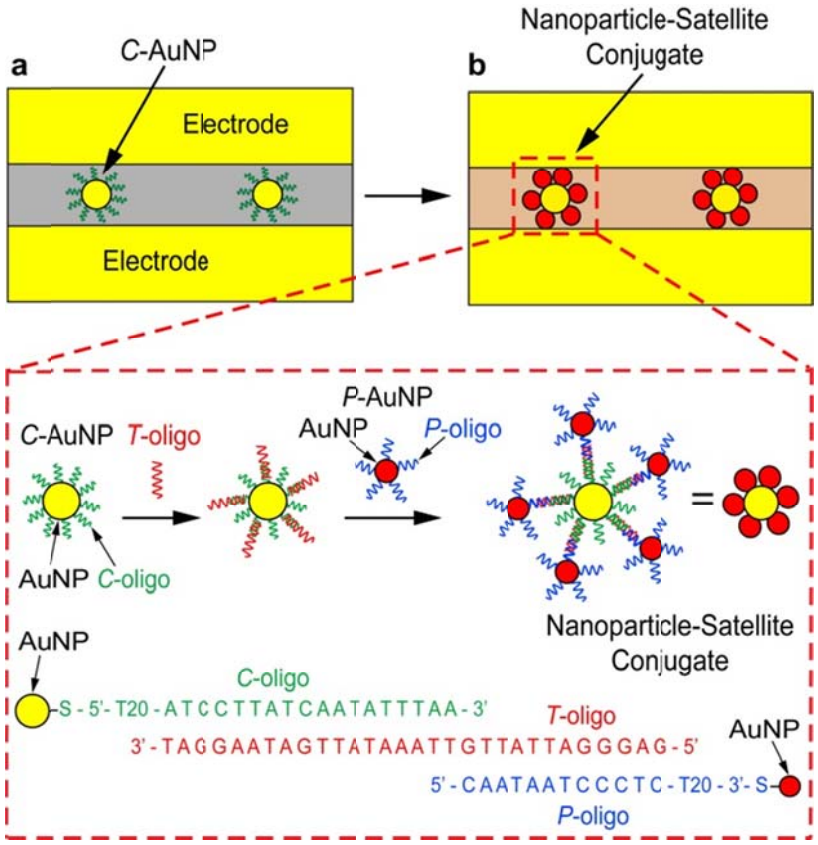

Figure 3-1 Schematic demonstration of amplification-free nanoparticle-bridge Oligonucleotide sensor. C-AuNPs placement between two electrodes (a). Formation of nanoparticle satellite conjugates (b).

3.2 Procedure of the Amplification-Free Nanoparticle-Bridge Oligonucleotide Sensor Fabrication

Procedure of the amplification-free nanoparticle-bridge Oligonucleotide sensor is shown in Figure 3-2. First, a ~100nm silicon dioxide layer is grown thermally on a (100) silicon wafer to function as an insulator. Using electron

beam lithography, deposition, and lift-off techniques, gold electrodes are made on the silicon dioxide substrate. Positively- and negatively-charged self-assembled monolayers (SAMs) are formed onto silicon dioxide and gold areas, respectively, using 3-aminopropyltriethoxysilane and 16-mercaptohexadecanoic acid. C-AuNPs are then placed between the gold electrodes via electrostatic funneling. Here, placing C-AuNPs at the center of the gap between two electrodes is very important to ensure that nanoparticle satellite conjugates can bridges two electrodes. After placement, positively-charged self-assembled monolayers are removed. APTES removal is essential to avoid loss of T-ssDNA. In other words, by removing APTES, T-DNA is just hybridized with C-DNA and is not lost onto silicon dioxide surface. By introducing T-ssDNA and then P-AuNPs solutions, nanoparticle satellite conjugates are formed through two hybridization reactions. Applying the voltage and measuring the current between two electrodes indicates that if T-ssDNA is present or not.

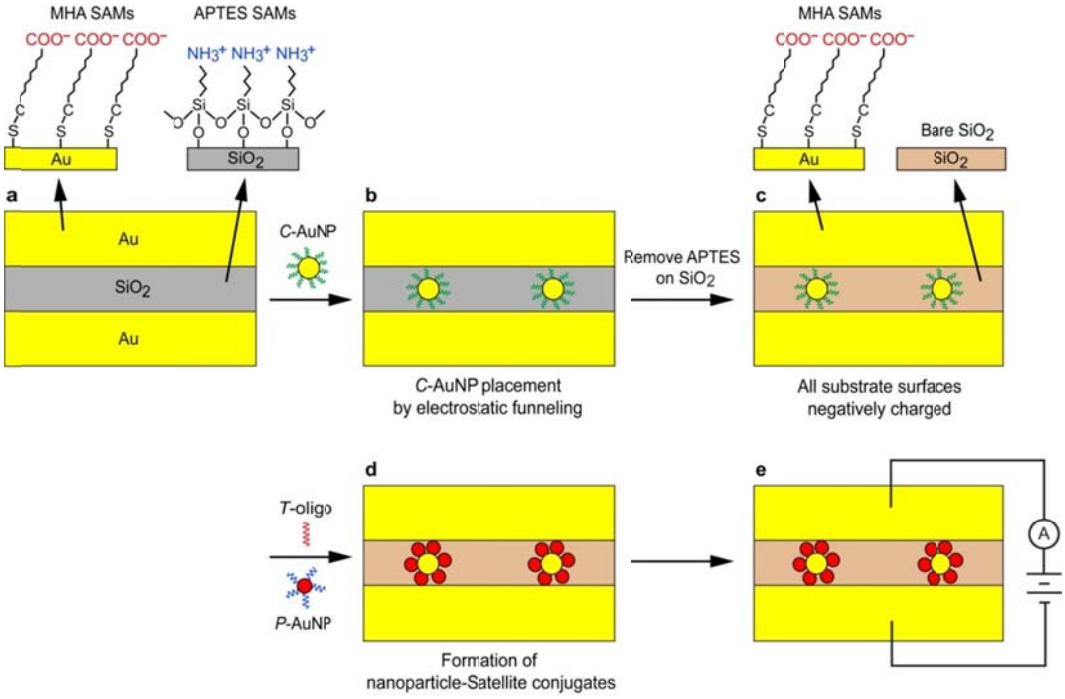

Figure 3-2 Schematic demonstration of nanoparticle-bridge Oligonucleotide sensor fabrication. Functionalization of SiO2 and Au surfaces with positively and negatively charged (SAMs), respectively (a). Placement of C-AuNPs onto the center locations of the electrode gap (b). Removal of APTES SAMs from SiO2 surface (c). Formation of nanoparticle-satellite conjugates (d). Producing an electrical sensor output by applying a voltage bias across the electrodes (e).

Chapter 4

Experimental Procedure

The procedure for fabrication of amplification-free nanoparticle-bridge oligonucleotide sensor was schematically illustrated in Figure 3-2. The main steps of fabrication are as following:

- Chip preparation
- Gold nanoparticle functionalization with single-strand DNAs (*AuNP-DNA*)
- Engineering of silicon dioxide and gold surfaces through the formation of Self-Assembled Monolayers (*SAMs*)
- Formation of nanoparticle satellite conjugates between two electrodes
- IV measurement and characterization

In this chapter, first background of experimental techniques which has been applied in our oligonucleotide detection method including immobilizing DNA strands onto gold nanoparticles, formation of Self-Assembled Monolayers (SAMs), and single particle placement via electrostatic funneling, is reviewed. Then, the materials, instrumentations, and procedures protocols utilized for fabrication of amplification-free nanoparticle-bridge oligonucleotide sensor are presented.

4.1 Background of DNA-Functionalized Gold Nanoparticles

By mixing alkanthiol-terminated oligonucleotides and gold nanopartilcles, oligonucleotides are immobilized onto gold nanoparticles surface through gold-thiol bond. In order to have a dense monolayer of oligonucleotides onto gold nanopartilcles surface, NaCl is added to the mixture to shield the charge repulsion between oligonucleotides.

The number of immobilized oligonucleotides onto gold nanoparticle surface depends on salt concentration [107, 108], gold nanoparticle size [107, 109], and Spacer (the region between the recognition sequence and the thiol modification site) Composition [110, 111].

4.1.1 Effect of salt on DNA surface loading

Loading density of the oligonucleotides increases with NaCl concentration which is mainly attributed to the screening effect of the concentrated counter-ions on the electrostatic repulsion force between the surface-bound oligonucleotide strands [107, 108] (Figure 4-1). Hurst et al. found that at high salt concentrations (between 0.7 and 1.0 M NaCl), maximum screening is achieved between neighboring oligonucleotides and loading remains relatively constant [107] (Figure 4-2).

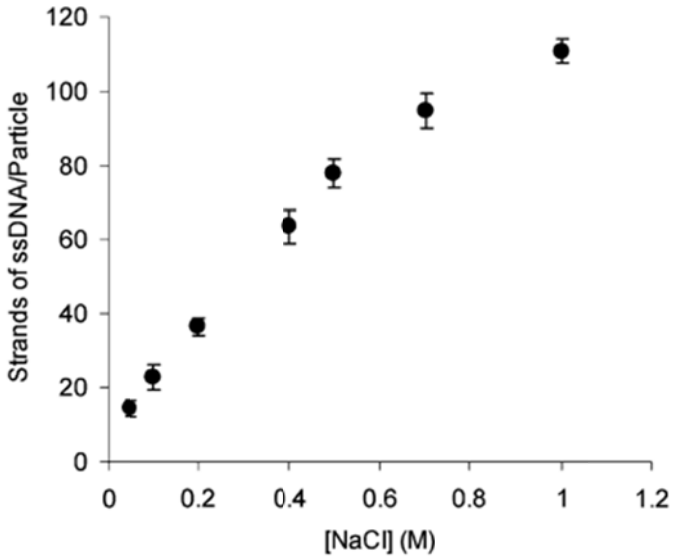

Figure 4-1 Surface density of the thiolated ssDNA on 13 nm gold nanoparticles as a function of NaCl concentration [108].

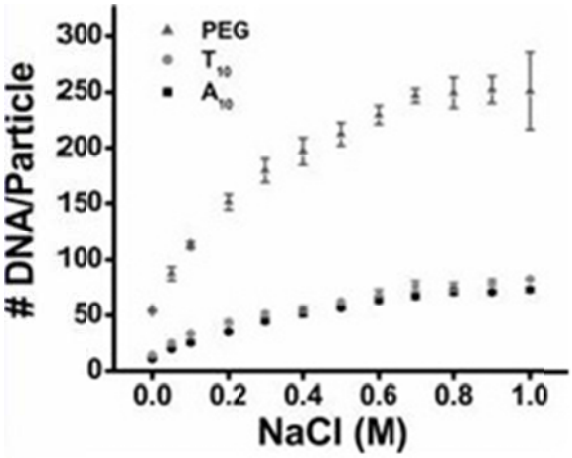

Figure 4-2 DNA loading vs NaCl concentration on 15-nm gold nanoparticles [107].

4.1.2 Effect of spacer type on DNA surface loading

Effect of spacer composition has also been investigated by researchers. The spacer role is to move recognition sequence further from the particle surface in order to reduce steric crowding of this region during hybridization. Poly-T, Poly-A, and PEG are three most common spacers.

Interactions between neighboring spacer regions and spacer region with gold determine the surface loading of gold nanoparticles. Poly-T and Poly-A spacers are composed of nucleobases and negatively-charged. Due to repulsion forces between strands and interaction tendency of nucleobases with gold surfaces, number of loaded DNA strands with nucleobase-containing spacers is less than that of with PEG-containing spacer (Figure 4-3).

It is known that the affinity of adenine nucleobase (A) with gold is stronger than thymine nucleobase (T) [111]. Oligonucleotides with poly-A spacer are more likely to lie on the gold surface and decrease surface density (Table 4-1). In other words, Poly-T spacer segments may orient perpendicular to gold nanoparticle surface promoting higher surface coverage [110].

Table 4-1 Comparison of surface coverage for A20 and T20 spacers [110].

Oligonucleotide	Surface coverage, pmol/cm^2
S3'A_{20}N12f	24±1
S3'T_{20}N12f	35±1

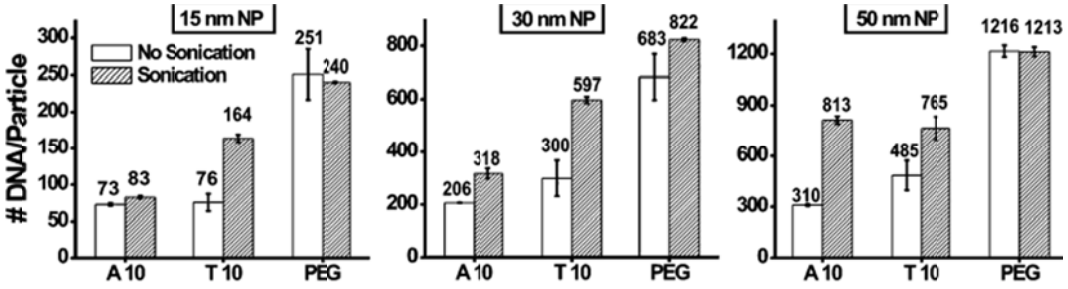

Figure 4-3 DNA loading values as a function of spacer for 15, 30, and 50-nm gold nanoparticles [107].

Table 4-2 Average values including standard deviations for particle sizes, absolute number of oligonucleotides per particle, surface Coverage, and effective footprint [109].

diameter (nm)	oligos/particle	coverage (oligos/cm^2)	footprint (nm^2)
10	68 ± 10	$2.0 \times 10^{13} \pm 2 \times 10^{12}$	4.9 ± 1
15	110 ± 10	$1.7 \times 10^{13} \pm 2 \times 10^{12}$	6.0 ± 1
20	180 ± 20	$1.4 \times 10^{13} \pm 1 \times 10^{12}$	7.0 ± 1
30	260 ± 10	$9.3 \times 10^{12} \pm 8 \times 10^{11}$	11 ± 1
40	430 ± 10	$8.5 \times 10^{12} \pm 4 \times 10^{11}$	12 ± 2
50	640 ± 80	$8.1 \times 10^{12} \pm 3 \times 10^{11}$	12 ± 1
60	890 ± 20	$7.8 \times 10^{12} \pm 1 \times 10^{12}$	13 ± 2
80	1400 ± 100	$7.1 \times 10^{12} \pm 9 \times 10^{11}$	14 ± 2
100	2200 ± 200	$7.1 \times 10^{12} \pm 4 \times 10^{11}$	14 ± 1
150	5100 ± 100	$7.1 \times 10^{12} \pm 2 \times 10^{11}$	14 ± 2
200	8500 ± 200	$6.8 \times 10^{12} \pm 1 \times 10^{12}$	15 ± 2
planar gold	N/A	$5.8 \times 10^{12} \pm 7 \times 10^{11}$	18 ± 2

4.1.3 Effect of gold nanoparticle size on DNA surface loading

Effect of gold nanoparticle size on surface loading has also been explored. It has been found that as the nanoparticle size increases, surface density decreases which is attributed to the decrease in the curvature of the nanoparticle [107, 109]. As a result, DNA strands stand closer to each other and inter-strand repulsion increases (Tables 4-2).

The influence of gold nanoparticle size on surface density is more significant for PEG-containing spacer compared to poly-T or poly-A-containing spacers (Table 4-3).

Table 4-3 Comparison of surface coverage of DNA on 15 to 250 nm gold nanoparticles for different spacers from [107].

NP, nm	A_{10} spacer, pmol/cm^2	T_{10} spacer, pmol/cm^2	PEG spacer, pmol/cm^2
15	19	38	56
30	19	35	48
50	17	19	26
80	19	20	27
150	15	18	19
250	14	16	21

4.1.4 Dissociation and degradation of thiolated DNA on gold nanoparticles

Stability of DNA-functionalized gold nanoparticles is important for practical applications since many assays may require a high ionic strength. Temperature is the most important factor in DNA dissociation kinetics. The rate of DNA dissociation increases drastically with temperature [112, 113] (Figure 4-4).

Bhatt et al. found that the cleavage of thiol-Au bond should be an endothermic process. They also attributed the deceased DNA dissociation at low salt to the decreased OH- concentration close to the gold surface [112]. Based on these studies, if long-term storage is required, low-temperature and low-salt conditions are essential.

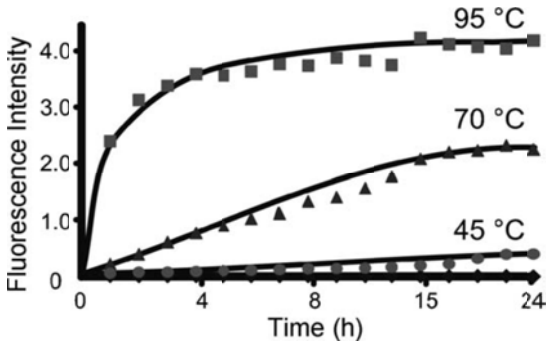

Figure 4-4 Curves showing fluorescence intensity at 520nm for Au-DNA conjugate samples heated at varying temperatures for 24h [113].

4.2 Background of Self-Assembled Monolayers (SAMs)

Self-Assembled Monolayers (SAMs) are organic highly ordered two-dimensional assemblies that form spontaneously onto a variety of surfaces by the adsorption of molecular constituents from solution or the gas phase. The molecules used to form SAMs have a head-group with a specific affinity for a surface. Aminosilanes on silicon/silicon oxide surfaces and sulfur-containing molecules on gold surfaces are two common adsorbate-substrate combinations [114-116].

4.2.1 Amino-terminated Self-Assembled Monolayers on Silicon Oxide Surface

Aminosilanes are widely used coupling agents for the modification of silicon surfaces. 3-Aminopropyltriethoxysilane (APTES) is one of the most commonly used aminosilanes to form amine-terminated SAMs on silicon surfaces. Chemical structure of APTES is shown in figure 4-5. APTES, due to its amino-terminal group, has been utilized in attachment of nanoparticles to silica substrates [117, 118] and biological applications such as DNA [119, 120] micro-arrays and protein [121] arrays.

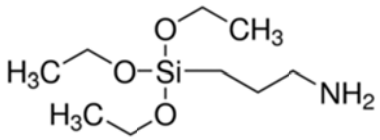

Figure 4-5 Chemical structure of APTES

Silanization is most common route for deposition of APTES onto OH-terminated silicon/silicon oxide surfaces. The SAMs formation is a multi-step process (figure 4-6). First, silane molecules are physisorbed at the hydrated silicon surface. Then, the Si(OC2H5)3 head-groups hydrolyzes into highly polar silanetriol Si(OH)3, in the presence of the water layer on the surface. At the end, these polar Si(OH)3 groups bonds covalently with the OH groups on substrate surface and silanol groups from neighboring molecules by creating a Si-O-Si network in the plane of the substrate [122-124].

The formation of APTES films on silicon surface is a complex process due to the presence of a reactive amino group in APTES and its inherent propensity to enter into competing reactions [125]. As a result of amino group presence, silane molecules can be incorporated into the layer through physiosorbtion, hydrogen-bonding, electrostatically reaction, covalently attachment to surface silanol groups or neighboring silane molecules in horizontal and/or vertical directions, and attachment to the surface in oligomeric form (Figure 4-7) [126, 127].

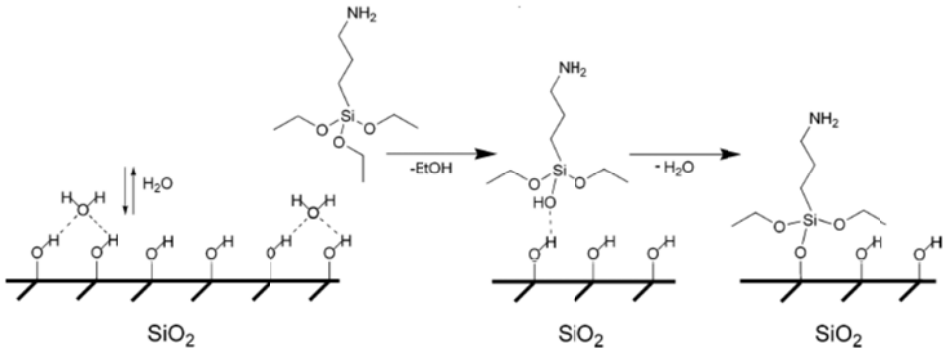

Figure 4-6 Schematic APTES hydrolysis followed by condensation [128].

Characterization of APTES films can be obtained by several techniques such as contact angle goniometry providing roughness of a SAMs, ellipsometry for the determination of the thickness, XPS for investigating the elemental composition of SAMs, FT-IR for identification of functional groups in SAMs, and AFM for measuring surface topology.

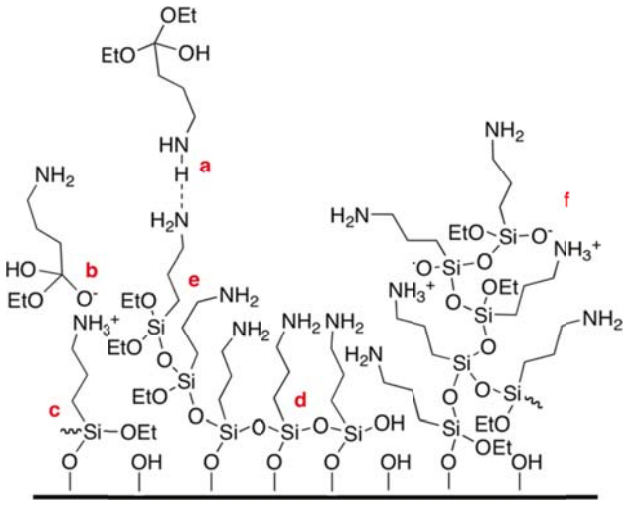

Figure 4-7 An APTES-derived layer with structural irregularities: individual silane molecules can be incorporated into the layer via (a) hydrogen bonding, (b) electrostatic attraction, (c) covalent bonding with the substrate, and (d) horizontal and (e) vertical polymerization with neighboring silanes; (f) oligomeric/polymeric silanes can also react/interact with functionalities present at the interface [126].

Several studies have been carried out to correlate nature and structure of APTES SAMs to reaction conditions such as solvent [129, 130], amount of water [131], reaction temperature and time [128], and silane concentration [128, 131]. Kim et al found that in an anhydrous toluene solution, APTES films grow by both covalent and noncovalent adsorption of APTES while in aqueous solutions APTES films grow by electrostatic interactions/or hydrogen bonding [130]. In general, APTES film thickness is mainly a function of time (figure 4-8). APTES concentration and reaction temperature influence surface roughness [128].

Zeta potential of amino-terminated SAMs was observed to switch from positive to negative values as the pH shifts from acidic to basic at the point of shift of around 7.5 (figure 4-9) which was believed to be because of the presence of a Stern layer formed by negatively charged counterions, overcompensating the positive surface charge. [132, 133] .

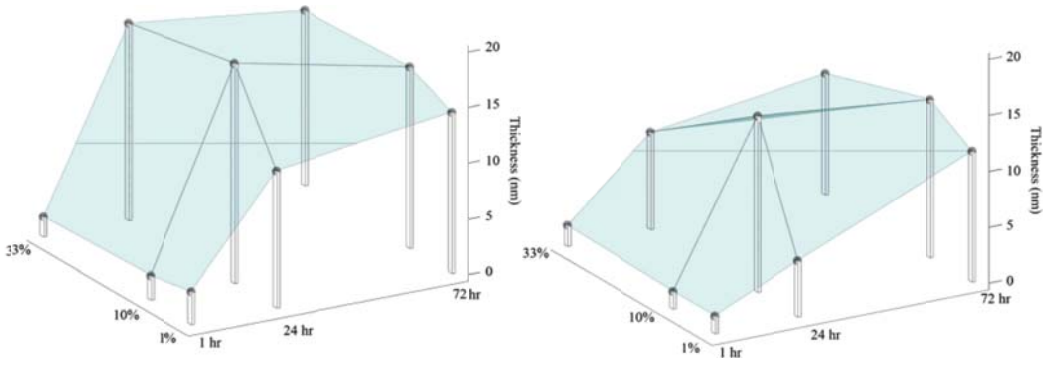

Figure 4-8 APTES film thickness as a function of temperature, (75C left, 25C right), time and APTES concentration [128].

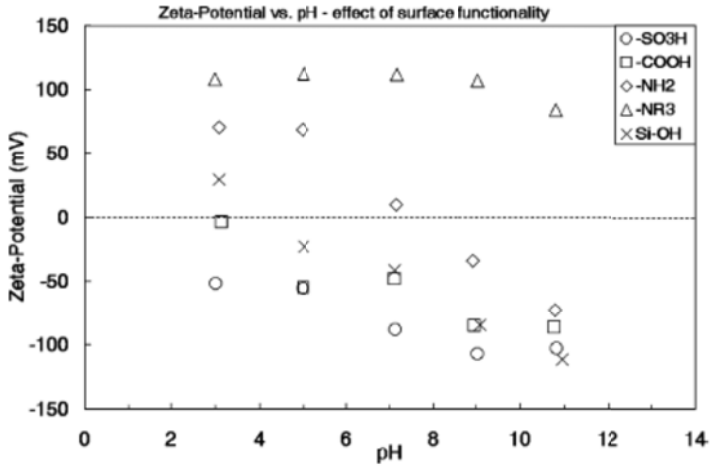

Figure 4-9 Zeta potentials of ionic SAMs [133]

4.2.2 Carboxyl-terminated Self-Assembled Monolayers on Gold Surface

SAMs formation of sulfur-containing alkanethiols on gold surface is a common technique to functionalize gold surface. After Nuzzo and Allara work [134] in which oriented monolayers formation by disulfide alkanethol on gold surface was shown, several studies have been done on characterization of SAMs on gold [135-137]. There are some factors that facilitate the adsorption of sulfur-contained thiols on gold as a monolayer system. First, gold is an inert metal and resistant to oxidation. The other factor is that gold has a strong affinity to sulfur. Also, long-chain alkanethiols form a densely-packed SAMs on gold surface.

Monolayers of organic compounds on gold surface can be formed in such a way that the carboxyl groups orient at the periphery of the monolayers (figure 4-10) [138-140] . Carboxyl-terminated SAMs constructed on metallic nanostructures add hydrophilic character to the surface [141].

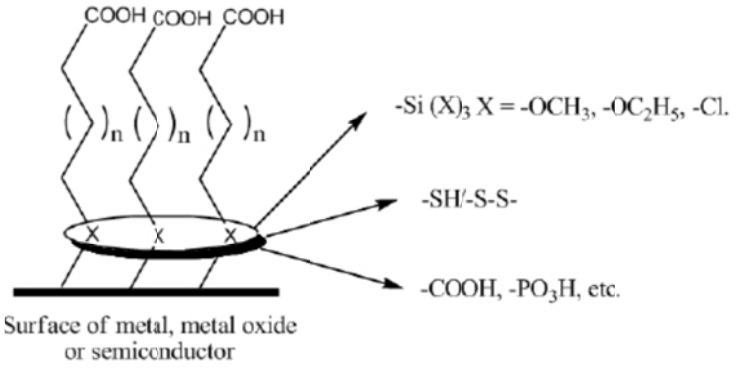

Figure 4-10 Schematic of carboxylic acid terminated SAMs [142].

Zeta potential of carboxyl-terminated SAMs is almost zero at pH around 3 but turns into negative values as pH increases [132, 133]. It was shown by Cheng et al. that carboxyl-terminated SAMs becomes 0%, 10%, 30%, 85%, and100% deprotonation at pH 3, 5, 7, 9, and 11, respectively (figure 4-11) [143].

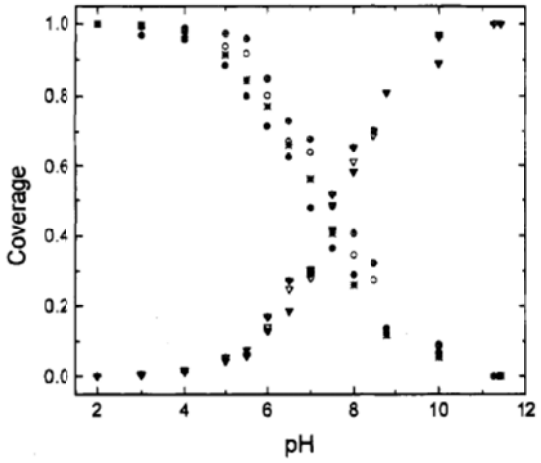

Figure 4-11 Plots of the surface coverages of carboxylic acid and carboxylate as a function of pH. Circles represent acid and triangles represent carboxylate anion [143]

4.3 Electrostatic Funneling

Electrostatic funneling is an approach for placement of charged nanoparticles onto specific locations on the surface. Figure 4-12 shows the concept of electrostatic funneling where interactions between nanoparticles and positively and negatively-charged areas of surface guide the placement of nanoparticles [144, 145]. The interaction between surface and charged nanoparticles occurs through double-layer.

Free ions in an aqueous solution can terminate electric field lines, and therefore can severely screen Coulomb interactions of charges. They also change the shape of the potential energy, making it go to zero exponentially beyond a characteristic distance called the Debye Length. In other words, the Debye length is the distance over which a charge is shielded by the ions in a solution. Debye length, which is usually denoted with K^{-1}, can be determined by

$$\frac{1}{\mathrm{K}} = \sqrt{\frac{\varepsilon_r \varepsilon_0 kT}{2e^2 N_A 1000 I_c}} \qquad (4\text{-}1)$$

Where ε_r is the dielectric constant of water; ε_0 is the permittivity of free space; k is the Boltzmann's constant; T is the absolute temperature; e is the electron charge; N_A is the Avogadro number; and I_c is the ionic strength of the electrolyte

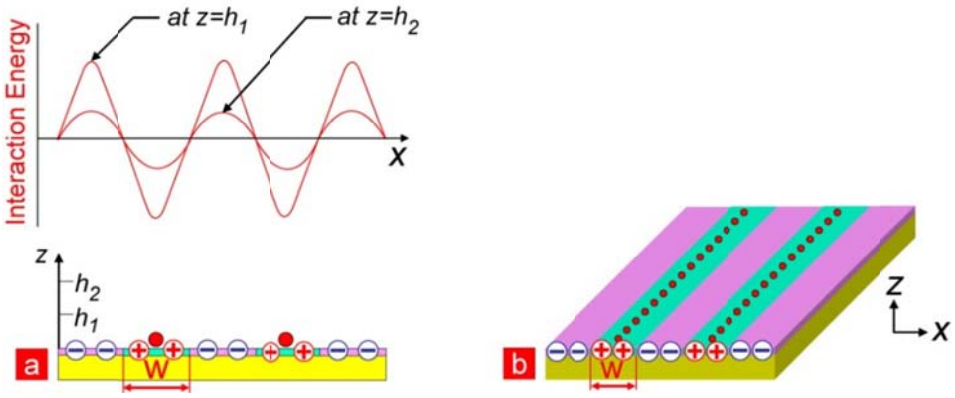

Figure 4-12 Wafer-scale nanoparticle placement with electrostatic funneling (a) A schematic of the electrostatic interaction energy in an aqueous solution for a negatively charged nanoparticle near a substrate surface functionalized with positively and negatively charged molecules. (b) The nanoparticles (red dots) are guided to the centers of positively charged lines (of width W) where the interaction energy is minimum [144].

4.4 Experimental Materials

4.4.1 Reagents

- Si wafer, test grade, p-type (100) (Nova electronic materials)
- E-beam photo resist ma-N 2401 (microchem)
- Photo resist developer ma-D 525 (microchem)
- 30-nm gold colloid (30-nm AuNP), Tannic surface (Nanocomposix) (Figure 4-13.a)
- 50-nm gold colloid (50-nm AuNP), Tannic surface (Nanocomposix) (Figure 4-13.b)
- Zonyl FSN-100, ((C2H4O)x(CF2)yC2H5FO) (Sigma-Aldrich)

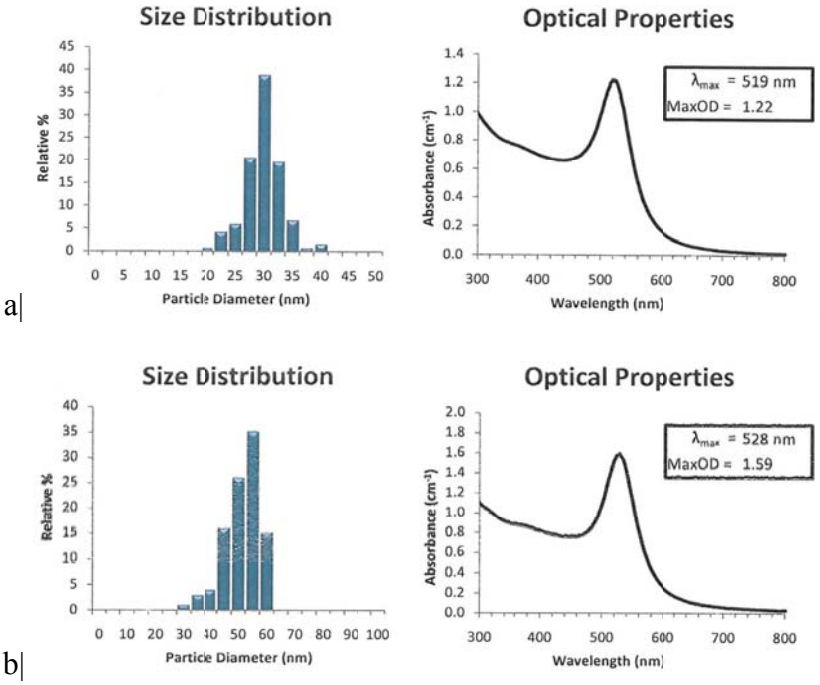

Figure 4-13 Properties of as-received (a) 30 and (b)50nm AuNPs

- Synthetic oligonucleotide probe-DNA (P-DNA) with disulfide linker (HPLC purified) (BioBasic) (Table 4-4)
- Synthetic oligonucleotide capture-DNA (C-DNA) with disulfide linker (HPLC purified) (BioBasic) (Table 4-4)
- Synthetic oligonucleotide target-DNA (T-DNA) (HPLC purified) (BioBasic) (Table 4-4)
- Synthetic oligonucleotide 1bp- mismatch target-DNA (T-DNA) (HPLC purified) (BioBasic) (Table 4-4)
- Synthetic oligonucleotide 3bp- mismatch target-DNA (T-DNA) (HPLC purified) (BioBasic) (Table 4-4)
- Synthetic oligonucleotide fluorescent marker-labeled probe-DNA with disulfide linker (HPLC purified) (BioBasic)
- Synthetic oligonucleotide fluorescent marker-labeled capture-DNA with disulfide linker (HPLC purified) (BioBasic)
- DTT (DL-Dithiothreitol), molecular biology grade ($HSCH_2CH(OH)CH(OH)CH_2SH$) (Sigma-Aldrich)
- NAP-5 column (GE Healthcare)
- Phosphate buffered saline, 10× concentrate, BioReagent (Sigma-Aldrich)
- Sodium chloride, ≥ 99.5% (NaCl) (Sigma-Aldrich)
- Sodium hydroxide (NaOH) (Sigma-Aldrich)

Table 4-4 Target, Capture, and Probe DNAs product information (all sequences are from 5' to 3')

T-DNA	Seq. : GAG GGA TTA TTG TTA AAT ATT GAT AAG GAT		
	Primer length: 30	Modification: None	Aggregate MW: 9363
	OD: 1	ug: 28.91	nmol: 3.09
C-DNA	Seq. : TTT TTT TTT TTT TTT TTT TTA TCC TTA TCA ATA TTT AA		
	Primer length: 38	Modification: 5' HS-SH C6	Aggregate MW: 11844
	OD: 1	ug: 34.02	nmol: 3.00
P-DNA	Seq. : CAA TAA TCC CTC TTT TTT TTT TTT TTT TT		
	Primer length: 32	Modification: 3' HS-SH C3	Aggregate MW: 9877
	OD: 4	ug: 142.48	nmol: 14.8
1bp mm T-DNA	Seq. : GAG GGA TTA TTG TTA AAT ATT CAT AAG GAT		
	Primer length: 30	Modification: None	Aggregate MW: 9323
	OD: 1	ug: 29.18	nmol: 3.13
3bp mm T-DNA	Seq. : GAG GGA TTA TTG TTA ACT ATT CAT AAC GAT		
	Primer length: 30	Modification: None	Aggregate MW: 9259
	OD: 1	ug: 30.00	nmol: 3.24

- Tris-EDTA buffer solution, molecular biology grade (NH2C(CH2OH)3+ C10H16N2O8+HCl) (Sigma-Aldrich)
- APTES (3-aminopropyltriethoxysilane) 99% (H2N(CH2)3Si(OC2H5)3) (Sigma-Aldrich)
- Sodium phosphate monobasic monohydrate, ≥ 98% (NaH_2PO_4.H2O) (Sigma-Aldrich)
- Sodium phosphate dibasic heptahydrate, ≥ 98% (Na_2HPO_4.7H2O) (Sigma-Aldrich)
- 16 MHDA (16-mercaptohexadecanoic acid) 90% (HS-(CH2)15-COOH) (Sigma-Aldrich)
- MHA (6-mercapto-1-hexanol) (Sigma-Aldrich)
- Hydrochloric acid (HCl)
- Denhardt's solution, molecular biology grade, lyophilized powder (50 mg Bovine Serum Albumin (BSA), 50 mg Polyvinylpyrrolidone (PVP), and 50 mg Ficoll) (Sigma-Aldrich)
- Triton X-100 solution, 10% in H2O, (Sigma-Aldrich)
- SSPE buffer, 20× concentrate, molecular biology grade (Sigma-Aldrich)
- DMSO (Dimethyl sulfoxide) ≥ 99.5% ((CH3)2SO)(Sigma-Aldrich)
- Acetone (C3H6O)
- Ethanol, 200 proof (C2H5OH)

4.4.2 Reagents Setup

- **Disulfide cleavage buffer** 200 mM phosphate buffer (pH = 8.0)
- **Exchange buffer** 10 mM phosphate buffer (pH = 7.5)
- **Salting buffer** 10× phosphate buffered saline + 3.46 M NaCl
- **Conjugate washing buffer** 10 mM phosphate buffer + 100 mM NaCl (pH = 7.5)
- **Storage buffer** Tris-EDTA buffer: 10 mM Tris-HCl, 1 mM disodium EDTA (pH = 8.0)
- **Hybridization buffer** 5× Denhardt's solution + 0.5% Triton X-100 + 6× SSPE + 10% DMSO + 45% water: 5 ml 50× Denhardt's, 2.5 ml 10% Triton X-100, 15 ml 20× SSPE, 5 ml DMSO , 22.5 ml DI water.
- **Hybridization washing buffer** 0.5% Triton X-100 + 6× SSPE + 10% DMSO + 55% water: 2.5 ml 10% Triton X-100, 15 ml 20× SSPE, 5 ml DMSO , 27.5 ml DI water.
- **Low Stringency wash buffer** 0.1% Triton X-100 + 2× SSPE + water: 100 µl 10% Triton X-100, 1000 µl 20× SSPE, 8900 µl DI water.
- **High Stringency wash buffer** 0.1% Triton X-100 + 0.5× SSPE + water: 100 µl 10% Triton X-100, 250 µl 20× SSPE, 8900 µl DI water.
- **Ultra-high Stringency wash buffer** 0.1% Triton X-100 + 0.1× SSPE + water: 100 µl 10% Triton X-100, 50 µl 20× SSPE, 8900 µl DI water.

4.5 Experimental Instruments

- Scanning electron microscope (SEM) equipped with e-beam writer, Zeiss 1540
- Atomic Force Microscopy (AFM), (AFM-DI-Dimension 5000)
- E-beam evaporator, AJA international
- Oxidation furnace, Tystar
- Electrical test, Agilent 4155C
- UV/VIS Spectrometer, PerkinElmer Lambda 35
- Fluorescence Spectrophotometer
- Nanodrop Spectrophotometer, NanoDrop 1000
- Centrifuge, Eppendorf 5418
- Cole-Parmer hot plate
- Ultra-sonicator
- UV-Ozone cleaner
- Tube rotator, Labquake
- pH meter, Oakton
- Millipore DI Water purification system

4.6 Experimental Procedure

4.6.1 Chip Preparation

The goal of this section is to make a comb structure pattern of 100 nm silicon dioxide trenches separated by gold. Here, three important issues should be paid attention. First, the negative e-beam resist is very sensitive to moisture, so the wafer should be heated at 200 °C for dehydration. Second, during evaporation of gold onto wafer, chromium is deposited first to act as an adhesive between silicon dioxide wafer and gold. Third, after final cleaning, chips should be immersed in ethanol to break the gold oxide layer formed during the cleaning. Gold oxide prohibits the proper formation of SAMs. Below, experimental steps for fabrication of chip are presented.

1| Clean (100) Si wafer (4” dia.) in acetone using ultrasonicator at room temperature for 15 min. Wash with methanol and then DI water thoroughly. Dry with N2.

2| Grow 100 nm dry SiO2 layer on Si wafer using oxidation furnace.

3| Cut SiO2 wafer into small SiO2 wafer pieces (1 cm × 1 cm).

4| Clean SiO2 wafer piece in acetone using ultrasonicator at room temperature for 15 min. Wash with methanol thoroughly. Dry with N2.

5| Dehydrate the SiO2 wafer piece at 200 °C for 20 min.

6| Spin coat the negative e-beam resist ma-N 2401 onto SiO2 wafer piece at 3000 rpm for 30 sec immediately after dehydration.

7| Pre-bake the SiO2 wafer piece at 90 °C for 1 min.

8| Expose the ebeam resist using e-beam writer with 200 $\mu C/cm^2$ dose.

9| Develop the SiO2 wafer piece using developer ma-D 525 for 10 sec (gently shaking). Wash with DI water gently for 5 min. Dry with N2.

10| Deposit 5 nm Cr + 15 nm Au onto SiO2 wafer piece using AJA e-beam evaporator.

11| Lift-off the photo resist using acetone in ultrasonicator for 30 min.

12| Clean the gold-coated SiO2 wafer piece by Acetone and UV-ozone cleaner at room temperature for 10 and 20 min, respectively. Repeat step 12 five times.

13| Cut the gold-coated SiO2 wafer piece into a small ~ 5×5 mm piece having comb-structure pattern (Chip).

14| Immerse the chip into 1.5 ml ethanol overnight (more than 10 hr) to break the gold oxide.

The schematic representation of e-beam lithography and image of the chip are shown in figures 4-14 and 4-15, respectively.

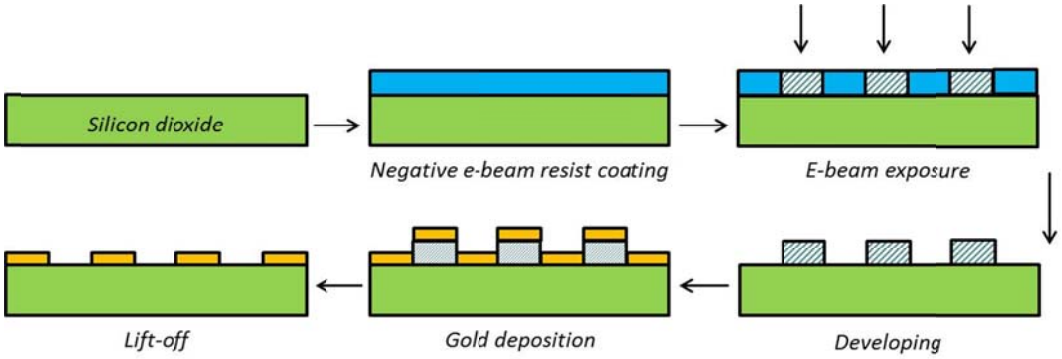

Figure 4-14 Schematic demonstration of e-beam lithography

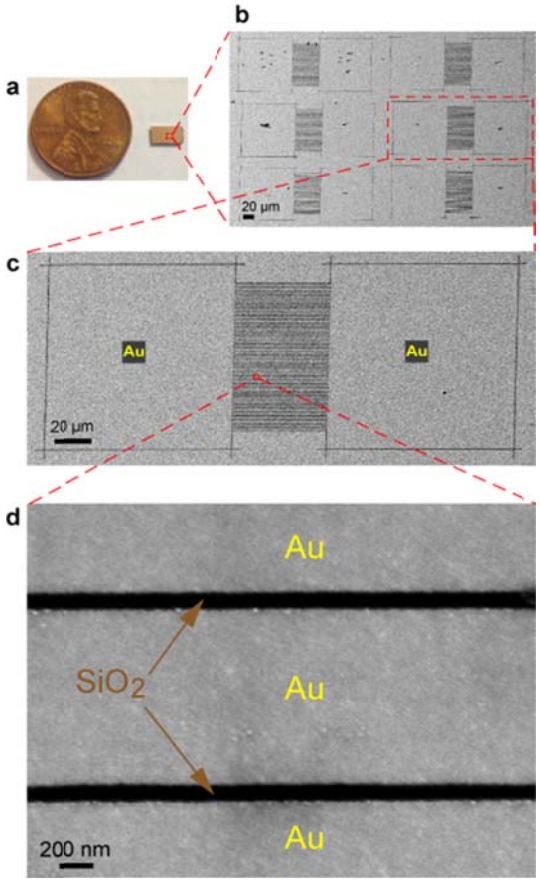

Figure 4-15 SEM images of the comb-structure patterns onto chip

4.6.2 Gold Nanoparticle Functionalization with Single-Strand DNAs (DNA-AuNP)

The goal of this section is to immobilize probe and capture DNAs onto 30 and 50 nm AuNPs, respectively. The DTT is used to cleave the disulfide functionality of as-received DNAs to turn them into thiolated single strands. The immobilizing of DNA single strands is occurred through the thiol-gold bond. The NaCl is added to the mixture of AuNPs and DNAs to shield the repulsion between DNA strands and increase the number of immobilized DNAs. The gold nanoparticles are first capped with surfactant FSN layer. The FSN layer stabilize gold nanoparticles in the presence of high salt concentration and also inhibits non-specific adsorption of nucleobases which leads to upright orientation of immobilized DNA strands [108]. Below, experimental steps for synthesis of DNA-AuNPs are presented.

4.6.2.1 30 nm AuNP functionalization with probe-DNA (P-AuNP)

15| Centrifuge 14.8 nmol probe-DNA (P-DNA) for 3 min at 3000 rpm.

16| Prepare 1 ml of 0.1 M DTT in disulfide cleavage buffer.

17| Add 125 µl of DTT solution to 14.8 nmol P-DNA tube, wrap the tube in aluminum foil and shake it for 2-3 h on rotating shaker.

Disulfide functionality of oligonucleotides is cleaved by DTT through the following reactions:

For 5’ Thiols: R–S–S–(CH2)6–Oligo + DTT → HS–(CH2)6–Oligo

For 3’ Thiols: Oligo–(CH2)3–S–S–(CH2)3–OH + DTT → Oligo–(CH2)3–SH

18| Allow the excess storage buffer to flow through the Nap-5 column. Equilibrate Nap-5 column with 15 ml of exchange buffer. Allow the buffer to enter the gel bed by gravity flow.

19| Load 125 µl P-DNA solution (step 17) onto Nap-5 column and allow entering the gel bed completely.

20| Add 375 µl of exchange buffer to Nap-5 column and allow entering the gel bed completely.

21| Elute purified P-DNA using 500 µl exchange buffer.

The schematic representation of NAP-5 instruction is shown in figure 4-16. purification of oligonucleotides is occurred through gel filtration process in which oligonucleotides are separated on the basis of size. Oligonucleotides move through a porous matrix. Larger oligonucleotides enter less into the pores or excluded from the matrix and thus elute first, while smaller oligonucleotides diffuse further into the pores and therefore move through the matrix more slowly and elute last.

22| 15 minutes before the end of P-DNA purification, pipette 950 µl 30-nm AuNP into a 2-ml microcentrifuge tube.

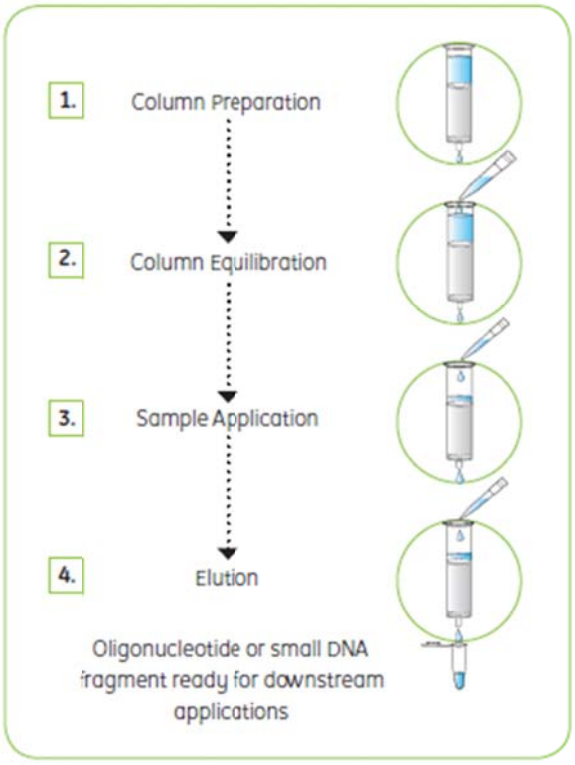

Figure 4-16 Schematic demonstration of NAP-5 instruction

23| Prepare 1 ml of 1 wt.% Zonyl FSN-100 in DI Water.

24| Add 50 µl of 1 wt.% Zonyl FSN-100 to 950 µl 30-nm Au-NP to stabilize Au-NP, vortex for 10 sec and let shake for 15 min.

25| Add 125 µl of purified P-DNA (step 21) to AuNP solution (step 24).

26| Add 111 µl of salting buffer to AuNP solution to obtain a final concentration of 0.45 M NaCl.

27| Vortex AuNP solution for 10 seconds, wrap in foil, and place on rotating shaker overnight.

28| Centrifuge DNA-functionalized gold nanoparticles (P-AuNP) for 10 min at 10,000 rpm; remove supernatant, and resuspend in 1 ml of conjugation washing buffer. Repeat step 15 four times.

29| Centrifuge DNA-functionalized gold nanoparticles (P-AuNP) for 10 min at 10,000 rpm; remove supernatant, resuspend in 1 ml of storage buffer, and store at 4 °C.

In the mixture of 30-nm AuNP and probe-DNA:

Concentration of NaCl is (5×111)/(950+50+125+111) = 0.45 M

Buffer strength is [((125×10) + (111×100)) / (950+50+125+111)] = 10mM

4.6.2.2 50-nm AuNP functionalization with capture-DNA (C-AuNP)

30| Perform steps 15-29 using 3.0 nmol capture-DNA (C-DNA) and 50-nm AuNP in lieu of probe-DNA (P-DNA) and 30-nm AuNP .

The schematic representation of gold nanoparticle functionalizing with DNAs is shown in figure 4-17.

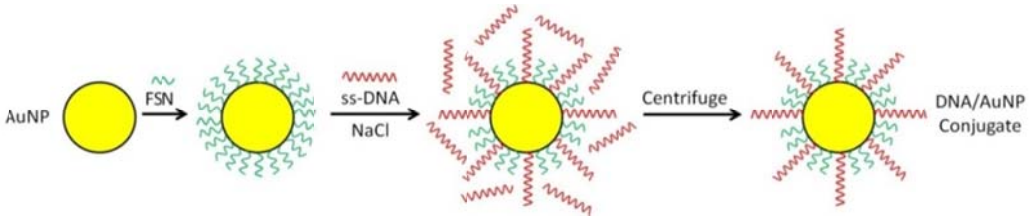

Figure 4-17 Schematic demonstration of gold nanoparticle functionalizing with DNAs

4.6.3 Quantification of oligonucleotides loaded onto gold nanoparticles

The goal of this section is to determine surface density of immobilized DNA strands onto gold nanoparticles. The importance of surface density is based on this factors that low surface density reduce stability of gold nanoparticles while working at high salt concentrations and on the other hand, high surface density reduce the hybridization efficiency. To determine the surface density, fluorescent-labeled probe and capture DNA are used. Synthesis of fluorescent DNA-AuNPs is carried in accordance with the procedure used for regular DNA. After synthesis, concentration of gold nanoparticles is measured through UV-Vis spectroscopy. To measure the concentration of fluorescent-labeled probe or capture DNA, mercaptohexanol (MCH) is used to displace the immobilized fluorescent-labeled DNA from the gold nanoparticle surface. After measuring the intensity of fluorescent-labeled DNA through fluorescent spectroscopy and interpolating that in standard calibration curve of known concentrations, the concentration of fluorescent-labeled capture or probe DNA is calculated. Knowing the concentrations of both gold nanoparticle and DNA, surface density is obtained. Below, experimental steps for determination of surface density is presented.

4.6.3.1 Quantification of loaded P-DNAs on 30-nm AuNPs

31| Perform steps 15-28 using 14.8 nmol fluorescent marker-labeled probe DNA (P*-DNA) in lieu of probe-DNA (P-DNA).

32| Take 200 µl of DNA-functionalized gold nanoparticles (P*-AuNP) to Nanodrop spectrophotometer to determine gold nanoparticle concentration via Beer's Law.

33| Add 400 µl 0.7M NaCl 10mM PB (pH 7.5) and 84.6 µl 2vol.% MCH in 0.3M NaCl 10mM PB (pH 7.5) to remaining 800 µl of DNA-functionalized gold nanoparticles (P*-AuNP). Shake the mixture for four hours to displace P*-DNA (figure 4-18).

In this mixture:

Final concentration of salt is 0.3 M

Final concentration of MCH is 10 mM

Final buffer strength is 10 mM

34| Centrifuge the solution of displaced P*-DNAs and 30-nm AuNPs for 10 min at 10,000 rpm. Take 200 µl from top portion of solution (Fig 4-18) to fluorescence spectrophotometer. Determine the concentration of P*-DNA using standard calibration line.

35| Ratio of P*-DNA concentration to AuNPs concentration determines the average number of loaded ss-DNA per AuNP.

4.6.3.2 Quantification of loaded C-DNAs on 50-nm AuNPs

36| Perform steps 31-35 using 3.0 nmol fluorescent marker-labeled capture DNA (C*-DNA) and 50-nm AuNPs in lieu of P*-DNA and 30-nm AuNPs.

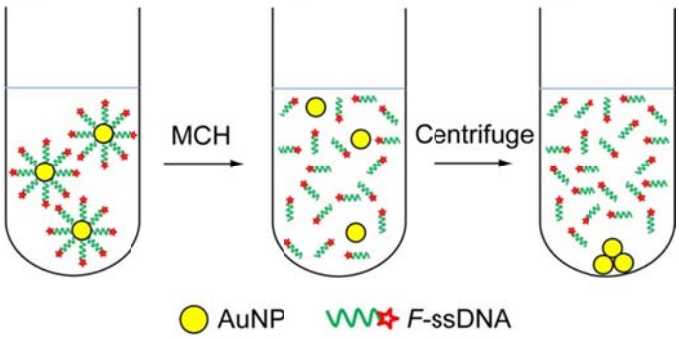

Figure 4-18 Schematic demonstration of fluorescent marker-labeled ss-DNA displacement from gold nanoparticles using MCH

4.6.4. Engineering of Silicon Dioxide and Gold Surfaces through the Formation of Self-Assembled Monolayers (SAMs)

Self-assembled monolayers are formed to guide C-AuNPs to center of the gap between two electrodes via electrostatic funneling. Positively-charged NH_3^+-terminated SAMs is formed onto silicon dioxide surface using APTES (3-aminopropyltriethoxysilane) and negatively-charged COO^--terminated SAMs is formed onto gold surface using 16-MHDA (16-mercaptohexadecanoic acid).

4.6.4.1. Formation of positively-charged SAM onto SiO2 surface

37| Prepare 500 µl of 0.5 vol.% APTES (3-aminopropyltriethoxysilane) in ethanol. Vortex for 10 sec.

38| Add 2 µl of 0.1 M NaOH in ethanol to APTES solution.

39| Immerse the chip into APTES solution at room temperature for 40 min.

40| Rinse the chip with ethanol thoroughly three times.

4.6.4.2. Formation of negatively-charged SAM onto Au surface

41| Prepare 500 µl of 10 mM 16-MHDA (16-mercaptohexadecanoic acid) in ethanol

42| Add 5 µl of HCl to 16-MHDA solution

43| Immerse the chip in 16-MHDA solution at room temperature for 2.5 h.

44| Rinse the chip with ethanol thoroughly three times. Dry with N2.

4.6.5. Formation of Nanoparticle Satellite Conjugates between two Electrodes

Nanoparticle satellite conjugates are formed via five main steps. First, C-AuNPs are accurately placed between two electrodes. Second, free amine-terminated SAM onto silicon dioxide surface is removed to avoid attachement and loss of target DNA. Third, target DNA is hybridized with capture DNA onto C-AuNPs. Fourth, stringency washing is carried out to de-hybridize mismatched target DNA from capture DNA in order to ensure that just complementary DNA is detected, and fifth, P-AuNPs are introduced for hybridization between target DNA and probe DNA. Below, experimental steps for formation of nanoparticle satellite conjugates is presented

4.6.5.1. Accurate placement of *C*-AuNPs between two electrodes onto the center of SiO2 surface

45| Place 10 µl of C-AuNP onto pattern area of the chip inside hybridization chamber Wait for 15 min.

46| Wash the chip with DI water.

4.6.5.2. Removing free APTES molecules from SiO2 surface

47| Immerse the chip into hybridization buffer at 42 °C for 2.5 h.

4.6.5.3. Hybridization of Target DNA (T-DNA) with C-DNA onto C-AuNP

48| Prepare 2 ml of T-DNA in hybridization buffer.

49| Immerse the chip into T-DNA solution at room temperature for 3, 20, 68, 96 h for 5nM, 50 pM, 500 fM, and 50 fM T-DNA, respectively. Shake gently using orbital shaker.

50| Wash the chip with hybridization washing buffer three times to remove all unhybridized T-DNA.

4.6.5.4. Stringency washing

51| Immerse the chip into low stringency wash buffer at room temperature for 10 min.

52| Immerse the chip into high stringency wash buffer at room temperature for 10 min.

53| Immerse the chip into ultra-high stringency wash buffer at room temperature for 10 min.

4.6.5.5. Pre-hybridization of P-DNA of P-AuNP with T-DNA onto C-AuNP

54| Immerse the chip into 250 µl of hybridization buffer at room temperature for 10 min.

4.6.5.6. Hybridization of P-DNA of P-AuNP with T-DNA onto C-AuNP

55| Centrifuge 150 µl of P-AuNP at 10,000 rpm for 10 min. Remove supernatant and resuspend in hybridization buffer.

56| Immerse the chip into P-AuNP solution at room temperature for 4 h. Wash with DI water and dry with N2.

4.6.6. I-V measurement and SEM characterization

57| Get I-V measurements and do SEM to investigate the formation of nanoparticle satellite conjugates and sensitivity of the sensor.

Chapter 5

Results and Discussion

5.1 Characterization and Quantitative Analysis of Oligonucleotide-Functionalized Gold Nanoparticles

Figures 5-1 and 5-2 show the UV-vis spectra of non- and DNA-functionalized 30 and 50 nm gold nanoparticles, respectively. After functionalization, only a small shift in the surface plasmon band from 519 to 523 nm and 527 to 530nm was observed for 30 and 50-nm gold nanoparticles, respectively. The decrease in intensity of the plasmon band is due to a decrease in particle concentration during synthesis of the oligonucleotide-functionalized gold nanoparticles. Surface modification is not necessarily the cause of plasmon absorption wavelength shift; centrifugation of the Oligonucleotide - functionalized particles may affect the particle size distribution and consequently the position of the plasmon band [146]. In addition, Oligonucleotide - functionalized nanoparticles electrolyte could affect the plasmon band due to charge screening effects and a change in the dielectric constant of the medium [147]. Plasmon absorption wavelength shift is the main characterization tool which is monitored in most of biosensors which are utilizing surface plasmon resonance of gold nanoparticles [148-151].

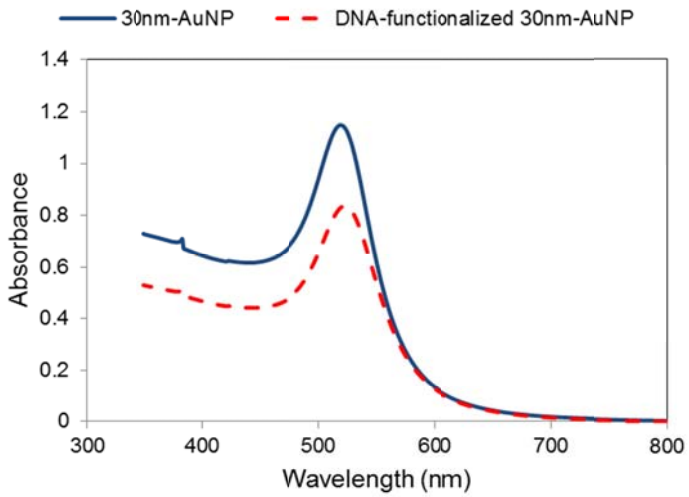

Figure 5-1 UV-vis spectra of non- and Oligonucleotide -functionalized 30-nm gold nanoparticles

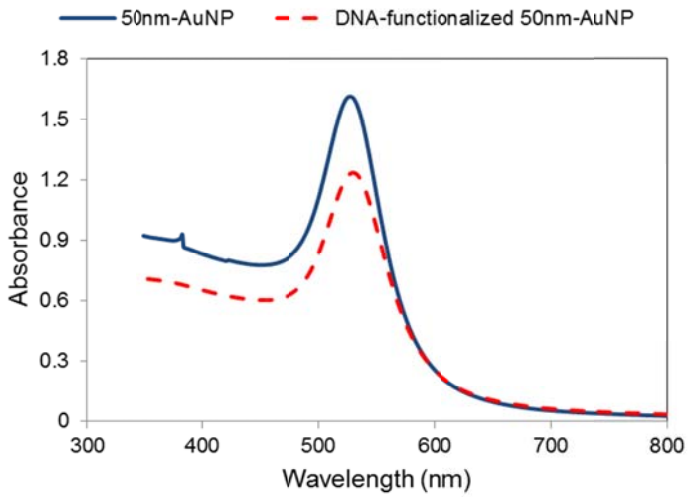

Figure 5-2 UV-vis spectra of non- and Oligonucleotide-functionalized 50-nm gold nanoparticles

Assuming the gold nanoparticle's extinction coefficient for oligonucleotide-functionalized gold nanoparticle which are 3.585×10^{9} and 1.935×10^{10} $M^{-1}cm^{-1}$ for 30 and 50nm AuNP, respectively, concentration of P-AuNP and C-AuNP was calculated to be 1.46×10^{11} and 3.44×10^{10} particles/ml, respectively. The concentration of fluorescent marker-labeled P-DNA and C-DNA was obtained from calibration line of known concentrations. Measuring the fluorescence intensity of fluorescent marker-labeled P-DNA and C-DNA using fluorescence Spectrophotometer and having a standard linear calibration curve from known concentrations of fluorescent marker-labeled P-DNA and C-DNA (figure 5-3), the concentration of P-DNA and C-DNA was calculated to be 57.3 and 39.7 nM, respectively, using 0.45M salt concentration and 49.6 and 29.2 nM using 0.25M salt concentration.

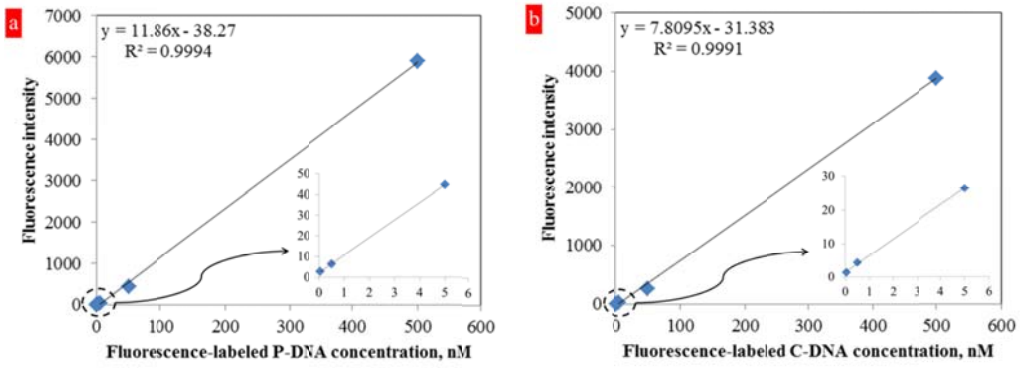

Figure 5-3 Standard linear calibration curves for fluorescence-labeled P-DNA (a) and C-DNA (b)

Oligonucleotide loading of the single-stranded thiolated capture and probe Oligonucleotide on 50-nm AuNPs (C-AuNP) and 30-nm AuNPs (P-AuNP), respectively, as a function of salt concentration is shown in figure 5-4. As seen, increase of Nacl concentration leads to higher immobilized DNA on gold nanoparticle which is due to screening effect of the counter-ions [108]. It should be noted that the oligonucleotide immobilization onto gold nanoparticles is obtained through covalent binding of thiol and gold.

To have oligonucleotide-functionalized gold nanoparticles that can be utilized in detection of bio-molecules, surface coverage and hybridization efficiency should be in a good balance. There is a minimum required number of immobilized oligonucleotide to stabilize gold nanoparticles. On the other hand, number of immobilized oligonucleotide should not be too high not to be capable of hybridization.

Oligonucleotide surface coverage increases with salt concentration due to reduced electrostatic repulsion between the negatively charged oligonucleotide strands. Spacer segments, here T20, also helps to reduce electrostatic and steric interactions between immobilized oligonucleotides and incoming complementary bio-molecules.

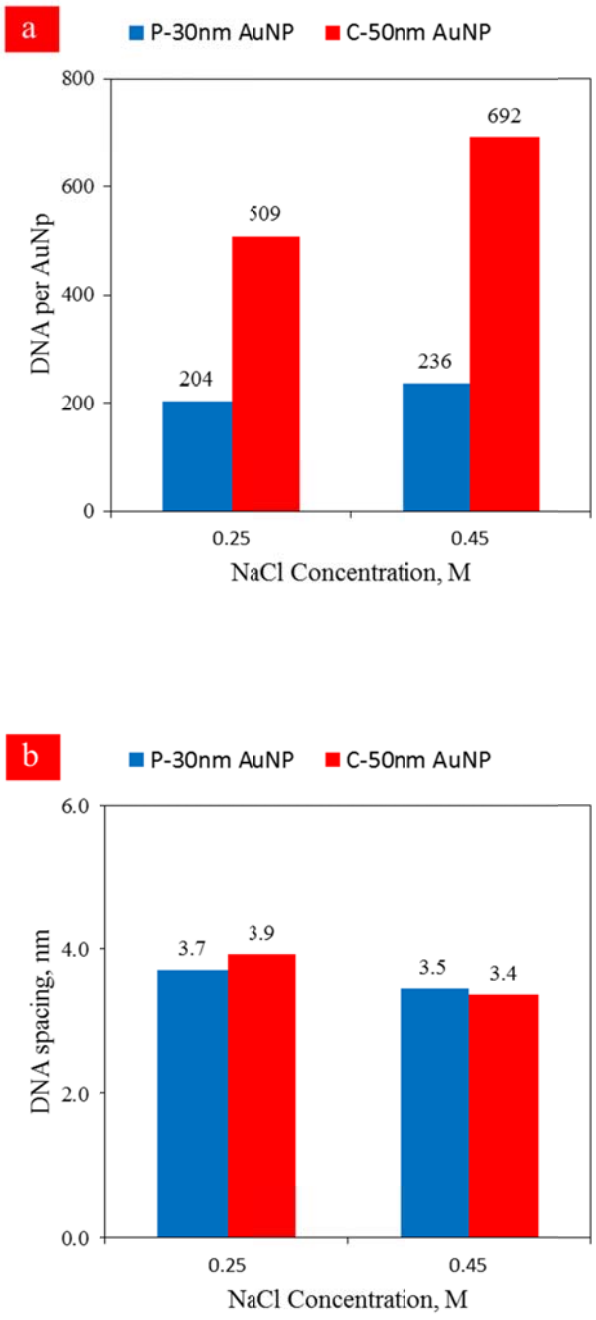

Figure 5-4 Number of DNA per gold nanoparticle (a) and immobilized DNA spacing (b) for P-AuNP and C-AuNP.

5.2 Formation of Self-Assembled Monolayers onto Silicon Dioxide and Gold Surfaces

Figure 5-5 shows the attachment of oligonucleotide-functionalized 30-nm AuNPs after formation of Self-Assembled Monolayers (SAMs). Oligonucleotide -AuNPs are suspended in 1mM PB at pH 7.5. As seen, oligonucleotide -AuNPs are only attached to positively-charged silicon dioxide surface and are repelled from the negatively-charged gold surface. This selectivity exhibits the proper formation of amino- and carboxyl-terminated SAMs onto silicon dioxide and gold surfaces, with positive and negative surface charge, respectively, which is similar to the observations of other groups [133].

Precise placement of oligonucleotide -AuNPs onto silicon dioxide area was investigated using a silicon dioxide substrate patterned with gold through electron-beam lithography (Figure 5-6). After placement of primary oligonucleotide -AuNPs via electrostatic funneling, secondary oligonucleotide -AuNPs are not able to attach to surface inside the holes due to repulsion between gold surface and oligonucleotide -AuNPs and between oligonucleotide -AuNPs themselves [145].

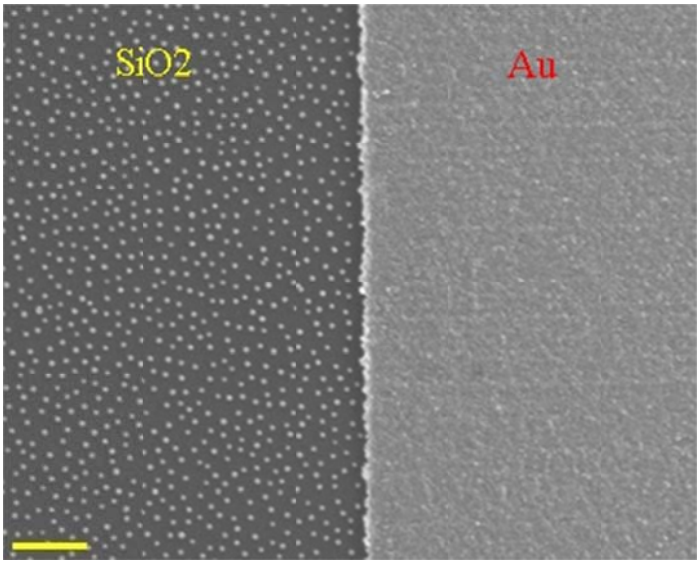

Figure 5-5 Oligonucleotide-functionalized 30nm AuNPs attachment on SiO_2 (dark) and Au (bright) surfaces (scale bar: 500nm)

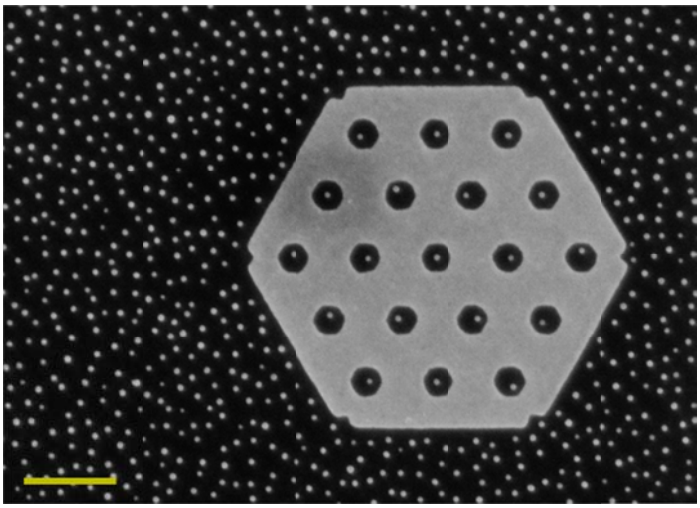

Figure 5-6 Singe particle placement of oligonucleotide-functionalized 30nm AuNPs (bright and dark areas are Au and SiO_2 surfaces; scale bar: 500nm)

5.3 Placement of C-AuNPs between Two Gold Electrodes

C-AuNPS are placed at the center of the gap between two electrodes through electrostatic funneling. The positively and negatively-charged SMAs push the negatively-charged C-AuNPs toward the center of the gap. The electrostatic interaction between C-AuNPs and surfaces of gold and silicon dioxide are the dominant mechanism of the placement [144].

SEM image of three placed C-AuNPs between two electrodes is shown in figure 5-7. Measuring the deviation of the C-AuNPs location from the center of the gap for hundred C-AuNPs shows that C-AuNPs were placed onto the gap with high precision (figure 5-8).

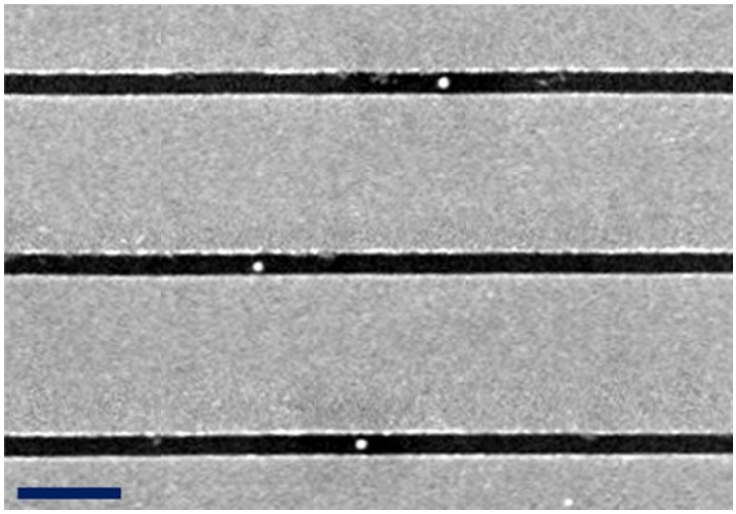

Figure 5-7 SEM images of three C-AuNPs placed onto gap between two electrodes (scale bar: 500nm)

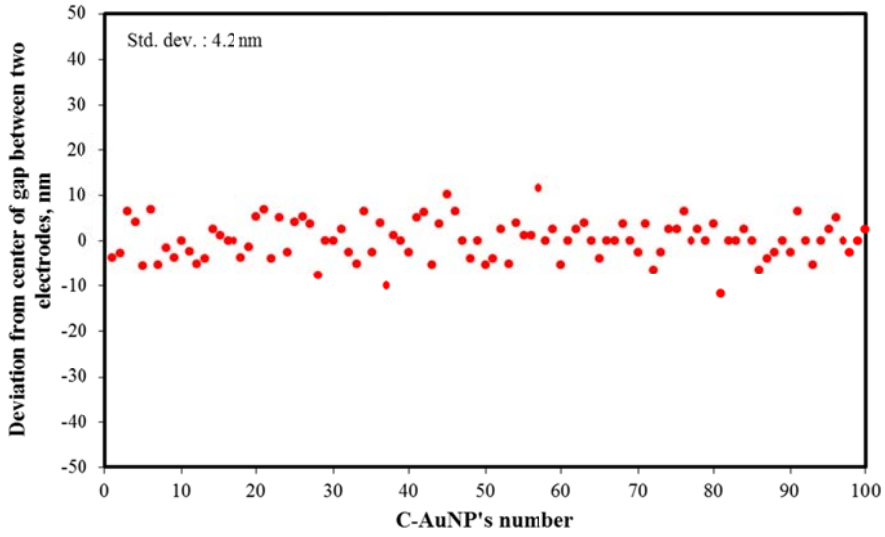

Figure 5-8 Deviation of C-AuNPs location from center of the gap between two electrodes for 100 C-AuNPs

Debye length for the C-AuNPs in 1mM PB at pH 7.50 can be calculated using equation 4-1. By inserting 0.001 $mol.m^{-3}$ for the ionic strength of the electrolyte (I_c), 8.85×10^{-12} $m^{-3}.kg^{-1}.s^{4}.A^{2}$ for the permittivity of free space (ε_0), 80.4 for the dielectric constant of water (ε_r), 1.38×10^{-23} $m^{2}.kg.s^{-2}.K^{-1}$ for the Boltzmann's constant (k), 298 K for the absolute temperature (T), 6.02×10^{23} mol^{-1} for the Avogadro number (N_A), and 1.6×10^{-19} coulomb for the electron charge (e), Debye length is calculated to be ~10 nM. This 10nm Debye length is not too short to leads to the attachment of C-AuNPs to walls and is not too long to hinder the attachment of C-AuNPs on the gap.

Number of placed C-AuNPs for each device of substrate is around 100-1000 particles. This number depends on concentration of C-AuNPs in buffer, pH and ion concentration of buffer, and placement duration. It should also be noted that pre-hybridization at 42 °C for 2.5 hour removes part of placed C-AuNPs from the surface in addition to amino-terminated SAMs.

The effect of buffer's ion concentration on Debye length and attachment of DNA-AuNPs can be seen in figure 5-9. Attachment of DNA-AuNPs on silicon dioxide increases with ion concentration due to reduced Debye length (equation 4-1) and repulsion between DNA-AuNPs (figure 5-12a and c). Comparing figures 5-12b and d show how increasing buffer's ion concentration from 1 to 10mM leads to less Debye length which leads to more than one DNA-AuNP attachment inside the holes.

The effect of buffer's pH on Debye length and attachment of DNA-AuNPs can be seen in figure 5-10. Attachment of DNA-AuNPs on silicon dioxide increases with decrease in buffer's pH. Amine-terminated SAM onto silicon dioxide layer exhibits more protonation at pH 6.0 than pH 7.0 which causes more attraction between silicon dioxide surface and DNA-AuNPs. Also, carboxyl-terminated SAM exhibits more deprotonation at higher pH which causes more repulsion between gold surface and DNA-AuNPs. These two phenomena lead to more attachment of DNA-AuNPs onto silicon dioxide surface and more than one DNA-AuNP attachment inside holes at lower pH.

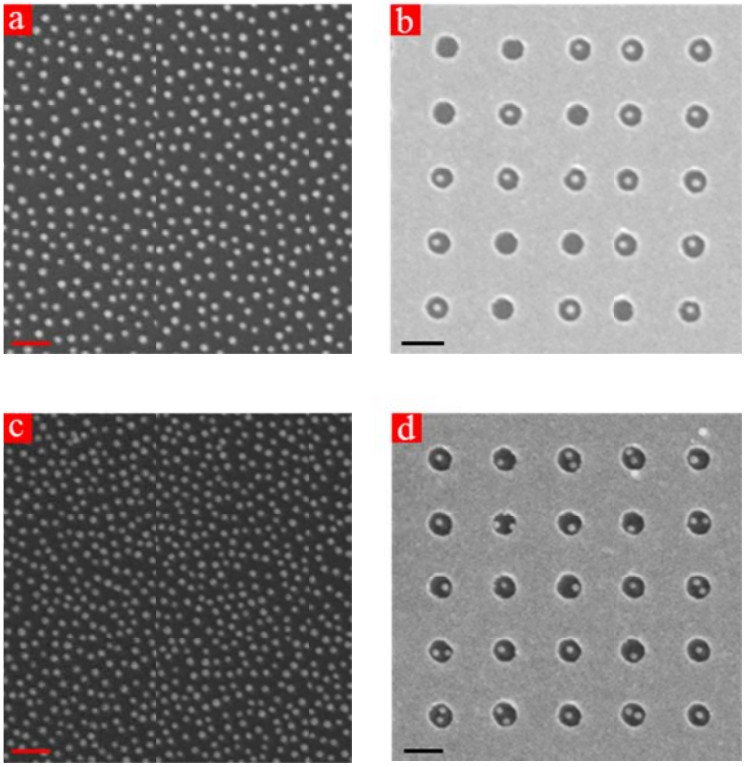

Figure 5-9 Effect of ion concentration on attachment of DNA-AuNPs at 1 mM PB pH 7.25 (a&b) and 10 mM PB pH 7.25 (c&d) (scale bars: 200nm)

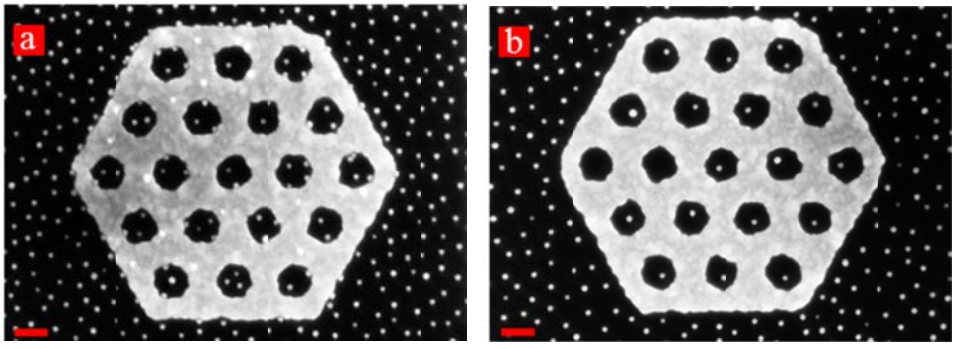

Figure 5-10 Effect of pH on attachment of DNA-AuNPs at 1 mM PB pH 6.0 (a) and 1 mM PB pH 7.0 (b) (scale bars: 200nm)

5.4 Formation of Nanoparticle Satellite Conjugates onto Silicon Dioxide Surface

Formation of nanoparticle satellite conjugates was first examined onto bare silicon dioxide surface. Figures 5-11 and 5-12 show SEM images of formed nanoparticle satellite conjugates for complementary and 1-bsae pair mismatched T-DNA at 5nM, 50 fM, and 100 aM concentrations. SEM images show that at high concentrations, central C-AuNPs are fully surrounded by P-AuNPs as a result of presence of sufficient T-DNA nearby and two hybridization reactions between first C-DNA and T-DNA and then T-DNA and P-DNA. At low concentration of 50 fM, central C-AuNPs are hybridized with average two P-AuNPs due to less availability of T-DNA. The lowest concentration of detected T-DNA on bare silicon dioxide was 100 aM. Most of the C-AuNPs were surrounded by zero or one P-AuNP.

Comparing SEM images of nanoparticle satellite conjugates for complementary and mismatched T-DNA shows that stringency washing was carried out successfully to differentiate complementary from mismatched T-DNA. High specificity is due to the sharp melting transitions of double stranded oligonucleotides formed between T-DNA and C-DNA-functionalized gold nanoparticles. Here, thermal stringency is not needed because of the salt dependency of hybridized C-AuNP and T-DNA.

Another accomplishment that should be noticed is that there is no attachment of P-AuNPs onto silicon dioxide surface which is due to APTES removal step after C-AuNPs placement.

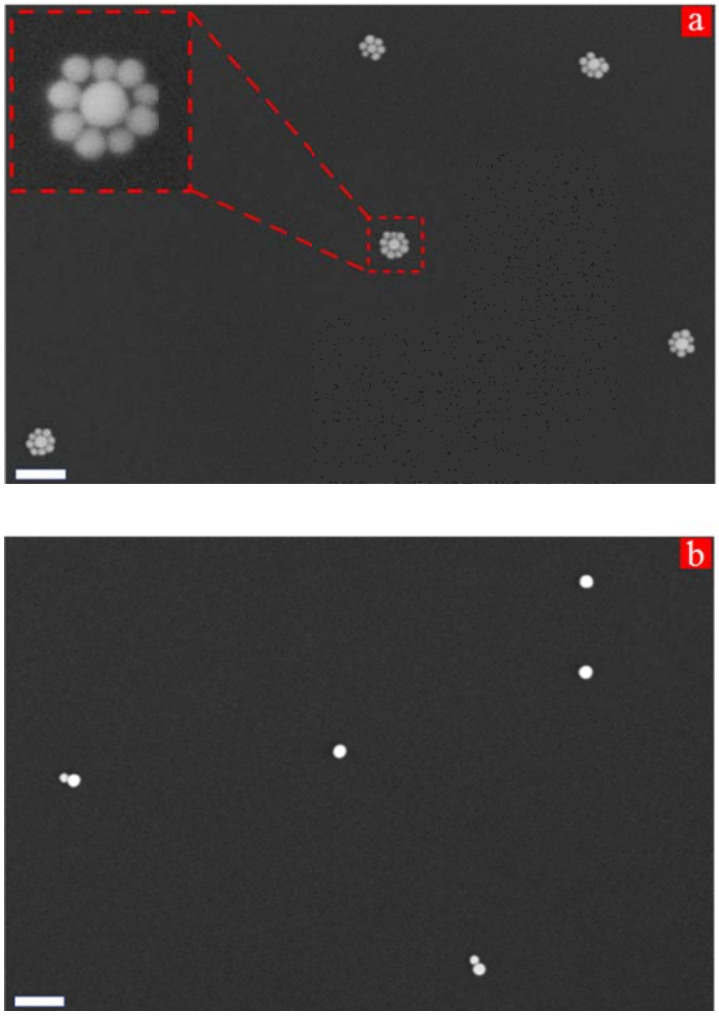

Figure 5-11 Formation of nanoparticle satellite conjugates onto silicon dioxide surface for 5 nM complementary (a) and 1-base pair mismatched (b) T-DNA (scale bars: 200nm)

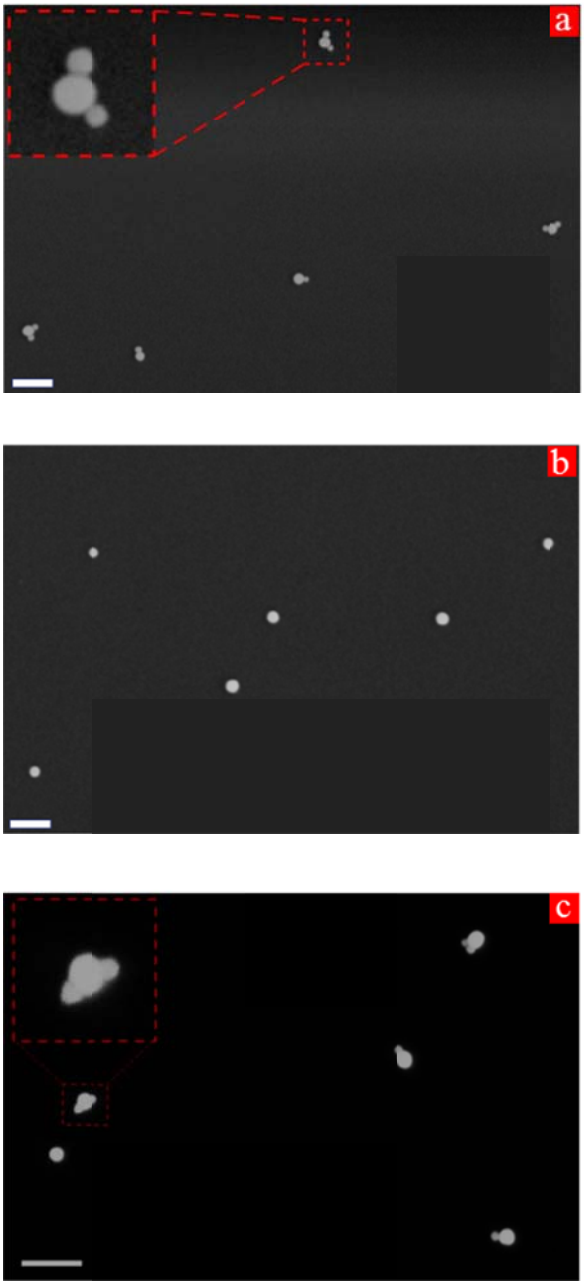

Figure 5-12 Formation of nanoparticle satellite conjugates onto silicon dioxide surface for 50 fM complementary (a) 50 fM 1-base pair mismatched (b), and 100 aM complementary (c) T-DNA (scale bars: 200nm)

5.5 Analysis of DNA Detection Using Amplification-Free Nanoparticle-Bridge DNA Sensor

5.5.1 SEM characterization

Figures 5-13 to 5-17 show SEM images of four nanoparticle satellite conjugates and statistical analysis of one device from each chip at 5nM, 50 pM, 500fM, 50 fM complementary T-DNA and 5nM 1-bp mismatched T-DNA, respectively. The number of the nanoparticle satellites (P-AuNPs) around each C-AuNP was counted using SEM to evaluate the statistics of nanoparticle satellite conjugates. The average number of nanoparticle satellites (P-AuNPs) per C-AuNP decreased with deceasing T-DNA. This value was 5.1±0.80, 3.9±0.60, 2.4±0.36, 0.7±0.16, and 0.5±0.15 for 5 nM, 50 pM, 500 fM, 50 fM complementary T-DNA, and 5 nM 1-bp mismatched DNA, respectively.

The hybridization time between C-DNA and T-DNA was 3, 20, 68, and 96 hours for 5 nM, 50 pM, 500 fM, and 50 fM complementary T-DNA. The hybridization time should be high enough to allow T-DNA strands reach C-AuNPs because migration of T-DNA in this detection method is just through passive thermal diffusion.

In our assay, hybridization between target oligonucleotide and capture oligonucleotide is controlled by diffusion of target oligonucleotide. That is a reason why detection at low concentrations of target oligonucleotide takes long time.

Passive hybridization, in which no external force is involved, is limited by diffusion. Because diffusion coefficients of nucleic acids in aqueous solutions are about 10^{-7} cm^2 s^{-1}, the travelling time of nucleic acid is about 1mm in 24 hours [152]. Although in some hybridization stations convection motion is used to enhance hybridization, the effect is not significant. Even if hybridization is carried out for two days, small number of target oligonucleotides can react with capture oligonucleotides. The corresponding diffusion length, $l = \sqrt{Dt}$, is 1.3 mm for two days hybridization. Since capture oligonucleotides hybridize with nearby target oligonucleotides, most of the target oligonucleotides which are outside the diffusion length are wasted and not involved in detection.

The hybridization of target DNA with capture DNA on chip-based detection methods is considered to be based on a two-step mechanism. First, target DNA is adsorbed non-specifically on the surface and then diffuses along the surface towards the hybridization site. Since in our detection method, there is no adsorption of target to the surface, hybridization is controlled by diffusion of target oligonucleotide towards hybridization sites. Transportation of the target DNA in the solution is in accordance with convection diffusion equation which depends on concentration of target DNA, time, velocity, and diffusion coefficient. It was reported that rate-limiting step in passive hybridization is surface diffusion of target DNA [153].

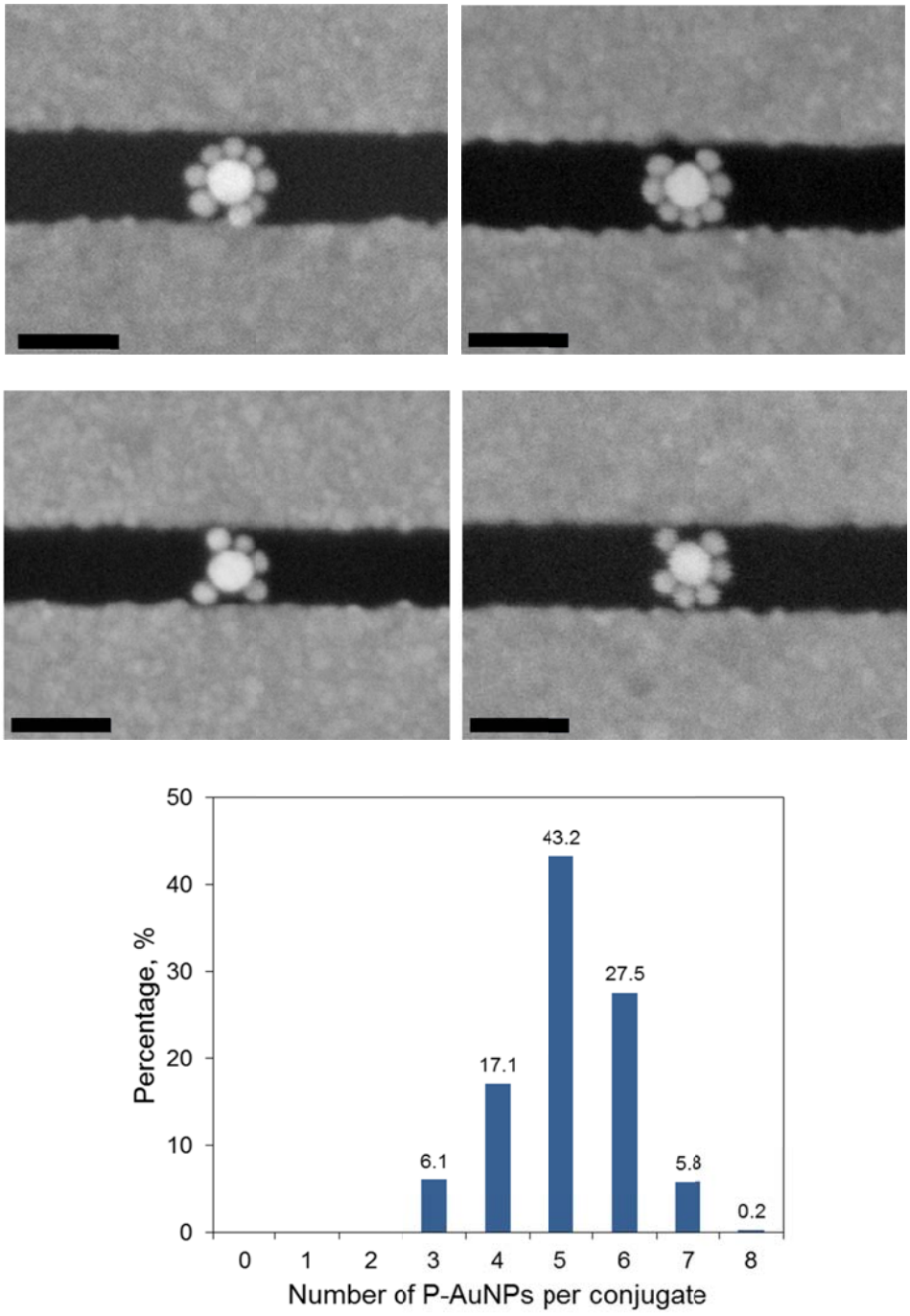

Figure 5-13 SEM images and statistical analysis of nanoparticle satellite conjugates at 5 nM T-DNA (scale bars: 100nm)

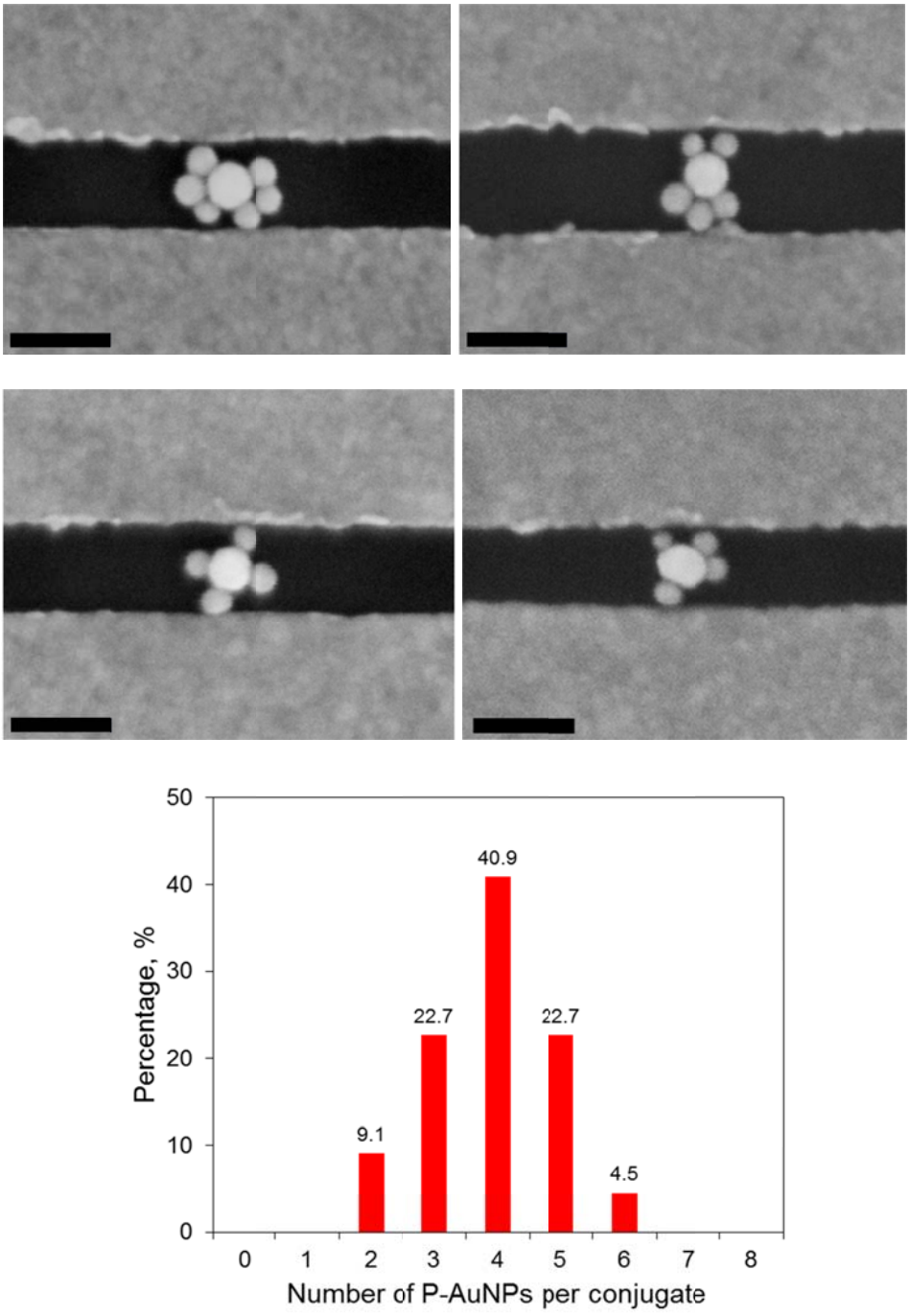

Figure 5-14 SEM images and statistical analysis of nanoparticle satellite conjugates at 50 pM T-DNA (scale bars: 100nm)

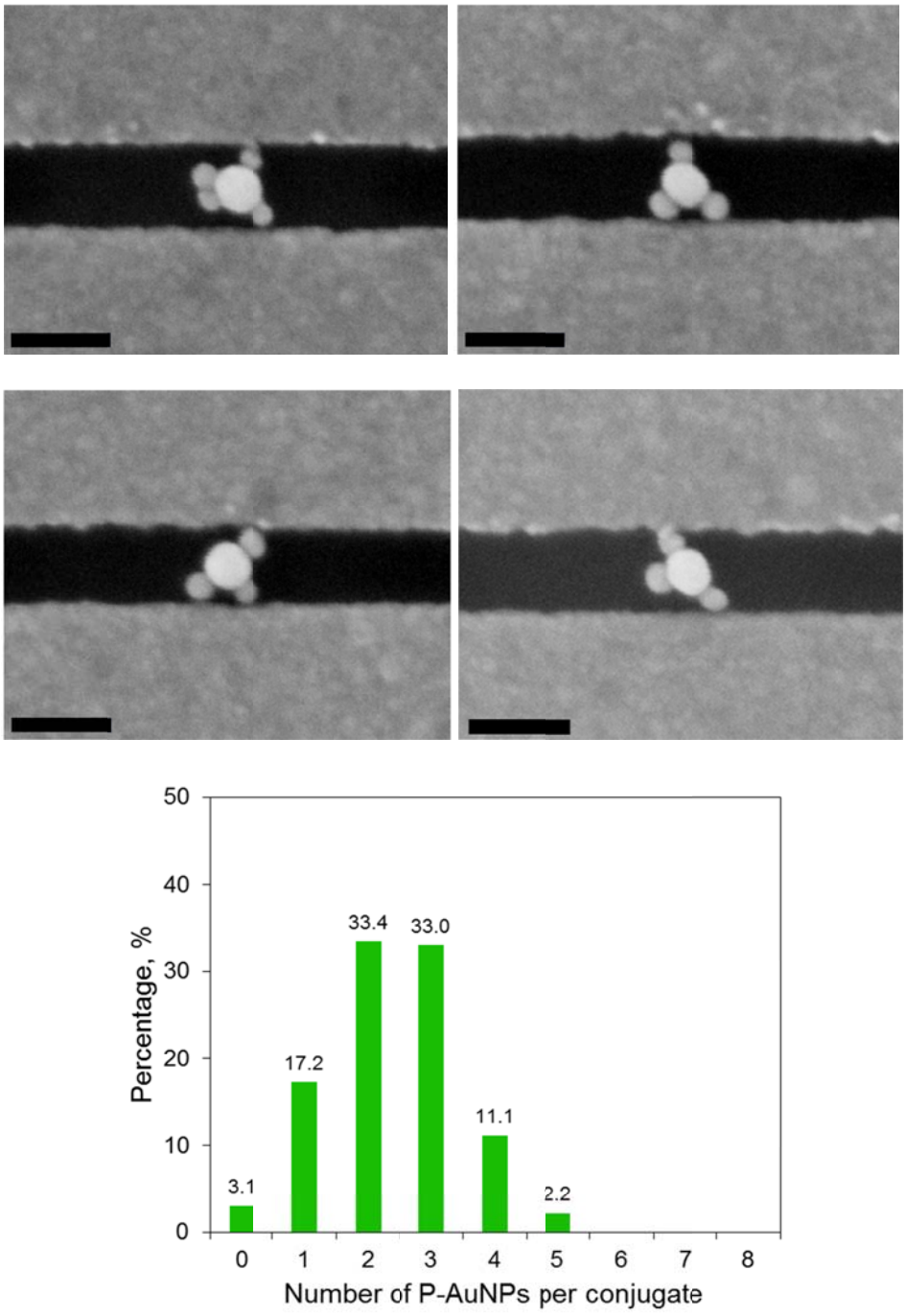

Figure 5-15 SEM images and statistical analysis of nanoparticle satellite conjugates at 500 fM T-DNA (scale bars: 100nm)

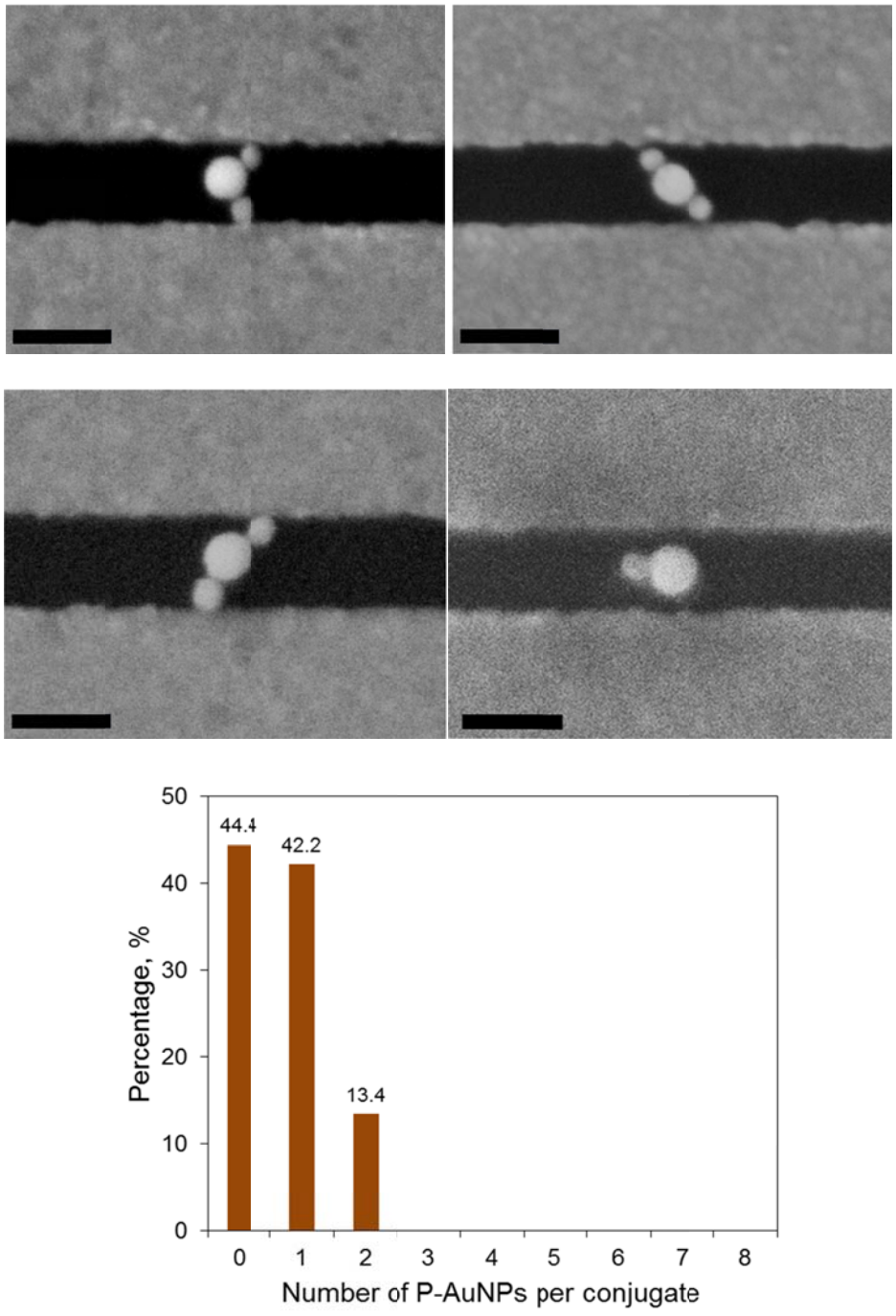

Figure 5-16 SEM images and statistical analysis of nanoparticle satellite conjugates at 50 fM T-DNA (scale bars: 100nm)

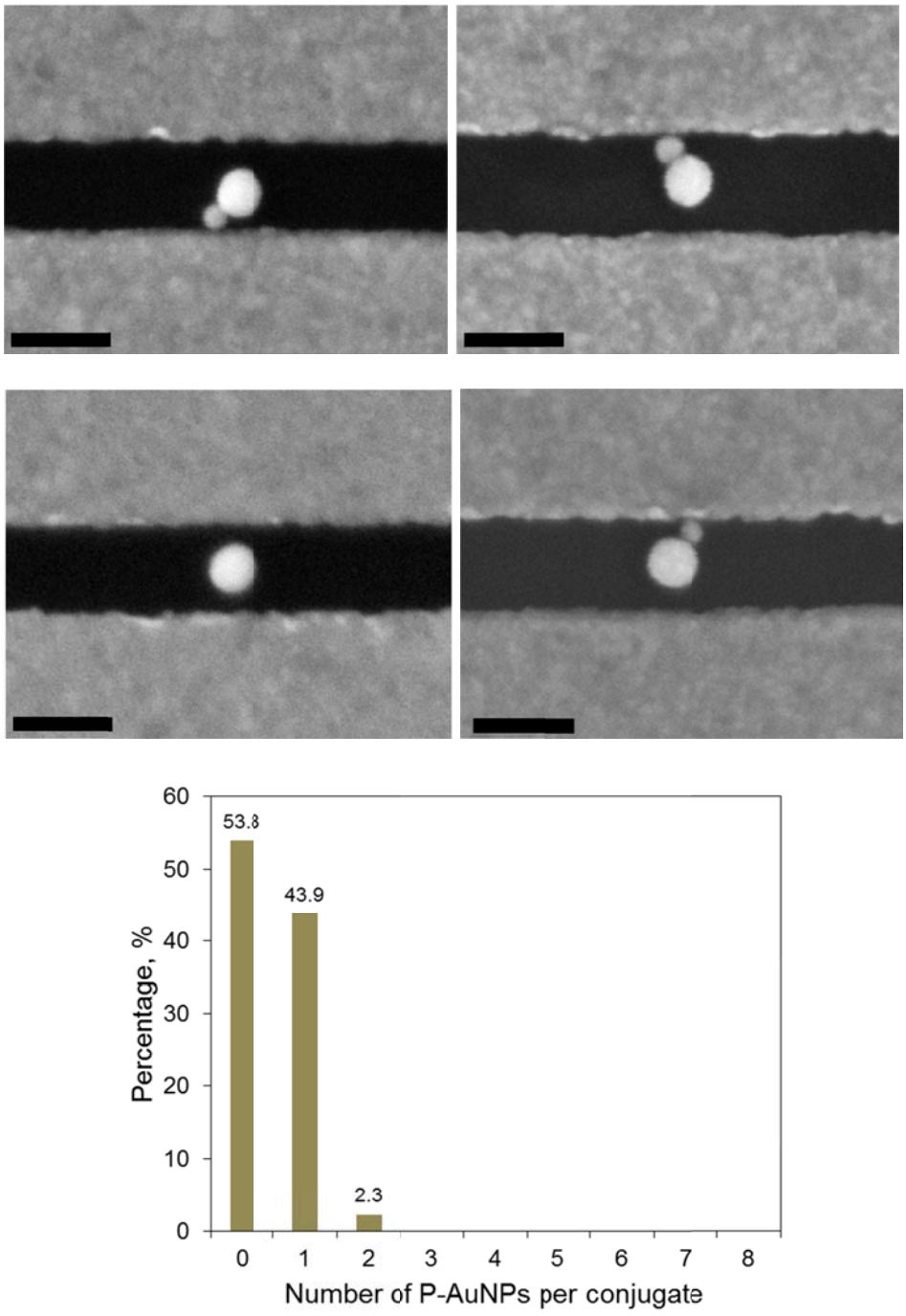

Figure 5-17 SEM images and statistical analysis of nanoparticle satellite conjugates at 5 nM 1-base pair mismatched T-DNA (scale bars: 100nm)

5.5.2 I-V measurements

Formation of nanoparticle satellite conjugates between two electrodes provide electrical path between two electrodes. Therefore, presence of T-DNA can be electrically detected through current-voltage (I-V) measurement. Applying voltage between two electrodes (V_{SD}) produces current (I_{SD}) if nanoparticle satellite conjugates were formed between two electrodes. Figures 6-16 to 6-20 show I-V measurements for 5nM, 50 pM, 500 fM, 50 fM T-DNA and 5nM 1-bp mismatched T-DNA, respectively.

Applying voltage produces higher current at high concentration of T-DNA which is due to the more number of formed nanoparticle satellite conjugates which provide electrical path between two electrodes.

I-V measurements comparison between 5 nM complementary and mismatched T-DNA (figures 5-18 and 5-22) approves the efficiency of stringency washing in distinguishing between complementary and mismatched T-DNA. As seen, applying voltage produced no current for 5 nM mismatched T-DNA since no nanoparticle satellite conjugate which bridges two electrodes was formed.

Based on I-V measurements and SEM characterizations, limit of detection in this amplification-free detection method is **50 fM** which is considered as an ultra-sensitive DNA sensor.

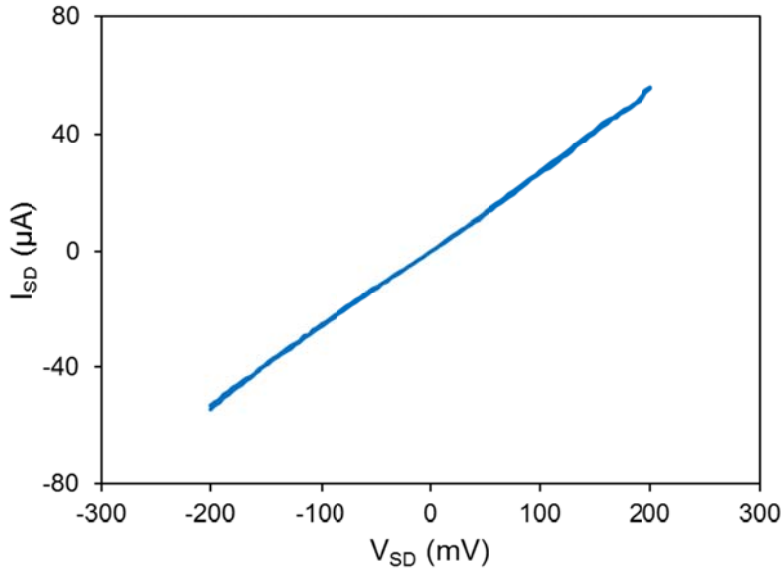

Figure 5-18 I-V measurement for 5 nM T-DNA (device is same as the one which was analyzed statistically in figure 5-13)

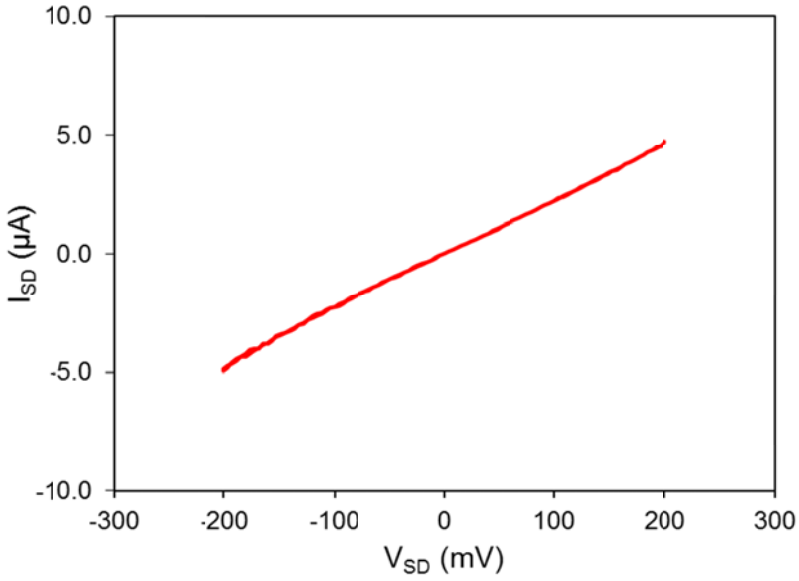

Figure 5-19 I-V measurement for 50 pM T-DNA (device is same as the one which was analyzed statistically in figure 5-14)

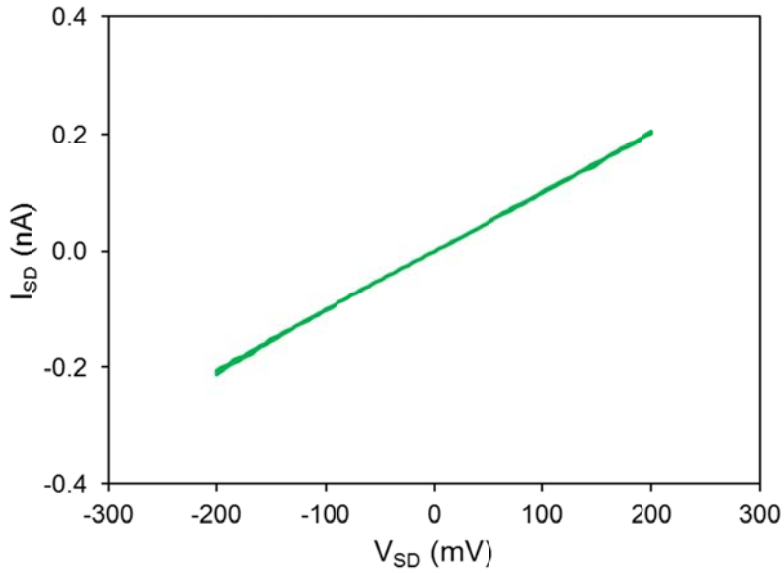

Figure 5-20 I-V measurement for 500 fM T-DNA (device is same as the one which was analyzed statistically in figure 5-15)

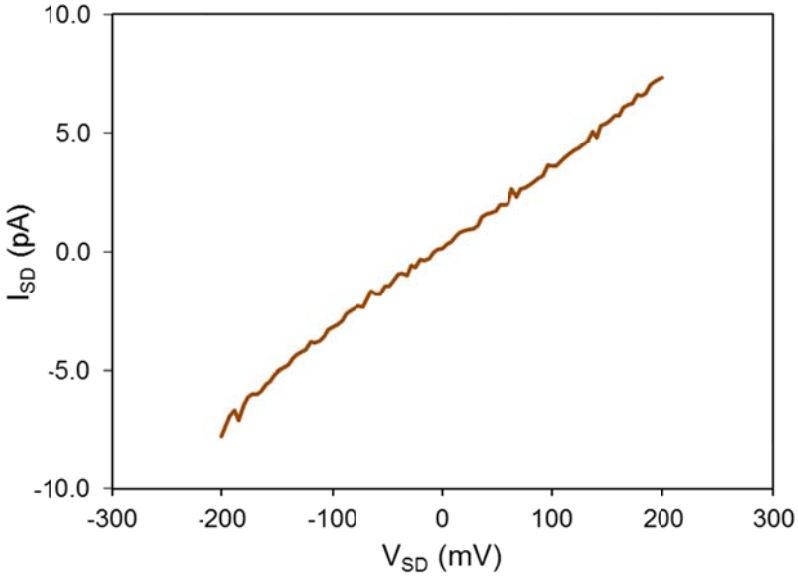

Figure 5-21 I-V measurement for 50 fM T-DNA (device is same as the one which was analyzed statistically in figure 5-16)

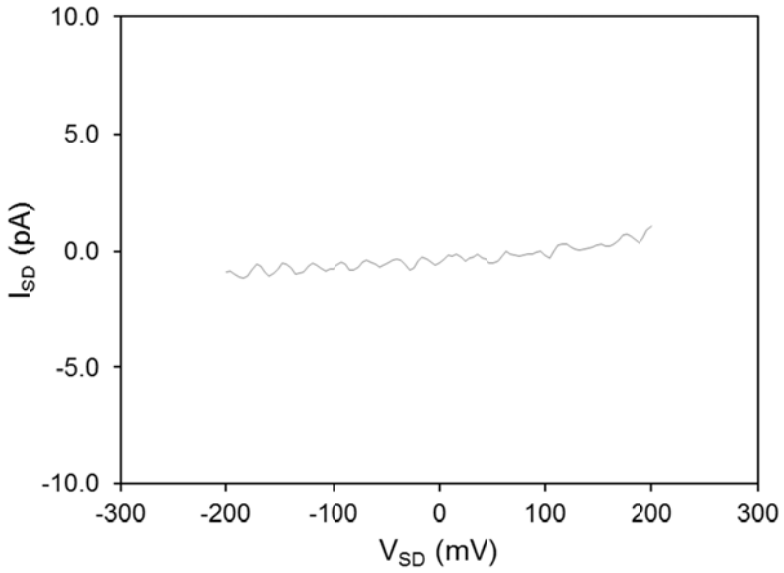

Figure 5-22 I-V measurement for 5 nM 1-bp mismatched T-DNA (device is same as the one which was analyzed statistically in figure 5-17)

Chapter 6

Conclusion and Future Work

6.1 Conclusion

In this research, a new amplification free oligonucleotide sensor was developed in which gold nanoparticles were used to electrically detect the oligonucleotide molecules. The summary of accomplishments is as following:

- Successful functionalizing of gold nanoparticles with thiolated single-stranded DNA molecules. Around 700 capture DNA and 240 probe DNA was immobilized onto 50 and 30 nm gold nanoparticles, respectively, with inter-molecular spacing of ~ 3.5 nm.
- Successful formation of amino- and carboxyl-terminated self-assembled monolayers (SAMs) onto silicon dioxide and gold surfaces.
- Accurate placement of DNA-functionalized gold nanoparticles onto specific locations of sensor via electrostatic funneling. Capture DNA-functionalized gold nanoparticles were placed between two electrodes with 4nm accuracy.
- Achieving a high level of sensitivity (**50 fM**) and selectivity in DNA detection without applying any kind of amplification technique. This detection method is combined with high specificity by not detecting the one base pair-mismatched oligonucleotide.

6.2 Future Work

6.2.1 Applying Electric Field to Accelerate Oligonucleotide Hybridization and Detection

DNA molecules are strongly charged due to the presence of phosphate groups on the phosphate-sugar backbone of the DNA. Hence, the movement and orientation of DNA molecule can be controlled by application of electric field. Direct current electric field and pulse electric field could be effective to accelerate and facilitate hybridization in this research.

DC electric field facilitates hybridization reaction by providing more DNA strands at the hybridization sites due to electrophoresis phenomenon [154-157]. Negatively-charged DNA strands are dragged towards higher potential electrode. Water electrolysis at voltages above 1.2 V SCE is the main drawback. To overcome this problem, a porous hydro gel permeation layer is used. Permeation layer allows running at voltages higher than 1.2V while protecting DNA strands from surface electrochemical reactions. Hybridization buffer is the other important key that provides DNA rapid transportation and facilitates hybridization by balancing acidic conditions at the anode surface and diminishing repulsion between DNA strands because of having a net positive charge. Since our proposed DNA detection method begins with accurate placement of DNA/AuNP

conjugate between two electrodes, applying permeation layer is not allowed. Therefore, applied voltage must be less than 1.2V.

Pulse electric field is another type of applied electric field that increases hybridization reaction kinetics by DNA desorption and reorientation which favors hybridization [153, 158-160]. The exerted torque on the DNA strand in an electric is the primary cause of DNA re-orientation. DNA strand in solution behaves as a rod-like polymer with charge distribution of 4.7×10^{-19} C/cm and is surrounded by a symmetrical counter-ions atmosphere36. Once the electric field is applied, counter-ions atmosphere losses its symmetry because of free ions flow along the DNA axis. Consequently, a torque arises from the interaction of the asymmetric counter-ions atmosphere with DNA strand re-orienting DNA strand along the electric field direction. The critical factor in pulse electric field application is the rise time. The rise time must be shorter than dielectric response time. The pulse time should also be in microsecond timescale. By applying pulse electric field, considering the pulse time, the migration of the DNA from the bulk is negligible. In this research, a proper electric field will be designed to facilitate and accelerate the hybridization reactions

6.2.2 Implementing Microfluidic System

Implementing microfluidic system could accelerate the hybridization, reduce the detection time, and likely increase the detection sensitivity. Recently,

devices consisting of microfluidic channels have been considered significantly in bio-detection methods [161, 162]. First advantage of using microfluidic system is that reduced volume of target bio-molecule is needed because microfluidics operates with the transfer and control of small amount of fluids in microscale flow configurations [163]. Requiring less volume of target bio-molecule makes the detection way more efficient and possible to have compact and portable systems.

The important aspect using microfluidic system is that the hybridization between capture and target oligonucleotide can be accelerated on microfluidic channels. In microfluidic system, ratio of surface to volume is large which leads to reduced diffusion distance. Therefore, mass transport of target bio-molecules is enhanced and hybridization of target bio-molecules with capture bio-molecules is accelerated. It would be more efficient if target bio-molecule could move and encounter all the capture bio-molecules. One possible way could be using a circulation microfluidic system.

References

1. Saiki, R., et al., *Enzymatic amplification of beta-globin genomic sequences and restriction site analysis for diagnosis of sickle cell anemia.* Science, 1985. **230**(4732): p. 1350-1354.
2. Liu, R.H., et al., *Self-contained, fully integrated biochip for sample preparation, polymerase chain reaction amplification, and DNA microarray detection.* Analytical chemistry, 2004. **76**(7): p. 1824-1831.
3. Asaga, S., et al., *Direct serum assay for microRNA-21 concentrations in early and advanced breast cancer.* Clinical chemistry, 2011. **57**(1): p. 84-91.
4. Nam, J.M., S.I. Stoeva, and C.A. Mirkin, *Bio-bar-code-based DNA detection with PCR-like sensitivity.* Journal of the American Chemical Society, 2004. **126**(19): p. 5932-5933.
5. Hill, H.D. and C.A. Mirkin, *The bio-barcode assay for the detection of protein and nucleic acid targets using DTT-induced ligand exchange.* Nat. Protocols, 2006. **1**(1): p. 324-336.
6. Park, S.-J., T.A. Taton, and C.A. Mirkin, *Array-based electrical detection of DNA with nanoparticle probes.* Science, 2002. **295**(5559): p. 1503-1506.

7. Kim, D., W.L. Daniel, and C.A. Mirkin, *Microarray-Based Multiplexed Scanometric Immunoassay for Protein Cancer Markers Using Gold Nanoparticle Probes.* Analytical Chemistry, 2009. **81**(21): p. 9183-9187.

8. Cao, Y.C., R. Jin, and C.A. Mirkin, *Nanoparticles with Raman spectroscopic fingerprints for DNA and RNA detection.* Science, 2002. **297**(5586): p. 1536-1540.

9. Kang, T., et al., *Patterned Multiplex Pathogen DNA Detection by Au Particle-on-Wire SERS Sensor.* Nano Letters, 2010. **10**(4): p. 1189-1193.

10. Jin, J.I.I. and J. Grote, *Materials Science of DNA*. 2011: CRC Press.

11. Hoffman, G.W. and D. Pörschke, *Cooperative nonenzymic base recognition. Kinetics of the binding of a base monomer to a complementary polynucleotide template.* Biopolymers, 1973. **12**(7): p. 1625-1638.

12. Chen, C., et al., *Kinetics and thermodynamics of DNA hybridization on gold nanoparticles.* Nucleic acids research, 2009. **37**(11): p. 3756-3765.

13. Chan, V., D.J. Graves, and S.E. McKenzie, *The biophysics of DNA hybridization with immobilized oligonucleotide probes.* Biophysical journal, 1995. **69**(6): p. 2243.

14. Nicoloso, M.S., et al., *MicroRNAs—the micro steering wheel of tumour metastases.* Nature Reviews Cancer, 2009. **9**(4): p. 293-302.

15. Iorio, M.V., et al., *MicroRNA gene expression deregulation in human breast cancer.* Cancer research, 2005. **65**(16): p. 7065-7070.

16. Yanaihara, N., et al., *Unique microRNA molecular profiles in lung cancer diagnosis and prognosis.* Cancer cell, 2006. **9**(3): p. 189-198.

17. Porkka, K.P., et al., *MicroRNA expression profiling in prostate cancer.* Cancer research, 2007. **67**(13): p. 6130-6135.

18. Akao, Y., Y. Nakagawa, and T. Naoe, *MicroRNA-143 and-145 in colon cancer.* DNA and cell biology, 2007. **26**(5): p. 311-320.

19. Tricoli, J.V. and J.W. Jacobson, *MicroRNA: potential for cancer detection, diagnosis, and prognosis.* Cancer Research, 2007. **67**(10): p. 4553-4555.

20. Lu, J., et al., *MicroRNA expression profiles classify human cancers.* nature, 2005. **435**(7043): p. 834-838.

21. Kirk, B.W., et al., *Single nucleotide polymorphism seeking long term association with complex disease.* Nucleic Acids Research, 2002. **30**(15): p. 3295-3311.

22. Duggan, D.J., et al., *Expression profiling using cDNA microarrays.* Nat Genet.

23. Oberst, R., et al., *PCR-based DNA amplification and presumptive detection of Escherichia coli O157: H7 with an internal fluorogenic probe*

and the 5' nuclease (TaqMan) assay. Applied and environmental microbiology, 1998. **64**(9): p. 3389-3396.

24. Saiki, R.K., et al., *Genetic analysis of amplified DNA with immobilized sequence-specific oligonucleotide probes.* Proceedings of the National Academy of Sciences, 1989. **86**(16): p. 6230-6234.

25. Ma, W., et al., *Attomolar DNA detection with chiral nanorod assemblies.* Nature communications, 2013. **4**.

26. Shafique, S., *Polymerase Chain Reaction*. Lulu.com.

27. Sano, T., C. Smith, and C. Cantor, *Immuno-PCR: very sensitive antigen detection by means of specific antibody-DNA conjugates.* Science, 1992. **258**(5079): p. 120-122.

28. Niemeyer, C.M., M. Adler, and R. Wacker, *Immuno-PCR: high sensitivity detection of proteins by nucleic acid amplification.* Trends in biotechnology, 2005. **23**(4): p. 208-216.

29. Chen, C., et al., *Real-time quantification of microRNAs by stem–loop RT–PCR.* Nucleic acids research, 2005. **33**(20): p. e179-e179.

30. Jiang, J., et al., *Real-time expression profiling of microRNA precursors in human cancer cell lines.* Nucleic acids research, 2005. **33**(17): p. 5394-5403.

31. Schmittgen, T.D., et al., *A high-throughput method to monitor the expression of microRNA precursors.* Nucleic acids research, 2004. **32**(4): p. e43-e43.

32. Adler, M., R. Wacker, and C.M. Niemeyer, *A real-time immuno-PCR assay for routine ultrasensitive quantification of proteins.* Biochemical and biophysical research communications, 2003. **308**(2): p. 240-250.

33. Lind, K. and M. Kubista, *Development and evaluation of three real-time immuno-PCR assemblages for quantification of PSA.* Journal of immunological methods, 2005. **304**(1): p. 107-116.

34. Niemeyer, C.M., M. Adler, and R. Wacker, *Detecting antigens by quantitative immuno-PCR.* Nature protocols, 2007. **2**(8): p. 1918-1930.

35. Ali, M.M., et al., *Rolling circle amplification: a versatile tool for chemical biology, materials science and medicine.* Chemical Society Reviews, 2014. **43**(10): p. 3324-3341.

36. Mashimo, Y., et al., *Detection of small RNA molecules by a combination of branched rolling circle amplification and bioluminescent pyrophosphate assay.* Analytical and bioanalytical chemistry, 2011. **401**(1): p. 221-227.

37. Zhou, Y., et al., *A dumbbell probe-mediated rolling circle amplification strategy for highly sensitive microRNA detection.* Nucleic acids research, 2010. **38**(15): p. e156-e156.

38. Wen, Y., et al., *DNAzyme-based rolling-circle amplification DNA machine for ultrasensitive analysis of microRNA in Drosophila larva.* Analytical chemistry, 2012. **84**(18): p. 7664-7669.

39. Hong, C.-Y., et al., *Direct detection of circulating microRNAs in serum of cancer patients by coupling protein-facilitated specific enrichment and rolling circle amplification.* Chemical Communications, 2014. **50**(25): p. 3292-3295.

40. Konry, T., et al., *Ultrasensitive Detection of Low-Abundance Surface-Marker Protein Using Isothermal Rolling Circle Amplification in a Microfluidic Nanoliter Platform.* Small, 2011. **7**(3): p. 395-400.

41. Schweitzer, B., et al., *Immunoassays with rolling circle DNA amplification: a versatile platform for ultrasensitive antigen detection.* Proceedings of the National Academy of Sciences, 2000. **97**(18): p. 10113-10119.

42. Liu, D., et al., *Rolling Circle DNA Synthesis: Small Circular Oligonucleotides as Efficient Templates for DNA Polymerases.* Journal of the American Chemical Society, 1996. **118**(7): p. 1587-1594.

43. Dong, H., et al., *MicroRNA: function, detection, and bioanalysis.* Chemical reviews, 2013. **113**(8): p. 6207-6233.

44. Alhasan, A.H., et al., *Scanometric microRNA array profiling of prostate cancer markers using spherical nucleic acid–gold nanoparticle conjugates.* Analytical chemistry, 2012. **84**(9): p. 4153-4160.

45. Wang, Y., et al., *Nanopore-based detection of circulating microRNAs in lung cancer patients.* Nature nanotechnology, 2011. **6**(10): p. 668-674.

46. Calin, G.A., et al., *Frequent deletions and down-regulation of micro-RNA genes miR15 and miR16 at 13q14 in chronic lymphocytic leukemia.* Proceedings of the National Academy of Sciences, 2002. **99**(24): p. 15524-15529.

47. Van Ness, J., L.K. Van Ness, and D.J. Galas, *Isothermal reactions for the amplification of oligonucleotides.* Proceedings of the National Academy of Sciences, 2003. **100**(8): p. 4504-4509.

48. Zhang, Y. and C.-y. Zhang, *Sensitive detection of microRNA with isothermal amplification and a single-quantum-dot-based nanosensor.* Analytical chemistry, 2011. **84**(1): p. 224-231.

49. Wang, G.-l. and C.-y. Zhang, *Sensitive detection of microRNAs with hairpin probe-based circular exponential amplification assay.* Analytical chemistry, 2012. **84**(16): p. 7037-7042.

50. Jia, H., et al., *Ultrasensitive detection of microRNAs by exponential isothermal amplification.* Angewandte Chemie International Edition, 2010. **49**(32): p. 5498-5501.

51. Arnold, E. and S.G. Sarafianos, *Molecular biology: An HIV secret uncovered.* Nature, 2008. **453**(7192): p. 169-170.

52. Merkoçi, A., *Nanoparticles-based strategies for DNA, protein and cell sensors.* Biosensors and Bioelectronics, 2010. **26**(4): p. 1164-1177.

53. Cioffi, N., et al., *Electrosynthesis and characterization of gold nanoparticles for electronic capacitance sensing of pollutants.* Electrochimica Acta, 2011. **56**(10): p. 3713-3720.

54. Lin, Y.-W., C.-W. Liu, and H.-T. Chang, *DNA functionalized gold nanoparticles for bioanalysis.* Analytical Methods, 2009. **1**(1): p. 14-24.

55. Zanoli, L.M., R. D'Agata, and G. Spoto, *Functionalized gold nanoparticles for ultrasensitive DNA detection.* Analytical and bioanalytical chemistry, 2012. **402**(5): p. 1759-1771.

56. Sperling, R.A., et al., *Biological applications of gold nanoparticles.* Chemical Society Reviews, 2008. **37**(9): p. 1896-1908.

57. Alivisatos, A.P., et al., *Organization of'nanocrystal molecules' using DNA.* 1996.

58. Pellegrino, T., et al., *On the development of colloidal nanoparticles towards multifunctional structures and their possible use for biological applications.* small, 2005. **1**(1): p. 48-63.

59. Nicewarner Peña, S.R., et al., *Hybridization and enzymatic extension of Au nanoparticle-bound oligonucleotides.* Journal of the American Chemical Society, 2002. **124**(25): p. 7314-7323.

60. Mirkin, C.A., et al., *A DNA-based method for rationally assembling nanoparticles into macroscopic materials.* Nature, 1996. **382**(6592): p. 607-609.

61. Elghanian, R., et al., *Selective colorimetric detection of polynucleotides based on the distance-dependent optical properties of gold nanoparticles.* Science, 1997. **277**(5329): p. 1078-1081.

62. Storhoff, J.J., et al., *One-pot colorimetric differentiation of polynucleotides with single base imperfections using gold nanoparticle probes.* Journal of the American Chemical Society, 1998. **120**(9): p. 1959-1964.

63. Taton, T.A., C.A. Mirkin, and R.L. Letsinger, *Scanometric DNA array detection with nanoparticle probes.* Science, 2000. **289**(5485): p. 1757-1760.

64. Taton, T.A., G. Lu, and C.A. Mirkin, *Two-Color Labeling of Oligonucleotide Arrays via Size-Selective Scattering of Nanoparticle Probes.* Journal of the American Chemical Society, 2001. **123**(21): p. 5164-5165.

65. Storhoff, J.J., et al., *Homogeneous detection of unamplified genomic DNA sequences based on colorimetric scatter of gold nanoparticle probes.* Nature biotechnology, 2004. **22**(7): p. 883-887.

66. He, L., et al., *Colloidal Au-enhanced surface plasmon resonance for ultrasensitive detection of DNA hybridization.* Journal of the American Chemical Society, 2000. **122**(38): p. 9071-9077.

67. Kai, E., et al., *Detection of PCR products in solution using surface plasmon resonance.* Analytical chemistry, 1999. **71**(4): p. 796-800.

68. Miao, W. and A.J. Bard, *Electrogenerated chemiluminescence. 80. C-reactive protein determination at high amplification with [Ru (bpy) 3] 2+-containing microspheres.* Analytical chemistry, 2004. **76**(23): p. 7109-7113.

69. Miao, W. and A.J. Bard, *Electrogenerated chemiluminescence. 72. Determination of immobilized DNA and C-reactive protein on Au (111) electrodes using tris (2, 2'-bipyridyl) ruthenium (II) labels.* Analytical chemistry, 2003. **75**(21): p. 5825-5834.

70. Ding, C., et al., *Ultrasensitive chemiluminescence quantification of single-nucleotide polymorphisms by using monobase-modified Au and CuS nanoparticles.* Biosensors and Bioelectronics, 2010. **25**(5): p. 1082-1087.

71. Richter, M.M., *Electrochemiluminescence (ecl).* Chemical Reviews, 2004. **104**(6): p. 3003-3036.

72. Zhu, D., et al., *PCR-free quantitative detection of genetically modified organism from raw materials. An electrochemiluminescence-based bio bar code method.* Analytical chemistry, 2008. **80**(10): p. 3566-3571.

73. Shan, Y., J.-J. Xu, and H.-Y. Chen, *Distance-dependent quenching and enhancing of electrochemiluminescence from a CdS: Mn nanocrystal film by Au nanoparticles for highly sensitive detection of DNA.* Chemical Communications, 2009(8): p. 905-907.

74. Chai, Y., et al., *A novel electrochemiluminescence strategy for ultrasensitive DNA assay using luminol functionalized gold nanoparticles multi-labeling and amplification of gold nanoparticles and biotin–streptavidin system.* Chemical Communications, 2010. **46**(40): p. 7560-7562.

75. Thaxton, C.S., et al., *A Bio-Bar-Code Assay Based upon Dithiothreitol-Induced Oligonucleotide Release.* Analytical Chemistry, 2005. **77**(24): p. 8174-8178.

76. Stoeva, S.I., et al., *Multiplexed DNA Detection with Biobarcoded Nanoparticle Probes.* Angewandte Chemie International Edition, 2006. **45**(20): p. 3303-3306.

77. Nam, J.-M., C.S. Thaxton, and C.A. Mirkin, *Nanoparticle-based bio-bar codes for the ultrasensitive detection of proteins.* Science, 2003. **301**(5641): p. 1884-1886.

78. Thaxton, C.S., et al., *Nanoparticle-based bio-barcode assay redefines "undetectable" PSA and biochemical recurrence after radical prostatectomy.* Proceedings of the National Academy of Sciences, 2009. **106**(44): p. 18437-18442.

79. Stoeva, S.I., et al., *Multiplexed detection of protein cancer markers with biobarcoded nanoparticle probes.* Journal of the American Chemical Society, 2006. **128**(26): p. 8378-8379.

80. AbduláAziz, M., *Amperometric immunosensing using an indium tin oxide electrode modified with multi-walled carbon nanotube and poly (ethylene glycol)–silane copolymer.* Chemical communications, 2007(25): p. 2610-2612.

81. Gao, Z. and Z. Yang, *Detection of microRNAs using electrocatalytic nanoparticle tags.* Analytical chemistry, 2006. **78**(5): p. 1470-1477.

82. Shiddiky, M.J., M.A. Rahman, and Y.-B. Shim, *Hydrazine-catalyzed ultrasensitive detection of DNA and proteins.* Analytical chemistry, 2007. **79**(17): p. 6886-6890.

83. Lee, T.M.-H., H. Cai, and I.-M. Hsing, *Effects of gold nanoparticle and electrode surface properties on electrocatalytic silver deposition for electrochemical DNA hybridization detection.* Analyst, 2005. **130**(3): p. 364-369.

84. Das, J. and H. Yang, *Enhancement of Electrocatalytic Activity of DNA-Conjugated Gold Nanoparticles and Its Application to DNA Detection.* The Journal of Physical Chemistry C, 2009. **113**(15): p. 6093-6099.

85. Selvaraju, T., et al., *Nanocatalyst-based assay using DNA-conjugated Au nanoparticles for electrochemical DNA detection.* Langmuir, 2008. **24**(17): p. 9883-9888.

86. Weizmann, Y., F. Patolsky, and I. Willner, *Amplified detection of DNA and analysis of single-base mismatches by the catalyzed deposition of gold on Au-nanoparticles.* Analyst, 2001. **126**(9): p. 1502-1504.

87. Liu, T., J.a. Tang, and L. Jiang, *Sensitivity enhancement of DNA sensors by nanogold surface modification.* Biochemical and biophysical research communications, 2002. **295**(1): p. 14-16.

88. Liu, T., J.a. Tang, and L. Jiang, *The enhancement effect of gold nanoparticles as a surface modifier on DNA sensor sensitivity.* Biochemical and Biophysical Research Communications, 2004. **313**(1): p. 3-7.

89. Xu, H., et al., *Magnetically assisted DNA assays: high selectivity using conjugated polymers for amplified fluorescent transduction.* Nucleic acids research, 2005. **33**(9): p. e83-e83.

90. Gabig-Ciminska, M., et al., *Electric chips for rapid detection and quantification of nucleic acids.* Biosensors and Bioelectronics, 2004. **19**(6): p. 537-546.

91. Freitas, P., et al., *Magnetoresistive biochips.* Europhysics News, 2003. **34**(6): p. 224-226.

92. Smistrup, K., et al., *On-chip magnetic bead microarray using hydrodynamic focusing in a passive magnetic separator.* Lab on a Chip, 2005. **5**(11): p. 1315-1319.

93. Jarvius, J., et al., *Digital quantification using amplified single-molecule detection.* Nature methods, 2006. **3**(9): p. 725-727.

94. Martins, V., et al. *Use of magnetoresistive biochips for monitoring of pathogenic microorganisms in water through bioprobes: Oligonucleotides and antibodies*. in *Technical Proceedings of the 2005 NSTI Nanotechnology Conference and Trade Show*. 2005.

95. Alivisatos, A.P., *Less is more in medicine.* Scientific American, 2007. **17**: p. 72-79.

96. Wuister, S.F., et al., *Temperature-dependent energy transfer in cadmium telluride quantum dot solids.* The Journal of Physical Chemistry B, 2005. **109**(12): p. 5504-5508.

97. Zhang, C.-Y., et al., *Single-quantum-dot-based DNA nanosensor.* Nature materials, 2005. **4**(11): p. 826-831.

98. Han, M., et al., *Quantum-dot-tagged microbeads for multiplexed optical coding of biomolecules.* Nature biotechnology, 2001. **19**(7): p. 631-635.

99. Hahm, J.-i. and C.M. Lieber, *Direct ultrasensitive electrical detection of DNA and DNA sequence variations using nanowire nanosensors.* Nano letters, 2004. **4**(1): p. 51-54.

100. Woolley, A.T., et al., *Direct haplotyping of kilobase-size DNA using carbon nanotube probes.* Nature biotechnology, 2000. **18**(7): p. 760-763.

101. Wang, J., A.-N. Kawde, and M. Musameh, *Carbon-nanotube-modified glassy carbon electrodes for amplified label-free electrochemical detection of DNA hybridization.* Analyst, 2003. **128**(7): p. 912-916.

102. Li, J., et al., *Carbon nanotube nanoelectrode array for ultrasensitive DNA detection.* Nano letters, 2003. **3**(5): p. 597-602.

103. Wang, J., G. Liu, and M.R. Jan, *Ultrasensitive electrical biosensing of proteins and DNA: carbon-nanotube derived amplification of the recognition and transduction events.* Journal of the American Chemical Society, 2004. **126**(10): p. 3010-3011.

104. Cui, Y., et al., *Nanowire nanosensors for highly sensitive and selective detection of biological and chemical species.* Science, 2001. **293**(5533): p. 1289-1292.

105. Patolsky, F., et al., *Electrical detection of single viruses.* Proceedings of the National Academy of Sciences of the United States of America, 2004. **101**(39): p. 14017-14022.

106. Chen, R.J., et al., *Noncovalent functionalization of carbon nanotubes for highly specific electronic biosensors.* Proceedings of the National Academy of Sciences, 2003. **100**(9): p. 4984-4989.

107. Hurst, S.J., A.K. Lytton-Jean, and C.A. Mirkin, *Maximizing DNA loading on a range of gold nanoparticle sizes.* Analytical chemistry, 2006. **78**(24): p. 8313-8318.

108. Zu, Y. and Z. Gao, *Facile and Controllable Loading of Single-Stranded DNA on Gold Nanoparticles.* Analytical Chemistry, 2009. **81**(20): p. 8523-8528.

109. Hill, H.D., et al., *The role radius of curvature plays in thiolated oligonucleotide loading on gold nanoparticles.* ACS nano, 2009. **3**(2): p. 418-424.

110. Demers, L.M., et al., *A fluorescence-based method for determining the surface coverage and hybridization efficiency of thiol-capped oligonucleotides bound to gold thin films and nanoparticles.* Analytical chemistry, 2000. **72**(22): p. 5535-5541.

111. Kimura-Suda, H., et al., *Base-Dependent Competitive Adsorption of Single-Stranded DNA on Gold.* Journal of the American Chemical Society, 2003. **125**(30): p. 9014-9015.

112. Bhatt, N., et al., *Dissociation and degradation of thiol-modified DNA on gold nanoparticles in aqueous and organic solvents.* Langmuir, 2011. **27**(10): p. 6132-6137.

113. Herdt, A.R., et al., *DNA dissociation and degradation at gold nanoparticle surfaces.* Colloids and Surfaces B: Biointerfaces, 2006. **51**(2): p. 130-139.

114. Faucheux, N., et al., *Self-assembled monolayers with different terminating groups as model substrates for cell adhesion studies.* Biomaterials, 2004. **25**(14): p. 2721-2730.

115. Onclin, S., B.J. Ravoo, and D.N. Reinhoudt, *Engineering silicon oxide surfaces using Self-Assembled monolayers.* Angewandte Chemie International Edition, 2005. **44**(39): p. 6282-6304.

116. Smith, R.K., P.A. Lewis, and P.S. Weiss, *Patterning self-assembled monolayers.* Progress in Surface Science, 2004. **75**(1): p. 1-68.

117. Chen, C.-F., et al., *Electrostatic assembly of gold colloidal nanoparticles on organosilane monolayers patterned by microcontact electrochemical conversion.* Langmuir, 2006. **22**(18): p. 7819-7824.

118. Enders, D., et al., *Reversible adsorption of Au nanoparticles on SiO2/Si: An in situ ATR-IR study.* Surface Science, 2006. **600**(6): p. L71-L75.

119. Conzone, S.D. and C.G. Pantano, *Glass slides to DNA microarrays.* Materials Today, 2004. **7**(3): p. 20-26.

120. Falsey, J.R., et al., *Peptide and small molecule microarray for high throughput cell adhesion and functional assays.* Bioconjugate chemistry, 2001. **12**(3): p. 346-353.

121. Doh, J. and D.J. Irvine, *Immunological synapse arrays: patterned protein surfaces that modulate immunological synapse structure formation in T cells.* Proceedings of the National Academy of Sciences, 2006. **103**(15): p. 5700-5705.

122. Aswal, D.K., et al., *Self assembled monolayers on silicon for molecular electronics.* Analytica Chimica Acta, 2006. **568**(1–2): p. 84-108.

123. Brzoska, J.B., I.B. Azouz, and F. Rondelez, *Silanization of Solid Substrates: A Step Toward Reproducibility.* Langmuir, 1994. **10**(11): p. 4367-4373.

124. Wasserman, S.R., Y.T. Tao, and G.M. Whitesides, *Structure and reactivity of alkylsiloxane monolayers formed by reaction of alkyltrichlorosilanes on silicon substrates.* Langmuir, 1989. **5**(4): p. 1074-1087.

125. Kim, J., G.J. Holinga, and G.A. Somorjai, *Curing Induced Structural Reorganization and Enhanced Reactivity of Amino-Terminated Organic Thin Films on Solid Substrates: Observations of Two Types of Chemically*

and Structurally Unique Amino Groups on the Surface. Langmuir, 2011. **27**(9): p. 5171-5175.

126. Zhu, M., M.Z. Lerum, and W. Chen, *How to prepare reproducible, homogeneous, and hydrolytically stable aminosilane-derived layers on silica.* Langmuir, 2011. **28**(1): p. 416-423.

127. Asenath Smith, E. and W. Chen, *How To Prevent the Loss of Surface Functionality Derived from Aminosilanes.* Langmuir, 2008. **24**(21): p. 12405-12409.

128. Howarter, J.A. and J.P. Youngblood, *Optimization of silica silanization by 3-aminopropyltriethoxysilane.* Langmuir, 2006. **22**(26): p. 11142-11147.

129. Vandenberg, E.T., et al., *Structure of 3-aminopropyl triethoxy silane on silicon oxide.* Journal of Colloid and Interface Science, 1991. **147**(1): p. 103-118.

130. Kim, J., et al., *Formation, structure, and reactivity of amino-terminated organic films on silicon substrates.* Journal of Colloid and Interface Science, 2009. **329**(1): p. 114-119.

131. Zhang, F. and M.P. Srinivasan, *Self-Assembled Molecular Films of Aminosilanes and Their Immobilization Capacities.* Langmuir, 2004. **20**(6): p. 2309-2314.

132. Zhu, P., et al., *Investigation of Apatite Deposition onto Charged Surfaces in Aqueous Solutions Using a Quartz-Crystal Microbalance.* Journal of the American Ceramic Society, 2003. **86**(5): p. 782-790.

133. Shyue, J.-J., et al., *Acid-base properties and zeta potentials of self-assembled monolayers obtained via in situ transformations.* Langmuir, 2004. **20**(20): p. 8693-8698.

134. Nuzzo, R.G. and D.L. Allara, *Adsorption of bifunctional organic disulfides on gold surfaces.* Journal of the American Chemical Society, 1983. **105**(13): p. 4481-4483.

135. Nuzzo, R.G., B.R. Zegarski, and L.H. Dubois, *Fundamental studies of the chemisorption of organosulfur compounds on Au(111). Implications for molecular self-assembly on gold surfaces.* Journal of the American Chemical Society, 1987. **109**(3): p. 733-740.

136. Laibinis, P.E., et al., *Comparisons of self-assembled monolayers on silver and gold. Mixed monolayers derived from HS(CH2)21X and HS(CH2)10Y (X, Y = CH3, CH2OH) have similar properties.* Langmuir, 1991. **7**(12): p. 3167-3173.

137. Bain, C.D., et al., *Formation of monolayer films by the spontaneous assembly of organic thiols from solution onto gold.* Journal of the American Chemical Society, 1989. **111**(1): p. 321-335.

138. Nakano, K., et al., *Cytochrome c Self-Assembly on Alkanethiol Monolayer Electrodes as Characterized by AFM, IR, QCM, and Direct Electrochemistry.* Langmuir, 2007. **23**(11): p. 6270-6275.

139. Sakuragi, N., S. Yamamoto, and Y. Koide, *A Self-Assembled Monolayers Assisted Solid-State Conversion of Boehmite Particles to Aluminum Oxide Film.* Journal of the American Chemical Society, 2007. **129**(33): p. 10048-10049.

140. Chi, Y.S. and I.S. Choi, *Fluoro-N,N,N',N'-Tetramethylformamidinium Hexafluorophosphate: A Reagent for Formation of Interchain Carboxylic Anhydrides on Self-Assembled Monolayers.* Langmuir, 2006. **22**(16): p. 6956-6960.

141. Eck, W., et al., *PEGylated Gold Nanoparticles Conjugated to Monoclonal F19 Antibodies as Targeted Labeling Agents for Human Pancreatic Carcinoma Tissue.* ACS Nano, 2008. **2**(11): p. 2263-2272.

142. Jadhav, S., *Self-assembled monolayers (SAMs) of carboxylic acids: an overview.* Open Chemistry, 2011. **9**(3): p. 369-378.

143. Cheng, S.S., D.A. Scherson, and C.N. Sukenik, *In Situ Attenuated Total Reflectance Fourier Transform Infrared Spectroscopy Study of Carboxylate-Bearing, Siloxane-Anchored, Self-Assembled Monolayers: A Study of Carboxylate Reactivity and Acid-Base Properties.* Langmuir, 1995. **11**(4): p. 1190-1195.

144. Ma, L.-C., et al., *Electrostatic funneling for precise nanoparticle placement: a route to wafer-scale integration.* Nano letters, 2007. **7**(2): p. 439-445.

145. Huang, H.-W., et al., *Single-particle placement via self-limiting electrostatic gating.* Applied Physics Letters, 2008. **93**(7): p. 073110.

146. Kellenberger, E., *Colloidal Gold: Principles, Methods, and Applications. Hayat, MA., editor. Vol. 3*. 1991, San Diego, CA: Academic Press, Inc.

147. Mulvaney, P., *Surface plasmon spectroscopy of nanosized metal particles.* Langmuir, 1996. **12**(3): p. 788-800.

148. Huang, H., et al., *A novel label-free multi-throughput optical biosensor based on localized surface plasmon resonance.* Biosensors and Bioelectronics, 2009. **24**(7): p. 2255-2259.

149. Guo, L., et al., *Nanoarray-Based Biomolecular Detection Using Individual Au Nanoparticles with Minimized Localized Surface Plasmon Resonance Variations.* Analytical Chemistry, 2011. **83**(7): p. 2605-2612.

150. Guo, L., G. Chen, and D.-H. Kim, *Three-Dimensionally Assembled Gold Nanostructures for Plasmonic Biosensors.* Analytical Chemistry, 2010. **82**(12): p. 5147-5153.

151. Anker, J.N., et al., *Biosensing with plasmonic nanosensors.* Nat Mater, 2008. **7**(6): p. 442-453.

152. Nolte, D.D., *Invited review article: review of centrifugal microfluidic and bio-optical disks.* Review of scientific instruments, 2009. **80**(10): p. 101101.

153. Fixe, F., et al., *Electric-field assisted immobilization and hybridization of DNA oligomers on thin-film microchips.* Nanotechnology, 2005. **16**(10): p. 2061.

154. Edman, C.F., et al., *Electric field directed nucleic acid hybridization on microchips.* Nucleic Acids Research, 1997. **25**(24): p. 4907-4914.

155. Gurtner, C., et al., *Microelectronic array devices and techniques for electric field enhanced DNA hybridization in low-conductance buffers.* Electrophoresis, 2002. **23**(10): p. 1543-1550.

156. Heller, M.J., *An active microelectronics device for multiplex DNA analysis.* Engineering in Medicine and Biology Magazine, IEEE, 1996. **15**(2): p. 100-104.

157. Heller, M.J., A.H. Forster, and E. Tu, *Active microelectronic chip devices which utilize controlled electrophoretic fields for multiplex DNA hybridization and other genomic applications.* Electrophoresis, 2000. **21**(1): p. 157-164.

158. Cabeça, R., et al., *The effect of the shape of single, sub-ms voltage pulses on the rates of surface immobilization and hybridization of DNA.* Nanotechnology, 2009. **20**(1): p. 015503.

159. Fixe, F., et al., *Immobilization and hybridization by single sub-millisecond electric field pulses, for pixel-addressed DNA microarrays.* Biosensors and Bioelectronics, 2004. **19**(12): p. 1591-1597.

160. Fixe, F., et al., *An on-chip thin film photodetector for the quantification of DNA probes and targets in microarrays.* Nucleic acids research, 2004. **32**(9): p. e70-e70.

161. Noerholm, M., et al., *Polymer microfluidic chip for online monitoring of microarray hybridizations.* Lab on a Chip, 2004. **4**(1): p. 28-37.

162. Wang, Y., et al., *Microarrays assembled in microfluidic chips fabricated from poly (methyl methacrylate) for the detection of low-abundant DNA mutations.* Analytical Chemistry, 2003. **75**(5): p. 1130-1140.

163. Liu, R.H., et al., *Integrated microfluidic biochips for DNA microarray analysis.* 2006.

Biographical Information

Manouchehr Teimouri started his Ph.D. program in department of Materials Science and Engineering at the University of Texas at Arlington in January 2011and joined Dr. Seong Jin Koh's group in June 2011. Before that, he worked for 3 years from 2008-2010 as an oil and gas pipeline design and field engineer in Tehran, Iran. He received his M.Sc. and B.Sc. degrees in Materials Engineering from K.N. Toosi University of Technology and Amirkabir University of Technology (Tehran Polytechnic) in 2007 and 2004, respectively, in Tehran, Iran.